Monotonic Lateral Monopile Response in Weak Rock and the Influence of Crushed Rock due to Impact Driving

MSc. Thesis

C.Q.(Krijn) van Alphen

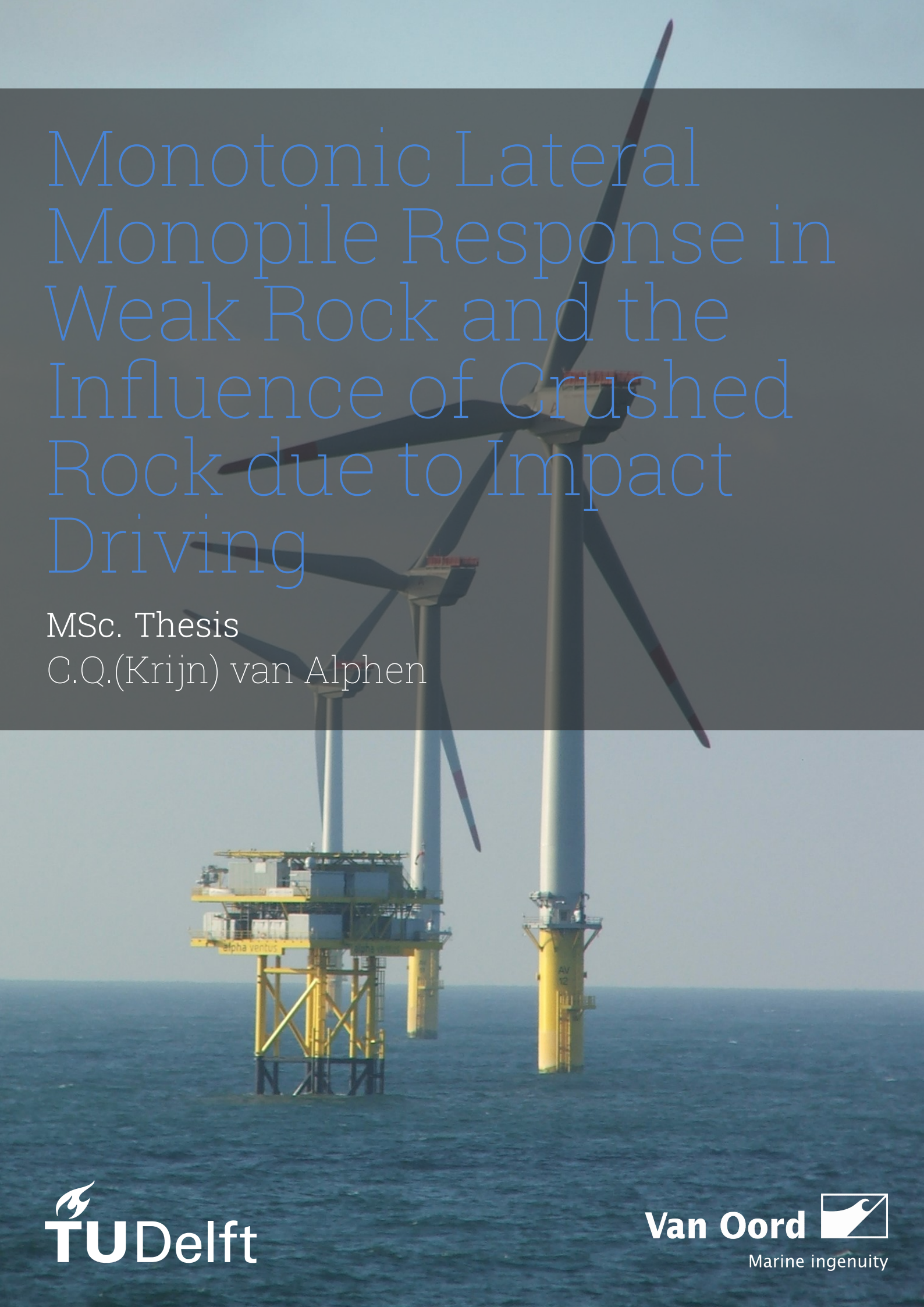

TU Delft

Van Oord
Marine ingenuity

Monotonic Lateral Monopile Response in Weak Rock and the Influence of Crushed Rock due to Impact Driving

by

C.Q.(Krijn) van Alphen

to obtain the degree of Master of Science
at the Delft University of Technology,
to be defended publicly on Tuesday August 29, 2023.

Student number:	4440595	
Project duration:	August 1, 2022 – August 31, 2023	
Thesis committee:	Dr. ir. R. B. J. Brinkgreve,	TU Delft, chair
	Prof. dr. ir. K. Gavin,	TU Delft
	Dr. ir. A. Tsouvalas	TU Delft
	Dr. ir. E. Kementzetzidis	TU Delft
	Ir. S. Brinkman,	Van Oord
	Ir. G. Chortis,	Van Oord

TU Delft

Preface

The thesis presented in this report marks the final step of my Master of Science Degree in Applied Earth Science at Delft University of Technology, completing the track in Geo-Engineering. The research has been performed at Van Oord Offshore Wind. I would like to thank Van Oord and the geotechnical team of the Offshore Wind Business Unit for providing me the opportunity to perform my thesis under their supervision and gain a valuable insights into the practical applications of geotechnical principles within the context of offshore wind projects.

Especially I would like to thank my two company supervisors George Chortis and Sanne Brinkman for the weekly meetings, random discussions, feedback and all other time and effort they put into my project with their daily supervision. I extend my appreciation to my university supervisors, Ronald Brinkgreve, Ken Gavin, Apostolos Tsouvalas, and Vagelis Kementzetzidis, for their support and guidance throughout this project.

Furthermore, I owe a great deal of gratitude to my family, friends and fellow students for their continuous support and encouragement.

With appreciation,

C.Q.(Krijn) van Alphen
Delft, August 2023

Summary

With the increasing demand for energy and the incentive to stop using fossil sources for energy generation, the demand for clean renewable energy sources is growing rapidly. Offshore wind has emerged as one of the most promising options for renewable energy generation and as a consequence is a booming industry. With the development of new wind farms all over the world, new geographical locations with challenging geological locations will be encountered. An example of challenging subsurface circumstances is a site consisting of weak rock. Currently monopiles are the most commonly used foundation type for offshore wind turbines (OWTs), due to its cost-effectiveness and ease of installation. The most widely used installation method is driving the monopile into the ground using an impact hammer. Driving a monopile into weak rock leads to crushing of the rock adjacent to the pile. A crushed zone is formed closely around the pile and cracks propagate further outwards of the crushed zone. The crushed zone around the monopile then in turn is expected to have an influence on the capacity of the laterally loaded structure. For future developments it is of interest to examine the influence on the lateral capacity and stiffness, to see whether driven installed monopiles have potential as a foundation type in weak rock.

This report therefore describes the investigation of the lateral monopile response in weak rock and the effect of a zone of crushed rock that is induced by driven installation. The goal of the investigation is to study the impact of the weaker zone around a monopile on the lateral response. The thesis focuses on the modelling of a monopile in a finite element model to examine the effect. The modelled monopile is compared to field tests that were done for the PhD dissertation of Lovera (2019) to be able to benchmark the model. To full-fill the research objective several steps were taken. The research can be divided into four parts to get to the final conclusion, being a literature review and three different models that are set up. The goal of the literature review and the two model in 2D are to act as a basis for the setup and inputs of the 3D model. The 3D model can then assess the effect of a crushed zone on the lateral capacity and stiffness of the pile. The literature review was done on multiple subjects related to the behaviour of rock around piles, for example crushing mechanisms of rock, bearing mechanisms under pile tips or pile driving tests.

Before setting up the models, different constitutive models and their pro's and cons were evaluated. A constitutive model is a way to mathematically describe the material mechanical behaviour under various loading conditions. It is used in finite element modelling to assign properties to a certain material body. Decisions on the preferred constitutive models per model then were made. For the crushed rock material it was decided that the HSsmall constitutive model was best applicable, as the crushed rock can be treated as a frictional material. For the intact rock the Hoek&Brown Softening constitutive model was decided to be best applicable, to allow for softening during the vertical push in the 2D model. For both crushed and intact rock also a Mohr-Coulomb material set was created to be used in the 3D model. This was done so the numerical models can be compared to models created by Lovera and because the post-peak behaviour of the intact rock outside the crushed zone is expected to not have a big influence on the lateral response in the 3D model.

The 2D model of a horizontal slice through the pile was set up to assess the strain patterns around a pile with a weak annulus around it. Next, the 2D axisymmetric vertical model was created to model a vertical push of a wished-in-place pile. The goal of the model was to see the effects of a vertical push. This is a simplified way of looking at this problem as the FEM numerical modelling software that was used is not ideal for modelling a complete driving sequence. Different model variations were created to compare the plastic regions that were induced in the models. The results of the vertical push could be used as indication for the thickness of a crushed zone that is included in the 3D model. Finally, multiple variations were created for the 3D model with different thicknesses of the crushed zone annulus and different properties of the crushed rock materials. The piles in the different models were loaded laterally

and the response is compared.

The results of the 2D horizontal model showed the strains were localized in the crushed zone, which is much softer than the intact rock. The results of the 2D axisymmetric vertical model showed a plastic zone reach deep into the geometry of the model. For a vertical push of a fixed length, the plastic zone reached 10 times the displacement or more. Different model variations with different residual strength values were also run. All models showed plastic or weakening region reaching a distance further than 2 wall thicknesses outside the pile. The fact that the plastic regions propagated deeper into the model than expected, combined with it not being a driving process but just a vertical push, led to the conclusion that the model was not a very reliable source. The size of the crushed zone therefore was altered for different 3D model variations. The results of the 3D model showed a significant impact of the introduction of a crushed zone on the global lateral pile stiffness. A model variation including a crushed zone showed a tangent initial global lateral stiffness drop of at least factor 10. For the base case of one wall thickness crushed zone with an average stiffness material set, the global stiffness dropped by a factor 27 even. Sensitivity checks are done on both the thickness of the crushed zone annulus as well as the stiffness properties of the material sets. The shape of the curves of the models including a crushed zone were non typical for a load-displacement curve, the curves showed a stiffening response for bigger displacements. The shape could be explained numerically considering the increase in stress-dependant stiffness in the crushed zone because of the high stresses that are present in the crushed zone due to the lateral loading. For the test results the increases in stiffness of the crushed rock due to increased stress also is an explanation for the displayed response, combined with compaction of open cracks outside which lead to increase in stiffness.

The research objective of this thesis is to examine the effect of a zone of crushed rock around a monopile on the lateral response. In conclusion it can be said that the impact of a crushed zone is big. The models that included a zone of crushed rock showed that pile response was highly influenced by the crushed rock area. For initial tangent global lateral stiffness of the pile this could be up to an order of magnitude compared to only intact rock. When taking into account that disturbance of rock is evident when impact driving a pile into it, this leads to the conclusion that it is important to include a crushed zone in future monopile designs in weak rock conditions. The stiffness parameters of the crushed rock are essential when modelling the lateral pile response in weak rock.

Contents

List of Figures

List of Tables

Nomenclature

Abbreviations

Abbreviation	Definition
HB	Hoek&Brown
HBS	Hoek&Brown Softening
HSsmall	Hardening Soil with small-strain stiffness
MC	Mohr-Coulomb
OnPT	Onshore Pile Test
OWT	Offshore Wind Turbine
WIP	Wished-In-Place

Symbols

Symbol	Definition	Unit
c	Cohesion	[kN/m^2]
D	Pile Diameter	[m]
E	Young's Modulus	[kN/m^2]
E_{50}^{ref}	Secant stiffness in standard drained triaxial test	[kN/m^2]
E_{oed}^{ref}	Tangent stiffness for primary oedometer loading	[kN/m^2]
E_{ur}^{ref}	Unloading/reloading stiffness from drained triaxial test	[kN/m^2]
F_x	Equivalent force	[kN]
G_0^{ref}	Reference shear modulus at very small strains	[kN/m^2]
GSI	Geological Strength Index	[-]
L	Embedment Depth	[m]
m	Power Function	[-]
m_b	Reduced value of intact rock parameter	[-]
m_{bres}	Residual reduced value of intact rock parameter	[-]
m_i	Dimensionless parameter for intact rock	[-]
p_{ref}	Power for stress-level dependency of stiffness	[kN/m^2]
s	Rock mass parameter	[-]
s_{res}	Residual rock mass parameter	[-]
t	Wall thickness	[m]
α	Factor for reducing tensile strength in HBS	[-]
γ	Fluidity	[1/day]
$\gamma_{0.7}$	Threshold shear strain	[-]
σ_{ci}	Uniaxial compressive strength	[kN/m^2]
σ'_{xx}	Effective stress in x-direction	[kN/m^2]
σ'_{yy}	Effective stress in y-direction	[kN/m^2]
σ'_{zz}	Effective stress in z-direction	[kN/m^2]
ϵ_{eq}^{p}	Equivalent strain	[-]
ϕ	Friction angle	[^{o}]
ψ	Dilation angle	[^{o}]
ν	Poisson's ratio	[-]
$\nu_{0.7}$	Poisson's ratio for unloading-reloading	[-]

1

Introduction

Since the industrial revolution the demand for energy has been ever-increasing, and over the last few decades, it has been exploding even. Non-renewable fossil energy sources like coal, oil, and gas have been the primary sources for energy generation, and they still contribute significantly to the energy mix in 2023. Over time however, concerns over climate change caused by the energy generation have grown as well. In 1979 the first World Climate Conference took place in Geneva, which led to the establishment of the World Climate Program. As awareness grew, the international community adopted the world's first greenhouse gas emission reduction treaty in 1997, the Kyoto Protocol. With urgency levels rising further, this finally led to the famous Paris Agreement in 2015, where 195 countries signed a legally binding agreement to cut green house emissions. The increasing concerns over climate change and agreements that arose with it, coupled with the finite nature of non-renewable sources, have driven the growing demand for renewable energy sources like wind, solar, and hydroelectric power.

Viewed as one of the most promising renewable energy sources, this trend is visible with offshore wind as well. The first offshore offshore wind farm in the world, the Vindeby Offshore Wind Farm, started operating in Denmark in 1991. By 2023, there are already 162 offshore operational offshore wind farms worldwide and many more are in development. It is anticipated that 330 GW (Lassen, 2022) of installed capacity of offshore wind is reached by 2030, coming from 34 GW in 2020. Figure 1.1 also visualizes the exponential growth of installed offshore wind capacity over the past fourteen years. The offshore wind industry is clearly booming and new wind farms will be developed in the coming years.

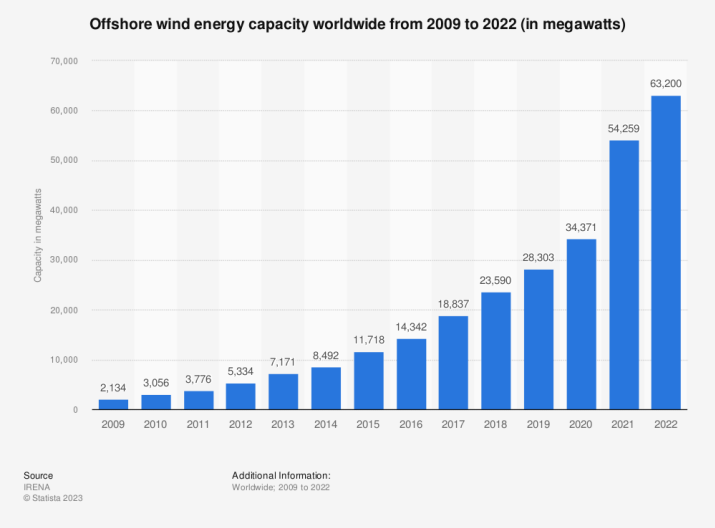

Figure 1.1: Installed offshore wind energy capacity worldwide from 2009 to 2022 (in megawatts). (IRENA, 2023)

With new sites for development of wind farms however, also new possibly challenging ground conditions are encountered. The ground conditions obviously have a significant effect on foundation design of an Offshore Wind Turbine (OWT). Foundation type and size then again have a big effect on project costs and timeline, making it a subject well worth investigating to be on top of things for future developments. This thesis will discuss the foundation of OWTs in such challenging conditions, specifically weak rock.

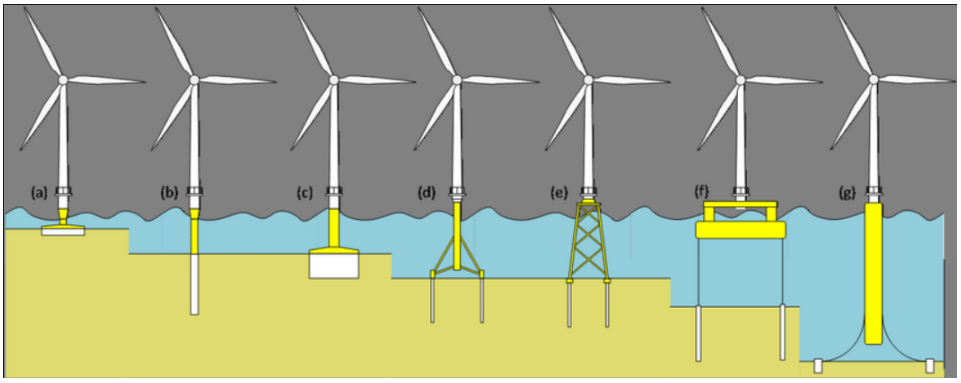

Figure 1.2: Graphic showing different ways of foundation for an OWT, being (a) Gravity based foundation, (b) monopile, (c) suction caisson, (d) tripod, (e) jacket, (f) tension leg platform and (g) ballast stabilised spar buoy (Houlsby and Byrne, private communication). (Beuckelaers, 2017)

Different variations of foundation exist for OWTs. Both bottom-fixed or floating foundations can be designed in multiple ways. Figure 1.2 shows seven different examples of foundations that are used. The most widely used foundation type is the monopile, more than 80% of the wind turbines currently installed in the North Sea are based on monopiles foundations for example (Sif Group, 2023). The reason it is so popular are the low fabrication and transportation costs, low risk profile and the ease of installation. It is therefore, that this thesis will focus on monopiles as a foundation type, it is shown at (b) in Figure 1.2.
A monopile is a foundation made up of an open-ended pile. Since significant lateral forces act on these foundations, monopile differ from typical foundation piles in terms of there length-to-diameter (L/D) ratio. The newest monopiles have diameters up to 11 meter, and 15 meter (Memija, 2023) is within reach with OWTs continue to grow in size.

Now, in sandy or clayey conditions monopiles are typically being driven into the ground using a hydrohammer. For rock conditions this usually is not a suitable technique as the rock is too hard to drive through. Hammering the monopile into hard rock can cause structural integrity issues, like buckling of the pile. In hard rock conditions alternative ways of installation can be used, like relieve drilling inside the pile or completely drilling out the complete volume of the monopile and filling it up with grout material to connect the monopile to the ground. For weak rock conditions, driving the pile to target depth should be feasible. The process of pile driving into weak rock however, is not well understood (Terente et al., 2017). Expected is that this driving will cause crushing and cracking of the rock around the monopile. Due to the significant lateral loading that happens at monopile foundations, the question is whether this remoulding and crushing has a big impact on the lateral response of the foundations.

Summing up, this thesis will look at monopile foundations for an OWT in weak rock conditions. It will focus on the effect on lateral response of crushed rock around a monopile that is induced by impact driven installation. This is of interest since the lateral ground response is important for the design of a monopile foundation.

2

Research Objective

As mentioned in the introduction, with higher demand for sustainable energy supply, new locations for offshore windfarms will be explored and developed over the next decade. By exploring new locations also new geological situations will be encountered. These new types of ground conditions potentially cause difficulties for foundation design. The knowledge on behaviour of weak rock in terms of lateral pile response is a topic where not much research has been done on yet. This is because for conventional, usually axially loaded, foundation structures the lateral capacity is not of as much interest as for monopiles. In order to prepare for future developments it is of interest to study the behaviour of a monopile in weak rock.

2.1. Starting Points

Starting point of this research is a PhD dissertation written by Anais Lovera in 2019. That research focusses on the same problem as this thesis, installation of monopiles in weak rock. Lovera performed onshore pile tests (OnPT) at a reduced scale. The tests included multiple piles, some driven, others drilled and grouted. This allowed for comparison in response for different installation method. Some piles were subjected to monotonic, some to cyclic loading. The results of these test are displayed in the thesis report and can therefore be used as a benchmark for a numerical model. For details of the pile testing, please refer to the thesis report of Lovera (2019).

The report provides test results of laboratory tests that were done on the weak rock samples, like an oedometer test, uniaxial test and triaxal tests. Furthermore it provides the lateral pile loading test results, observations at the site and also 2D and 3D numerical modelling of the problem. The input parameters that are used for the numerical modelling are also given. All this information together can be used to calibrate a new model and further investigate the numerical model as this was not the main focus of Lovera. The new numerical model has as a goal to better capture the behaviour that is seen during lateral loading of a pile in weak rock, rather than being a linear approximation. At the OnPT an annulus of remoulded rock and cracks around this zone were observed at ground level for the driven piles. These observations combined with results of the lateral loading tests show that the impact driving installation process has an influence on the lateral capacity.

2.2. Research Questions

The goal of the research is to assess the influence of the crushed zone that is created around a pile during impact driving into weak rock by creating a numerical model using more advanced constitutive models to describe the behaviour of weak rock under such loading conditions. The model presented before by Lovera contained only Mohr-Coulomb material sets, which yielded a linear stiffness response for lateral displacement of the pile. By introducing constitutive models that include for example stress-dependant stiffness or softening behaviour, the response can be estimated more carefully. Also a better insight of the mechanisms happening around the pile can be created in this way. The width of the remoulded rock annulus is observed to be one times the wall thickness and assumed to be equally thick along the whole length of the pile in the ground in the Lovera numerical model (see Figure 2.1). The

joint that is shown in the figure is a way in the numerical model to allow gapping to happen behind the pile. A more elaborate explanation on considerations for the constitutive modelling is given in chapter 5.

The research objective is captured in the main research question:

- What is the influence of a crushed rock zone induced by impact driving on the monotonic lateral monopile response in weak rock?

A list of sub-questions is investigated to support the answer to the main question:

- What rock behaviour aspects are important to be captured by the constitutive model? (Discussed in chapter 5)
- What is a suitable way to determine the remoulded zone and cracking around a monopile? (Discussed in chapter 4)
- How is the crushed zone around a monopile shaped for impact driving in terms of size and strength reduction? (Discussed in chapter 4)
- What parameters do influence the lateral pile response the most? (Discussed in chapter 7)

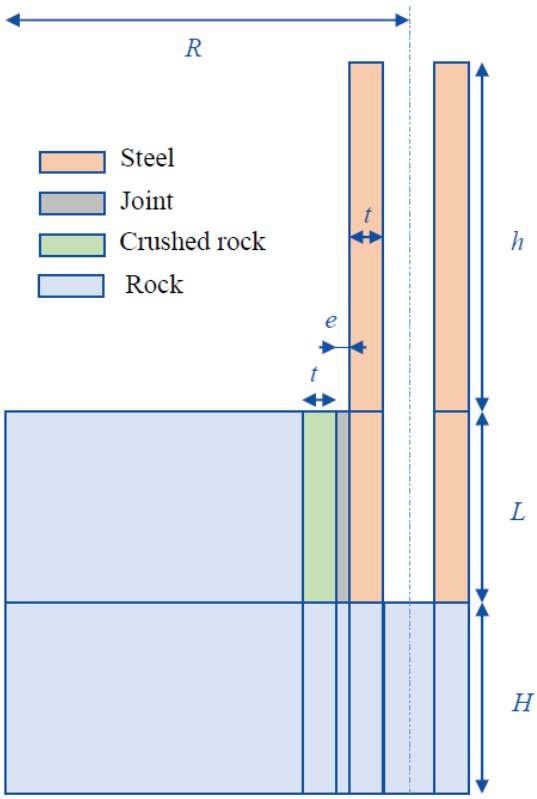

Figure 2.1: Geometry of 3D numerical model. (Lovera, 2019)

2.2.1. Limitations

The main focus and research objective of this study is to assess the lateral response of a monopile and the influence of the crushed zone of the pile. Since the crushed zone is induced during the impact driven installation, it was of interest to also look at a vertical push of the pile and see if a simplified situation could gain insight. However, since this was not the main goal of the research a limited investigation was done. It has to be noted that driving a pile into a rock is a process that is complex to define and includes impact forces propagating through pile and soil, and structural dynamics that are described very limited in this report. In the end it was considered proven that a crushed zone is present around a monopile and the effect of this crushed zone is investigated.

2.3. Thesis Outline and Methodology

In order to answer the research questions several steps are taken in the investigation. The structure of the research and outline of this thesis will be as follows.

1. The topic of the thesis is introduced and relevance of the investigation is illustrated.
2. The starting points and research objective of the investigation are explained, and also the limitations are discussed.
3. Relevant background knowledge on pile installation, lateral loading of monopiles and constitutive models is presented.
4. A literature review is done on the subject to establish the current knowledge on lateral loading in weak rock. Subjects that are looked into are crushing mechanisms of rock, typical bearing mechanisms under pile tips, modelling of pile penetration, testing of pile driving and remoulded zone around piles in different ground conditions.
5. Numerical models are created to investigate the typical strains during lateral loading when a crushed zone is included and to check the effect of a static vertical loading under a pile wall on a plastic zone that forms.

   (a) 2D plain-strain horizontal model (top view) to examine typical strain around a lateral moving monopile, used as help for constitutive model choice,
   (b) 2D axisymmetric vertical model to examine rock weakening around pile tip during static loading by a vertical push,
   Then based on the results of the 2D models a 3D model is created to investigate the impact of a crushed rock zone on the lateral response of a pile:
   (c) 3D model to examine the full soil-pile response during lateral loading.

   An elaborated description of the numerical models is given in chapter 5, where the constitutive models, parameter selection & calibration and model setups & geometries are discussed.

   The results of the 2D numerical modelling are used as prior information to the setup of the 3D model. The goal of the 2D horizontal model is to check typical strains around the monopile when a weak zone is present, this information is used for selection of the constitutive models in the 3D model. The 2D vertical model assesses the influence around the pile when a static vertical push is done, giving information on the size of the remoulded zone, which can also be used as input of the 3D model. The 3D numerical model calculates the lateral deflection at mudline for the monopile, this can be compared to the field tests done by Lovera to check if the effect of the crushed rock zone is correctly covered.
6. The results of all the three models are presented, showing the different sensitivity analysis that are done for the 2D and 3D models. Also the comparison of the 3D model to the OnPT data is presented.
7. The results and comparisons, as well as the validity of the model will be discussed in chapter 7.
8. Based on the literature found and the modelling results the research questions are answered and a conclusion is drawn of the effect of driven installation in weak rock. Finally the recommendations for future work are presented.

3

Background

3.1. Monopile Foundation

As mentioned in the introduction, a monopile is a foundation made up of one open-ended pile. Due to technological advances the size of OWT's have increased to impressive sizes in recent years, see Figure 3.2. The increase in size cuts the fabrication and installation costs per installed power output (Pisanò, 2019) and therefore makes developing windfarms with bigger OWT's of interest. With this surge in size of the OWT's, also the foundation size increases to be able to bear the structure. The geometry of a monopile makes that it cannot transfer moments and loads imposed on the foundation to axial loads along the piles, like a foundation with multiple piles can. The fact that a monopile has only one contact point with the ground leads to a laterally loaded structure, as shown in Figure 3.1. Due to the extensive lateral loading that happens on a monopile, the diameter is typically larger than that of piles in multiple piled foundations. Also the length-to-diameter (L/D) ratio is different because of the lateral load. Current designs for monopiles have diameters up to 11 meters and factories are being prepared to allow for construction of monopile with diameters up to even 15 meter in the future (Memija, 2023).

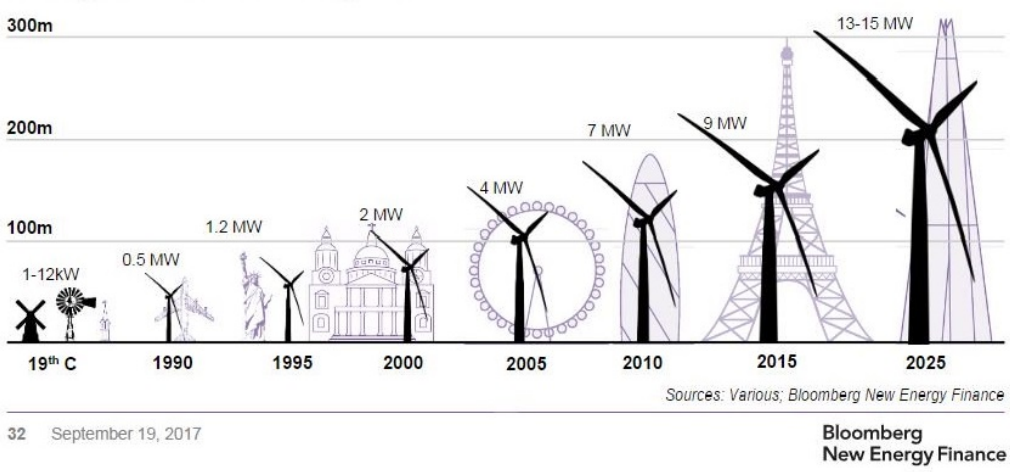

Figure 3.1: Evolution of wind turbine heights and output, from Bloomberg New Energy Finance's Future of Energy Summit, 2017.

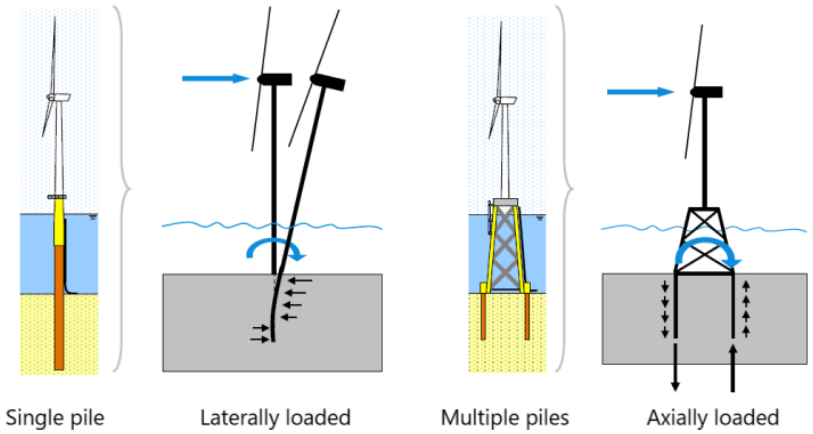

Figure 3.2: Loading of single pile foundation versus multiple pile foundation (Pisanò, 2021).

3.1.1. Wall Thickness

Since the monopiles are open-ended piles one of the dimensions of the structure is the thickness of the wall. In the investigation done is this report, the wall thickness is of importance as it is it used as a measure of the crushed zone that is formed around the foundation during installation. The thickness of the wall (t) compared to the diameter (D), or in other words the D/t ratio will influence the effect of installation as it is expected that a smaller wall thickness leads to a smaller crushed zone. Also the D/t ratio is expected to have an effect on the symmetry of the deformation around the pile wall. A large diameter with smaller wall thickness makes the shape more similar to a infinitely long wall, compared to a round pile shape. On top of that the plugging and induced radial stress at the pile tip is influenced by the D/t ratio (Lehane & Gavin, 1997, 2001). It has to be noted that the D/t ratio in the tests done by Lovera (2019) are lower than the typical D/t ratios used for monopiles. The D/t ratio used in the FEM models in this thesis is $1.2/0.035 = 34$, based on the OnPT that was done with smaller scale piles. For real scale, larger diameter, monopiles the D/t ratio can go up to 80, see Figure 3.3. A limiting factor to decreasing the wall thickness is the risk of buckling of the pile tip. Driving of the pile will cause high stress waves to move through the pile as it penetrates into the ground. When the pile wall is thin the risk of structural failure due to the resistance of the ground is bigger. Figure 3.4 shows piles that were extracted from the ground in the Rotterdam harbour and evidence of buckled pile toes. A widely used way to mitigate the risk of pile buckling is adding a driving shoe to the pile. A driving shoe is an increase in wall thickness for the lowest part of the pile, usually added at the inside of the open-ended pile.

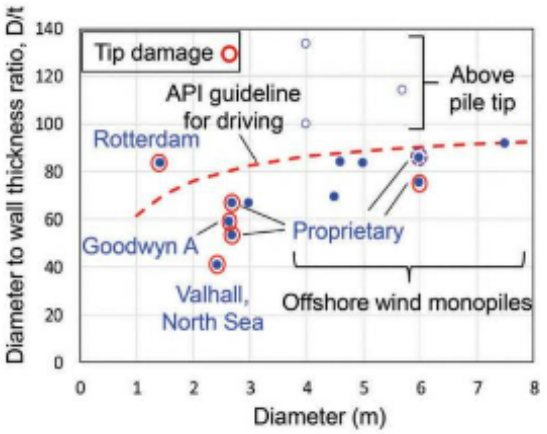

Figure 3.3: Trends for diameter and D/t in offshore wind industry and incidents of pile tip damage (Randolph, 2021).

Figure 3.4: Pile tip damage from Rotterdam harbour (Broos et al., 2017; Randolph, 2021).

3.1.2. Plugging

When the resistance due to the inner wall friction of an open-ended pile exceeds the base resistance of the soil, a plug starts forming inside the pile, see Figure 3.5. Based on industry practice plugging is not expected to happen in the large diameter monopiles. Also, jacked piles exhibit a greater tendency for plugging than impact driven piles (Fan et al., 2021). So although the plugging is happening in the jacking in this research, for driven piles it is not expected to happen. The 2D axisymmetric vertical models created in this thesis however have a tendency to show soil plugging when wishing in place the piles at deeper depths.

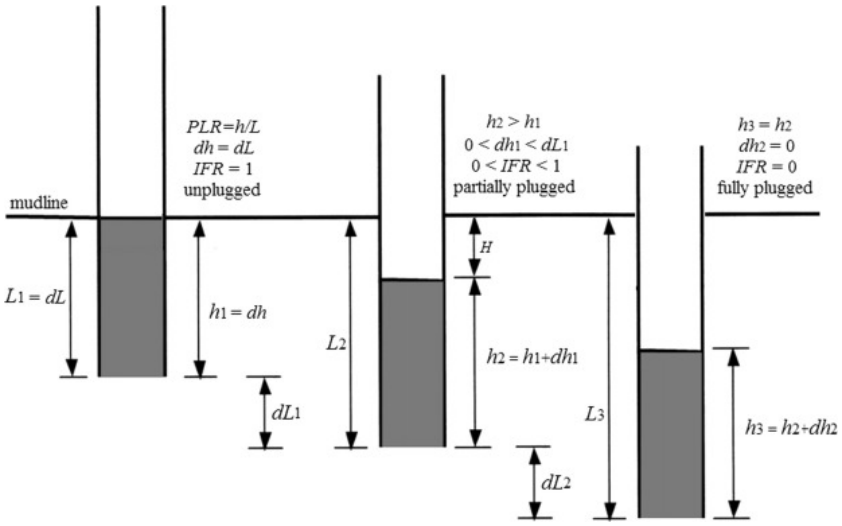

Figure 3.5: Mechanisms of soil plug formation op open-ended pile (Wang et al., 2020b).

3.2. Pile Installation

A monopile can be installed in different ways. The focus in this report is on the driven installation of a monopile as the effect of this installation method is assessed. Another way of installing a monopile, being drilling, is also discussed in this section.

3.2.1. Impact Driving

The process of driving a monopile into the ground is pretty straightforward when the vessel is positioned and the correct hydrohammer is present. The monopile is taken from the deck of an installation vessel, the hydrohammer is attached to the top. The monopile then is put op right and moved to the location where it should be installed. The procedure shown in Figure 3.6 is for a vibratory hammer, but for an impact hammer the sequence is exactly the same.

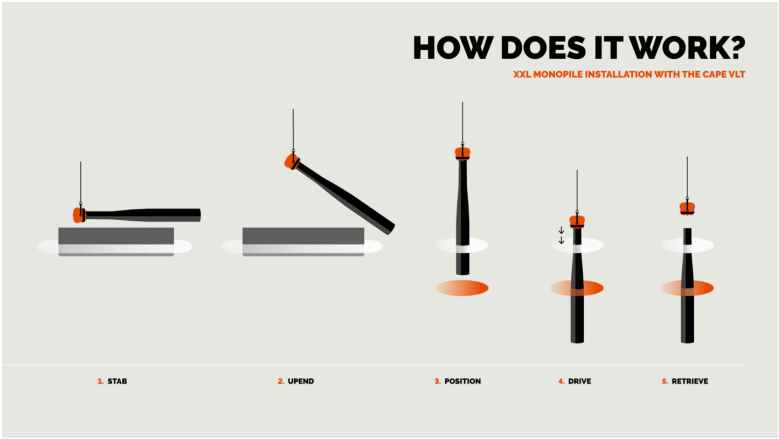

Figure 3.6: Graphic of the sequence of driving a pile into the ground, in this case a vibratory hammer by CAPE VLT.

3.2.2. Drilling

Using drilling for the installation of a monopile is a new technique. The first monopiles installed through drilling were installed in 2021 at the Saint-Nazaire wind farm of the coast of France. The sequence show in Figure 3.7 is similar to the one shown for impact driving, expect for the drill bit that is located inside the monopile. The graphic shows a drill-drive-drill sequence, but also drilling and then inserting the monopile is a possibility.

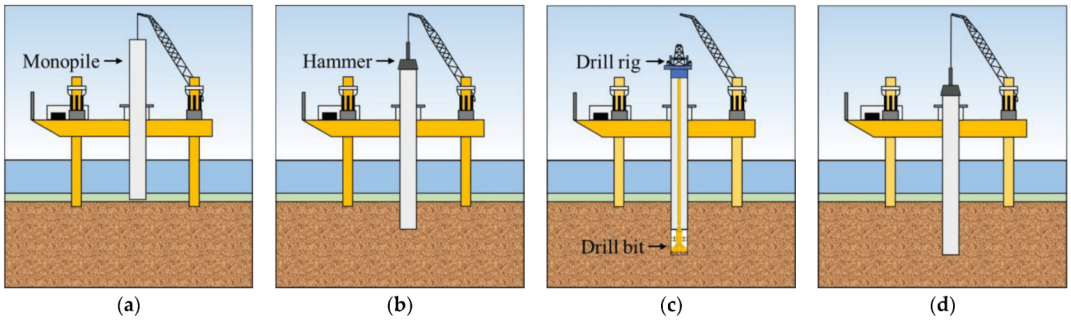

Figure 3.7: Graphic of the sequence of drilling a pile into the ground, using the monopile as a casing (Sun et al., 2023).

3.3. Lateral Loading

As mentioned before the monopile will be laterally loaded. The response of a pile can be rigid, semi-rigid, or flexible. The rigidity of the modelled piles is not extensively discussed in this report. However, to link pile deflection to rotation at mudline this has to be considered. Considering the low L/D value of the pile p5 ($3.2/1.2 = 2.67$) and the low D/t value (34) the pile is expected to act rigid. Especially for the beginning of the lateral loading, when the crushed rock has not become stiffer due to the stress increase, the pile will be rigid. The rigid deflection of a monopile is shown on the left in the schematic in Figure 3.8. Figure 3.9 shows the different ground components acting on a monopile and shows the rotation center of the monopile. The rotation center typically is $0.7 - 0.8 * L$ under mudline, for an L/D < 6 the rotation center moves towards 0.8 according to Wang et al. (2020a) and so that value will be used in this report.

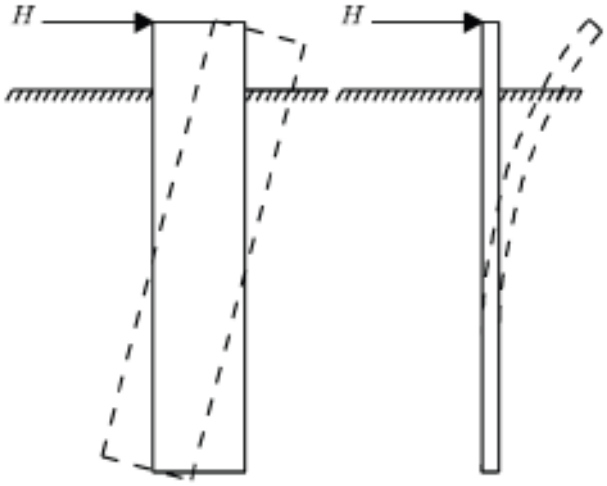

Figure 3.8: Difference between the rigid and the flexible pile behavior (Sørensen et al., 2012).

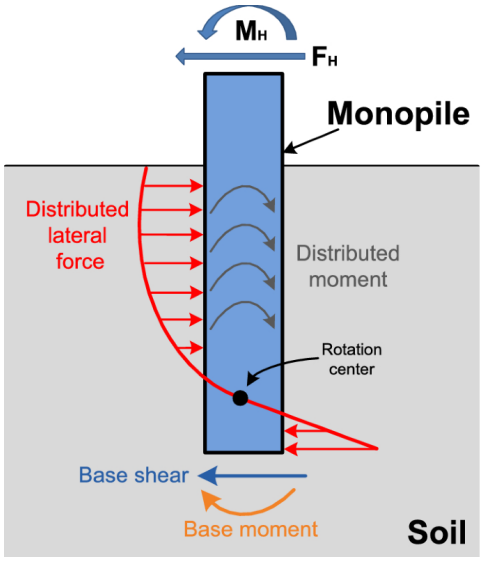

Figure 3.9: Components of ground reaction proposed by the PISA joint industry research project (Cao et al., 2023).

3.3.1. Typical Deflection

For the OWT to properly work, the permanent deformations around a monopile should not be too extensive. In order to meet the demands to have a functioning OWT, limits are set to the maximum deformations based on which a foundation design can be made. In the terms of lateral loading of the ground by a monopile foundation, the maximum deformations are expressed in deflection and rotation of the structure. First step in the design of a monopile is considering the ultimate limit state (ULS). For the ULS design extreme load cases are used, for example extreme winds or storm surges that occur once in a few years. The ULS design then leads to the minimal dimensions of the monopile required (Arany et al., 2017). In ULS designs deflections of up to 10% of the Diameter can still be allowed and if ULS failure occurs the whole structure collapses. To function, or for serviceability the limits set at the ULS are not enough. Therefore the serviceability limit state (SLS) is introduced. The SLS is a calculations of the stiffness of the foundation in the adjacent soil. The SLS sets a maximum to the allowed deflection and rotation at the mudline. The SLS value set for the maximum deflection at mudline is 0.03*Diameter and for the rotation of the monopile a maximum of 0.5^o is allowed (Gavin & Doherty, 2012; Jose & Mathai, 2016). Other design cases even state a maximum of 0.25^o of permanent rotation due to lateral loading (Charlton & Rouainia, 2022; Kaltekis et al., 2019).

3.4. Hoek&Brown Softening model

The Hoek&Brown Softening (HBS) model is a user-defined soil model that is created in PLAXIS. The HBS model is an implementation of the Hoek&Brown (HB) model but is further enhanced with the following constitutive features: (BENTLEY, 2019)

- The initial non-associativity with the ability the ability to simulate the non-linear evolution of the dilation in the post-peak regime,
- A softening rule implemented through two different implementations,
- A tension cut-off in the tensile regime of the stress space,
- A rate-dependent version of the HB model is here used to solve the mesh-dependency of the numerical solution when brittle failure is characterized by a strong concentration of strain in narrow shear bands.

Extra feature 1,3 and 4 are interesting for this investigation and a reason to use the HBS model instead of the HB model. The material sets created in this research were created as an HBS Strength Softening Model(SSM), which is one of the two softening rules that were implemented. This model also account for the non-linear dilatancy in its input, which was calibrated for the material set. Alejano et al. (n.d.) stated that a proper dilation angle for an average quality rock was 1/8 of the friction angle, based on which it is calibrated in the material sets.

The SSM model allows for the reduction of the m_b and s value as can be seen in Equation 3.1, where the softening rule is described mathematically.

$$\Gamma = \begin{bmatrix} m_b \\ s \end{bmatrix} = \begin{bmatrix} m_{b_o} - \left(\dfrac{m_{b_o} - m_{b_r}}{B_m + \varepsilon^p_{eq}} \right) \varepsilon^p_{eq} \\ s_o - \left(\dfrac{s_o - s_r}{B_s + \varepsilon^p_{eq}} \right) \varepsilon^p_{eq} \end{bmatrix} \tag{3.1}$$

Where B_{mb} and B_s are parameters governing the softening process and ϵ^p_{eq} is the equivalent strain or in other words cumulated value of deviatoric plastic strain.

m_b represents the reduced value of the intact rock parameter mi as defined in the Hoek&Brown model as:

$$m_b = m_i \exp\left(\frac{GSI - 100}{28 - 14D}\right) \tag{3.2}$$

with GSI being Geological Strength Factor and D the Disturbance Factor.

s is an auxiliary material constant for a rock mass:

$$s = \exp\left(\frac{GSI - 100}{9 - 3D}\right) \tag{3.3}$$

with GSI being Geological Strength Factor and D the Disturbance Factor. In Equation 3.1 m_b and s are described in their initial quantity m_{b0} and s_0 and their residual quantity m_{br} and s_r.

The introduction of the fluidity parameter (γ) allows for rate-dependant response in the HBS model. For inputs of $\gamma =< 0$ the model acts rate independent, so elasto-plastic. For inputs of $\gamma > 0$ the rate dependency is introduced and the model is visco-plastic. For the purpose of the viscous regularizing technique, the fluidity should be calibrated for an individual problem. Where for other engineering purposes the rate-effect could be of importance, in the context of the HBS model the rate dependency only has the goal to regularize strain localization.

4

Literature Review

A literature review is done to check the knowledge that is available on soil-structure interaction during pile penetration and underpin findings that are done in the modelling of this thesis. As starting point, (section 2.1) the thickness of the crushed rock annulus around the pile is based on observations at ground level and extruded into the ground with the same thickness. Extending this zone linearly is a simplified assumption that deserves a more thorough look in to. To get a better idea of the shape of the crushing, it is important to understand what happens under the pile tip during penetration. In order to understand this, areas of interest to review are: crushing mechanisms of rock, bearing mechanisms under piles, available modelling of pile penetration, testing on pile penetration and lateral pile load testing in varying ground conditions.

4.1. Crushing Mechanisms of Rock

A number of properties could affect the crushing behaviour of rock, such as strength, density, grain size/shape, mineral content, particle size and particle shape (Huang, 2016). The tensile strength of rock is typically weaker than the compressive strength of rock (Dai, 2002), the crushing behaviour of rock therefore is governed by cracks that are occur because of tensile loading. Boussinesq (1885) was the first to describe the stress field distribution under a point load. When rock is hit by a body, like a pile, a similar stress pattern starts. As the rock is intended by the body, tensile stress will start to develop at the edges of the pile (Nariseti, 2013). So although pile driving is a mainly compressive phenomena, as the pile is pushed into the ground, the crushing will be due to areas of high tension and shear stresses that develop. The simplified vertical push models also showed that the plastic zone was in accordance with areas of high shear stresses. Lindqvist et al. (1994) executed tests where rock samples were indented with impact loads which clearly visualises the multiple crushing and cracking mechanisms that occur, it shows a crushed zone that appears under the impacting body. In the OnPT test of Lovera (2019) also a crushed zone and cracks outside this zone were seen. The crushed zone was deduced to have much more impact than the cracks around it.

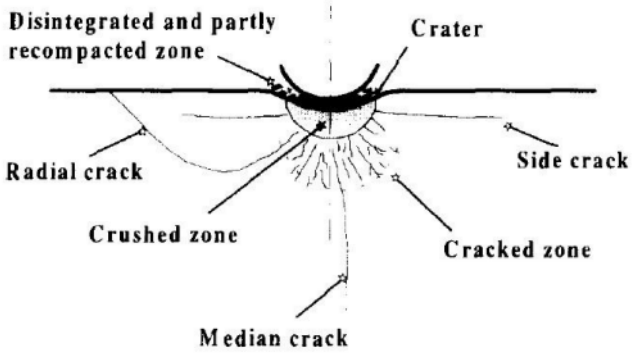

Figure 4.1: Schematic of resulting cracked zones under impact loading. (Lindqvist et al., 1994)

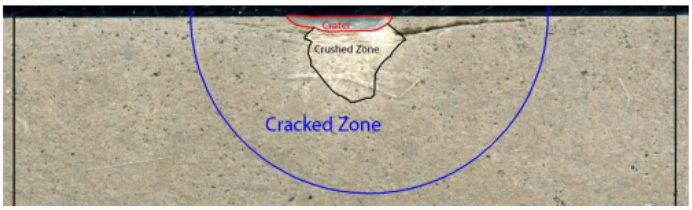

Figure 4.2: Picture of resulting cracked zones under impact loading. (Lindqvist et al., 1994)

4.2. Rock Behaviour under Compressive Loading

Figure 4.3 and Figure 4.4 show deformation curves for different rock masses. Figure 4.3 shows the results for different confining stresses. The graphs show that for multiple different rocks the response to normal loading gets stiffer as the deformation grows, especially when joints are present. The stiffening is also explained by the contact points between the two sides of a rock joint getting bigger as a joint is getting under bigger stress ((Hobbs, 1966)). The test shown in Figure 4.3

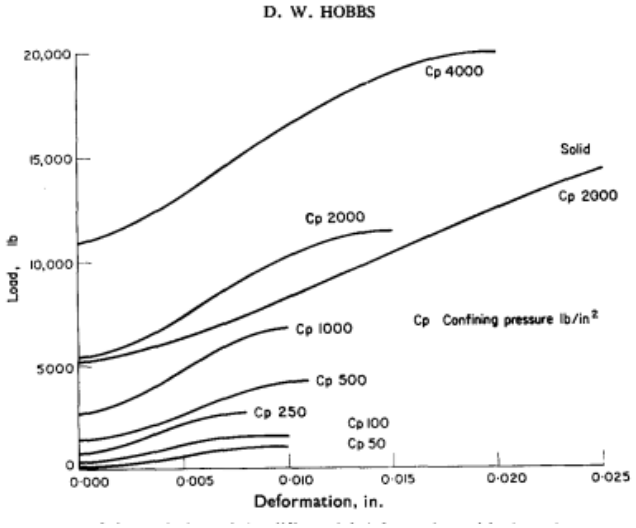

Figure 4.3: Load-deformation curve showing a overview of multiple different rock masses that were tested for different confining pressures by Hobbs (1966).

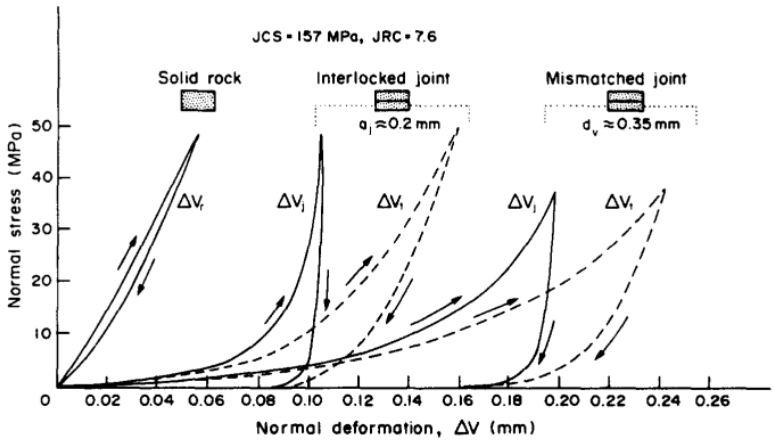

Figure 4.4: Stress-deformation curve showing the typcal shape for intact and jointed rocks. (Kulatilake et al., 2016).

4.3. Bearing Mechanisms under pile tips

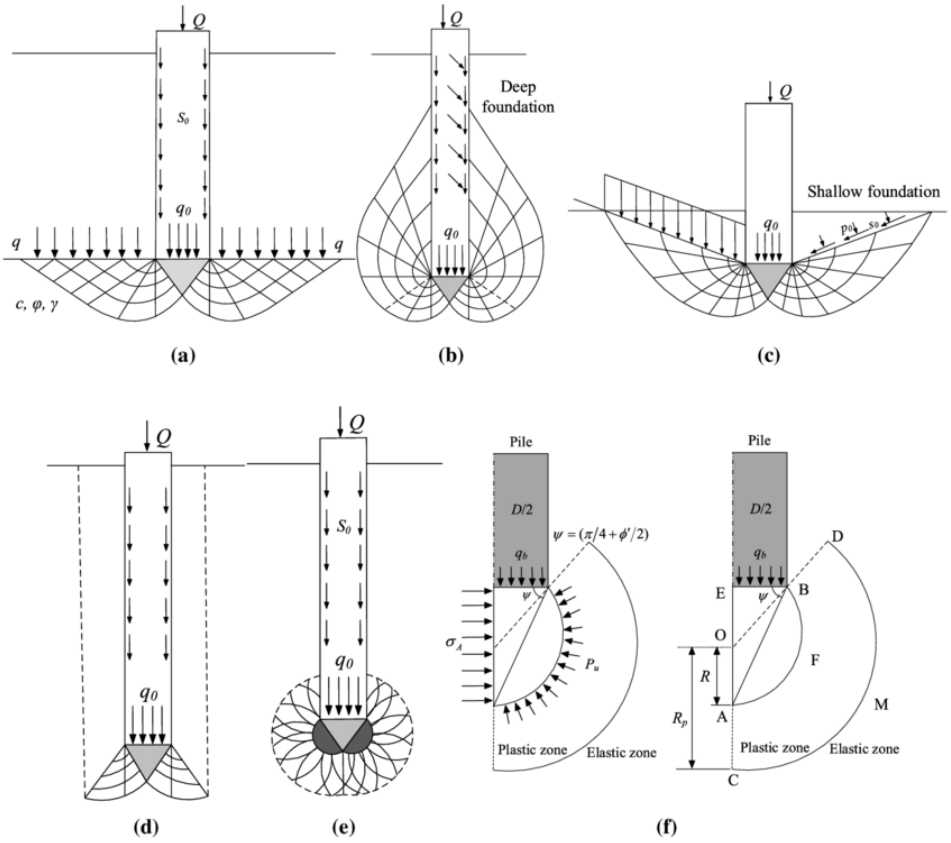

Figure 4.5: Different failure patterns around the pile tip assumed by different researchers: (a) Prandtl (1920), Reissner (1924) and Terzaghi (1943); (b) deep and (c) shallow foundations for sand and rock of de Beer (1945), Jaky (1948), Meyerhof (1951) and Serrano and Olalla (2002); (d) Berezantzev and Yaroshenko (1962) and Vesic (1963); (e) Bishop et al. (1945), Skempton et al. (1953) and Gibson (1950); and (f) Vesic (1972)

Xu et al. (2020) created an overview of failure patterns at the tip of foundation structures as assumed by different researchers. At (f) the pattern by Vesić (1972) is shown. The cavity expansion theory presented was originally proposed for sand conditions. Also, the cavity expansion theory is proposed for end bearing, which is a different situation than the dynamic loading during pile driving. The results of the experiment done by Xu et al. (2020) support the applicability of the spherical cavity expansion theory for for calculating the end-bearing capacity of piles socketed in weak rock and show that for weak rock the compression zone is consistent with the spherical failure pattern. Gharsallaoui et al. (2020) concluded that the cavity expansion theory for end bearing in rock mass is in good agreement with test results as well. It has to be noted that the experiment and theory by Vesić (1972) are based on a closed ended pile. A simple formula (4.1) to calculate the radius of the plastic zone under the pile tip is suggested by Yang (2006). Figure 4.6 graphically shows the calculated radius, R_u of the plastic zone.

$$R_u = \frac{D}{2cos\phi'_{cv}} \tag{4.1}$$

When calculations are done with different values for ϕ'_{cv} (30^o-40^o) it can be seen that the radius of the plastic zone outside the pile will be 7-14% of the pile diameter (D). That would be more than one times the wall thickness for the geometries of the pile by Lovera.

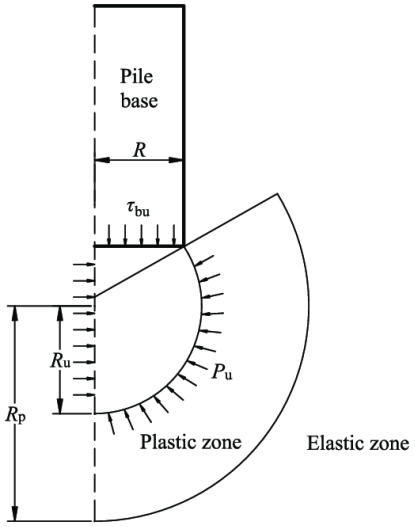

Figure 4.6: Cavity expansion under a pile tip. (Zhang et al., 2019)

4.4. Modelling of pile penetration

Modelling of end bearing of open-ended piles in rock was done by Jafari et al. (2019). Findings in terms of failure mechanisms at big depth were in accordance with the pattern shown at (b) in Figure 4.5. The model was made using Hoek&Brown and the conclusion was drawn that an elastic perfectly plastic model with HB failure criterion with the adapted modelling flow, results in an acceptable approximation of the bearing capacity of the pipe pile. The plastic zone under the pile was compared to the cavity expansion theory by Hamdi (2016) in the modelling done, and showed similarities.

When considering modelling of pile penetration it has to be noted that driving a pile into the ground is a dynamic process where stress waves travel up and down the pile after being impacted by the hammer. The stress waves will cause movement in radial, axial and torsional direction as the impacts that cause the stress wave are not perfectly aligned. The soil-pile interaction can cause damping of the stress waves before they reach the pile tip and wave dispersion also happens due to high frequency motions (Tsetas et al., 2021). Fan et al. (2021) performed centrifuge testing and numerical simulations of pile installation in sand. In this simulation they compared the results of jacking a pile versus driving a pile in terms of resulting void ratio and horizontal stress after installation. This is of interest as it gives an insight in the difference in soil response to these penetration methods. Since a vertical push is performed in this report, which can be compared to jacking of a pile, this then can be related to the difference in behaviour compared to driving. Also it gives insight to compare other literature sources that simulate a rigid body penetrating into rock.

The conclusions that Fan et al. (2021) drew were that the effect of the pile installation process on the surrounding soil can be substantial. The post-installation results for the jacked and impact driven pile were different in terms of both void ratio and stresses. The dynamic impact driving process leads to an area of densification much greater than that resulting from jacking in both the radial and vertical directions. The degree of densification due to impact driving is also much greater than following jacking. On the other hand the degree of the increase in the horizontal stress in jacked piles is significantly higher than in impact driven piles. see Figure 4.7. A study done by Jorna (2018) investigated pile tip deformation due to boulders that are encountered during monopile driving. The study also included dynamic and static loading cases and showed that for the static case all loading done on top of the pile is transferred to the boulder when crashing into it, while in the dynamic case this did not happen. It indicates that pushing of a static rigid body overestimates the load transfer to the pile tip compared to the real dynamic pile driving mechanism.

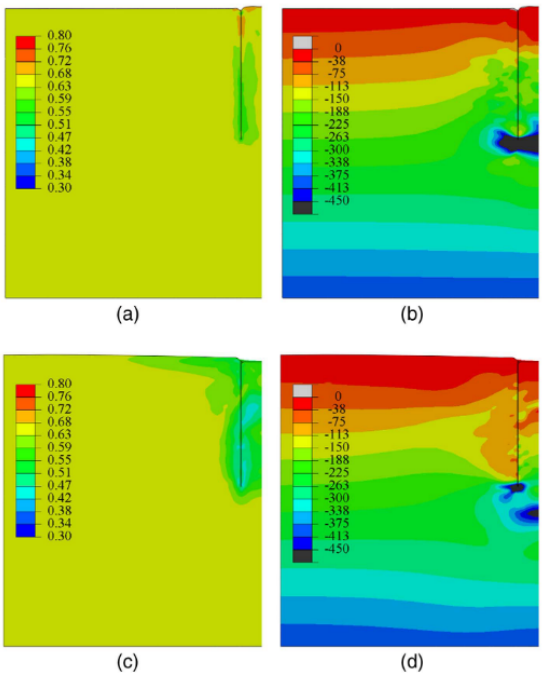

Figure 4.7: Numerical simulation results of open-ended pile penetration into sand by Fan et al. (2021). The figure shows post installation void ratio (a) and horizontal stress (b) after jacking of the pile and void ratio (c) and horizontal stress (d) after driving of the pile.

Zhang and Fatahi (2021) performed pile penetration in large-displacement software that made use of the discrete element method. The model includes a pile that is pressed into the ground as a rigid body. Although it has to be noted and is understood that this does not describe the dynamic process of driving a pile into the ground, it is still deemed a good indication for this study of the crushing of material happening around a pile wall when penetrating the ground. The results in Figure 4.8 show an unbonded zone around the pile wall of in the range of twice the wall thickness. When taking into account the findings of Fan et al. (2021) it can be said that the stresses under the pile are big in the jacking process that happens in the model of Zhang and Fatahi (2021), causing the unbonding of the elements. For a dynamic driving process the unbonding is expected to be be more severe in the closes vicinity of the pile but propagating less far outside the pile.

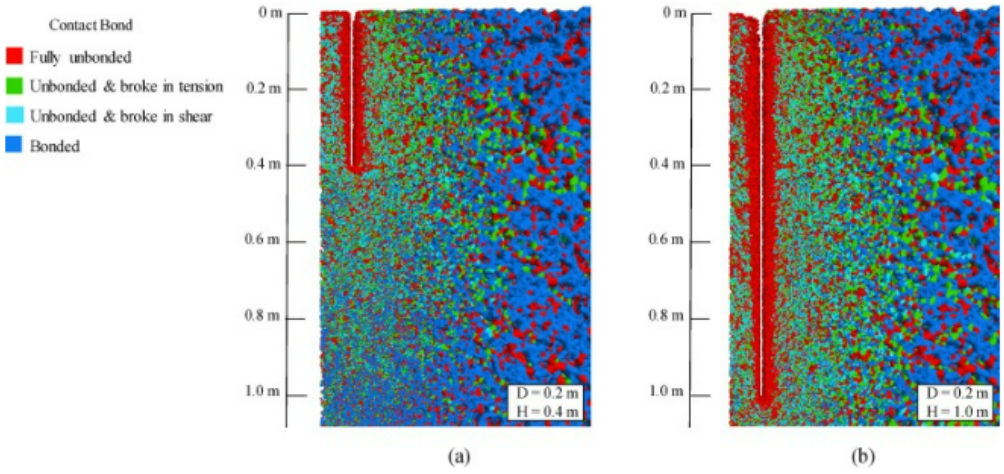

Figure 4.8: DEM model of penetration of an open ended pile, performed in weak rock (Zhang & Fatahi, 2021).

4.5. Testing of pile driving in weak rock

A test for open and closed ended piles was done by Alvarez-Borges et al. (2020). The test was performed on laboratory scale, in calcareous soft rock. The paper describes the crushed zone that is shaped around the piles. The zone is four times as big for the closed ended pile, but for the open-ended pile the relation of one times the wall thickness is presented again. Testing of open-ended piles penetrating into rock by Jafari et al. (2019) showed that the rock inside the pile is completely crushed. For piles with a D/t ratio up to 38 this is found to be true. This is D/t ratio that is in the range of the D/t ratio of the pile in this report. For bigger D/t ratios, which are common for large diameter piles, the complete crushing is not expected to happen, the effect of this can be a topic for future research.

4.6. Remoulded zone around piles in different ground conditions

For driving in weak rock Terente et al. (2015) indicates an annulus of weak rock around the pile, just like is seen at Lovera (2019). van Wijk (2022) addresses the weak zone to be one times the wall thickness for weak rock. Tomlinson and Woodward (2014) recommend to make use of driven methods for soils when calculating shaft frictions, because of the disintegration of the material around the pile. A experiment was done by Zhang et al. (2022) where an open ended pile was driven into weak rock and did penetrometer testing on the rock around the pile afterwards. The test was done on laboratory scale. The article shows a fitting curve of the reduced strength ratio outside the pile, the curves can be seen in Figure 4.9. It can be seen that the experiment results suggest the strength reduction of the rock due to the driving lasts two diamaters into the rock.

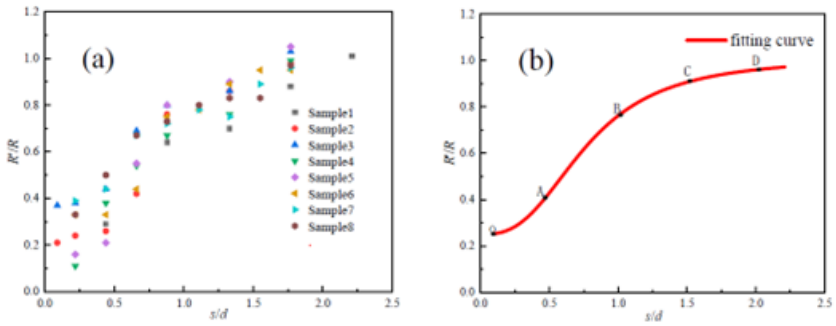

Figure 4.9: On the left, a graph showing the penetrometer tests done around a test pile. On the left the fitting curve of the reduced strength. (Zhang et al., 2022)

For brittle chalk, which differs in behaviour from the weak rock, an open ended pile driving experiment was done by Pedone et al. (2023). Chalk remoulds into a weak zone around the pile as well. The experiment yielded three zones to consider around the pile, a remoulded, a cracked and an intact part, a geometry of disintegration that is probable for weak rock as well.

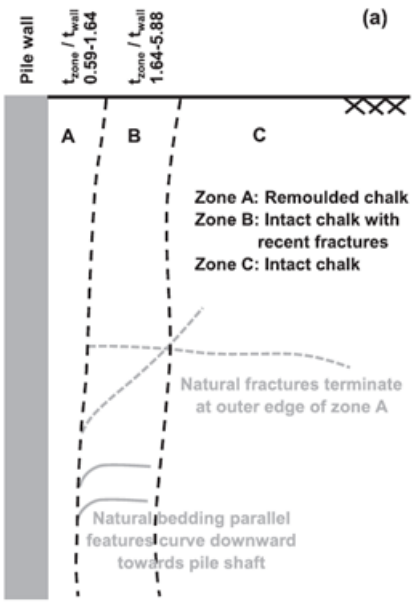

Figure 4.10: Geometry that is used in the experiment done by Pedone et al. (2023), showing the remoulded and fractured zones that are considered

4.7. Cyclic Behaviour for Lateral Loading

The graphs shown in this section are load-displacement curves for cyclic loading in sand, Figure 4.11 and Figure 4.12, and the cyclic results presented in the dissertation of Lovera, Figure 4.13 and Figure 4.14. Although cyclic loading is out of the scope of this thesis and not performed in the modelling, it can be used for explaination of the results. It can be seen that for sand conditions the cyclic loading repetition has a convex down shape for the loading part of the curve. The Lovera one however shows a convex down shape both for the loading and unloading part of the curve. So although the primary loading curve shows a different shape, the convex up shape found in the cyclic loading gives information that this behaviour is not uncommon for weak rock. The same shape was mentioned by Kementzetzidis et al. (2023) for cyclic lateral loading in soil and related to gapping or a zone of weaker material around the pile, which is the case for the situation in weak rock as well.

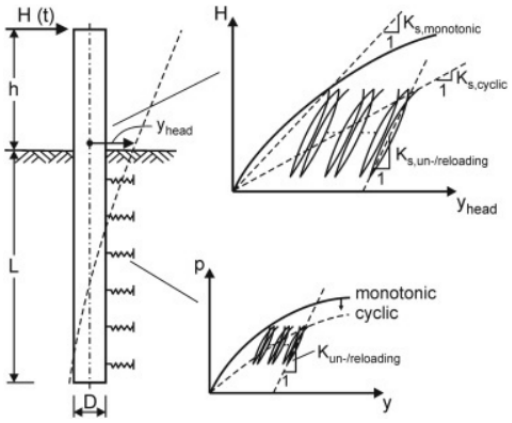

Figure 4.11: First example of typical cyclic loading curve in sand conditions. (Achmus et al., 2019).

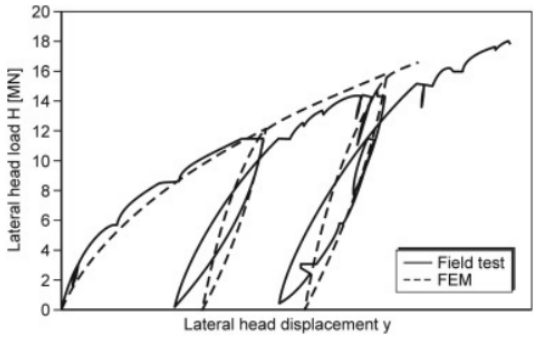

Figure 4.12: Second example of typical cyclic loading curve in sand conditions. (Achmus et al., 2019).

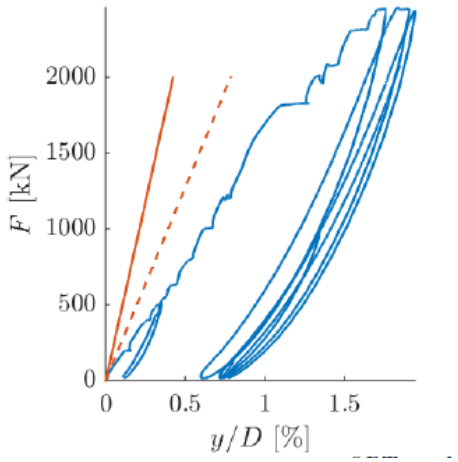

Figure 4.13: Load-displacement curve of pile p5 in the dissertation of Lovera (2019).

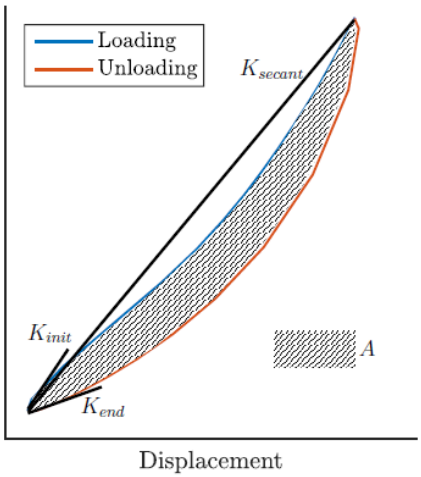

Definition of the secant stiffness (K_{secant}), the tangent initial stiffness (K_{init}), the final initial stiffness (K_{end}) and the area of the loading-unloading loop (A)

Figure 4.14: Area of unloading-reloading for the cyclic test resuts in weak rock (Lovera, 2019).

4.8. Conclusion

Summarizing the literature review, it can be said that no fixed conclusions is be made on the thickness of the crushed zone annulus around a pile for weak rock. Multiple sources indicate and discuss the presence of a crushed zone. Literature on crushing of rock and the penetration of a pile into rock also indicate that disturbance will happen around the pile. Quantifying the size however is hard, because of differing material or geometries in the executed models or tests that were looked at. Some sources are about close-ended piles for example, which will yield very different results from the open ended piles with a wall thickness-diameter ratio as small as that of a monopile. Through the findings of Alvarez-Borges et al. (2020) this can be correlated. Secondly the results differ from one wall thickness, to six wall thicknesses to two diameters, which is a wide range. A crushed zone of one wall thickness being observed multiple times. Also the amount of strength reduction in the rock is not know, and will be different for different materials, The 2D vertical numerical model will be run to see if a static vertical push and the resulting plastic zone matches results seen in literature. The 2D vertical model is not able to model the complete driving process though, and so will also only be a limited approximation. An explanation for the convex up shape of the load displacement curve is also given.

5

Numerical Modelling

In this research numerical modelling is used to examine the lateral pile response of the monopile. The calculations were done in PLAXIS 2D and PLAXIS 3D, commercial modelling software based on the finite element method (FEM) in 2D and 3D respectively. This chapter will describe the numerical models that were used and elaborate on parameter selection, model geometry and other relevant model details.

5.1. Constitutive Models

When using a Finite Element Method for numerical analysis, different constitutive models can be used. A constitutive model is a way to mathematically describe the material mechanical behaviour under various loading conditions. Since PLAXIS was used for the calculations, the choice of constitutive model was constrained by the options available in the software.

The materials to be modelled in this thesis are weak rock and after crushing, cohesion-less soil. That taken into account it was decided to take into consideration five constitutive models and compare them to see which ones were most suitable for the investigation. The five model taken into consideration are: Mohr-Coulomb (MC), Hoek&Brown (HB), Hoek&Brown with Softening (HBS), Hardening Soil (HS) and Hardening Soil with smalll-strain stiffness (HSsmall). The models are compared in Table 5.1. As mentioned in section 2.3 three different FE models are run to investigate the problem.

- 2D plain-strain horizontal model to examine typical strain around a lateral moving monopile,
- 2D axisymmetic and plain-strain vertical model to examine rock weakening around pile tip during driving process,
- 3D model to examine the lateral stiffness of the monopile.

For the different FE models, different features of the constitutive models are important. Therefore a choice of constitutive model was made separately for each FE model in order to fit the goal of the analysis. In general three constitutive models were used for two different materials, let alone parameters that were varied for sensitivity checks. The two materials are, again, intact weak rock and the crushed weak rock. The constitutive models picked were, Mohr-Coulomb and Hoek&Brown Softening for intact rock and Mohr-Coulomb and HSsmall for the crushed rock.

For the intact weak rock the Hoek&Brown softening model was used. The Hoek&Brown model is originally developed for rock masses(Hoek & Brown, 1997), and the most widely used constitutive model for rock materials (Hoek et al., 2002). The input parameters for this are also typical properties for rock and therefore convenient to describe the rock. The softening model addition was specifically chosen since the pile driving will induce crushing. The crushing makes that softening behaviour is of interest in the model. The Mohr-Coulomb model was selected as second option for the intact rock because for lateral loading the zone outside the crushed rock annulus is expected not to show big deformations and stay in the zone of elastic strains. Therefore a simple first order model that Mohr-Coulomb is will suffice, on top of that the simplicity will benefit the models running time. Finally, the Mohr-Coulomb

material model is needed to benchmark against available results.

The crushed rock can be treated as a cohesion-less material (Stevens et al., 1982),(Irvine et al., 2015),(Lovera, 2019) and the movement the pile is heavily influenced by small strains and the degradation of the stiffness of this zone which is located directly around the pile. Also, a second order approach that is stress dependant is desirable for an accurate ground model. Therefore this material is primarily assigned the HSsmall model. However, to compare results to available data and benchmark the results, also a material model is created in Mohr-Coulomb for the crushed rock.

A detailed description on the used configuration of constitutive models within the FE model geometries will be given in the Model Geometry subsections. Also, the reason for the choice per model will be elaborated.

Table 5.1: Constitutive models comparison.

Constitutive model	Pro	Con
Mohr-Coulomb	- Simple, easy to use -> first order approach of ground behaviour	Linear elastic -> no strain or stress dependant behaviour: - No stiffness degradation - No small strain stiffness - No softening
Hoek&Brown	- Created to describe the behaviour of rock - Includes parameters that are applicable for defining weathered rock - Non-linear failure envelope for small confining stress	- Linear elastic -> no strain or stress dependant behaviour: - No stiffness degradation - No small strain stiffness - No softening
Hoek&Brown with Softening - SSM (Strength Softening Model)	- Created to describe the behaviour of rock - Includes parameters that are applicable for defining weathered rock - Non-linear failure envelope for small confining stress - Includes softening	- No stiffness degradation - No small strain stiffness - Residual strength parameters arbitrary to fill in
Hardening Soil	- Second order approach of ground behaviour - Stress dependant behaviour	- No small strain stiffness - No softening
Hardening Soil with small - strain stiffness	- Second order approach of ground behaviour - Stress dependant behaviour - Small strain stiffness degradation	- No softening

5.2. Parameter selection and calibration

The constitutive models need input parameters. This section will describe and explain the chosen values for the parameters. Parameters were selected based on different sources. Since the goal is to compare results to OnPT done by Lovera (2019), parameter values were taken from her thesis or calibrated using laboratory test result in the thesis. Later on for comparison also parameters were taken from other literature sources or based on typical values for certain ground types, like a typical material set for a dense cohesionless material.

5.2.1. Available data

Available parameter in thesis for intact weak rock are shown in Table 5.2

Table 5.2: Intact rock parameters. (Lovera, 2019)

Parameter	Value
E (MPa)	5000
ν	0.3
c'ref (MPa)	1.66
ϕ' (°)	32
Tension cut-off (MPa)	1.57

Apart from the available parameters, also uniaxial and triaxial test results for the intact rock and an oedometertest result the crushed rock are given. Using the SoilTest facility of PLAXIS the material models are calibrated against the triaxial and uniaxial test for the intact rock.

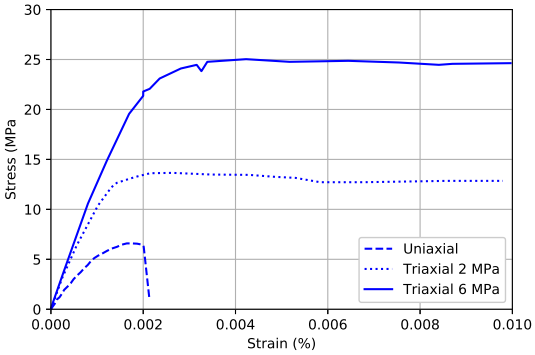

Figure 5.1: Results of the uniaxial and triaxial tests done on the intact weak rock material in dissertation of Lovera (2019).

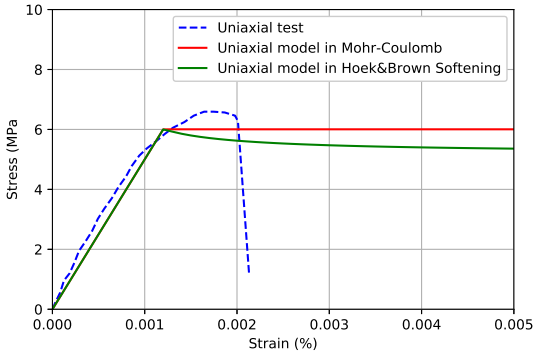

Figure 5.2: Uniaxial test results compared to results of a uniaxial test run in the SoilTest Facility.

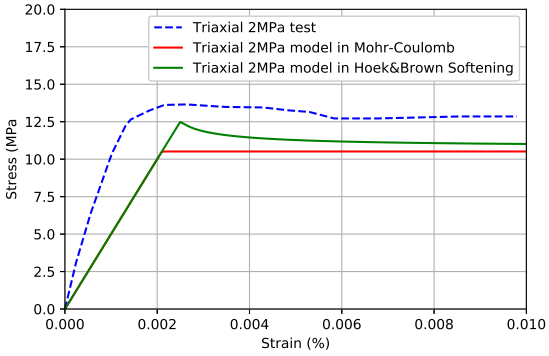

Figure 5.3: Triaxial test for a confining pressure of 2 MPa results compared to results of a triaxial test run in the SoilTest Facility.

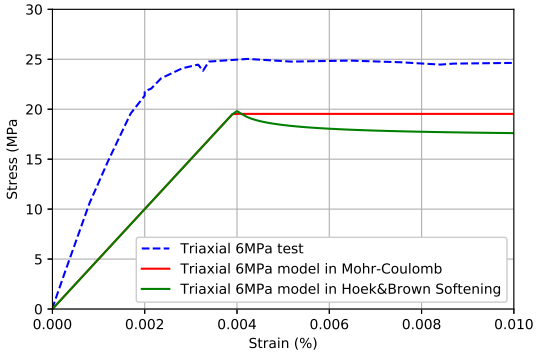

Figure 5.4: Triaxial test for a confining pressure of 6 MPa results compared to results of a triaxial test run in the SoilTest Facility.

Figure 5.1 to Figure 5.4 show the test data and fitting that is done to create material sets of parameters for the intact rock in PLAXIS for both Mohr-Coulomb and Hoek&Brown Softening. It can be seen that for the uniaxial test the stiffness in the elastic region is similar to the test data. For the triaxial tests however, the models predict a softer response than the actual test data. This is because the Mohr-Coulomb and Hoek&Brown Softening do not include stress-dependent stiffness. To be conservative and because the stress levels in the ground up to a depth of 10 meters do not come close to 2 or even 6 MPa, the value for stiffness is still taken as 5 GPa. An overview of the adopted parameters in the material sets can be found in Appendix A. The poisson's ratio ν was chosen based on the dissertation of Lovera. Disturbance Factor (D) was chosen to be 0 and the Geological Strength Index (GSI) was chosen to be 100, since the material before crushing was an undisturbed, intact rock. The value of 10 for m_i is typical for a limestone. $m_{\psi i}$ was chosen based on the relation stated in Alejano et al. (n.d.) which says the Hoek & Brown (1997) proposal of ϕ = $\psi/4$, ϕ = $\psi/8$ and ϕ = 0 for good, average and bad quality rock masses is starting to be widely used. The residual dilatancy parameter, being $m_{\psi res}$ was chosen 0 to make sure the dilatancy of the rock material drops to zero for big stresses. Parameters for residual strength, m_{res} and s_{res} are based on m and s being 10 and 1 respectively considering the chosen D and GSI. The residual strength values were varied in the different models. The uniaxial compressive strength (σ_{ci}) of the weak rock material was given in the dissertation of Lovera and is 6 MPa. The parameter governing the softening process ($B_m b$, B_s and B_ψ) are based on the information in the user manual (BENTLEY, 2019).

To calibrate the models for the crushed rock the oedometer test result was used, since this oedometer test was done on crushed material retrieved from the OnPT site. Available parameter in thesis for crushed rock are shown in Table 5.3

Table 5.3: Crushed rock parameters. (Lovera, 2019)

Parameter	Value
E (MPa)	60
ν	0.3
c'ref (MPa)	0
ϕ' (°)	32

Again using the SoilTest facility, material models are fitted over the test data to create sets of parameters that fit the ground behaviour.

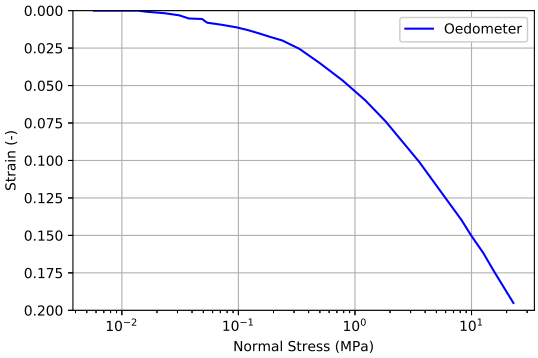

Figure 5.5: Results of the oedometer test done on the crushed weak rock material in dissertation of Lovera (2019).

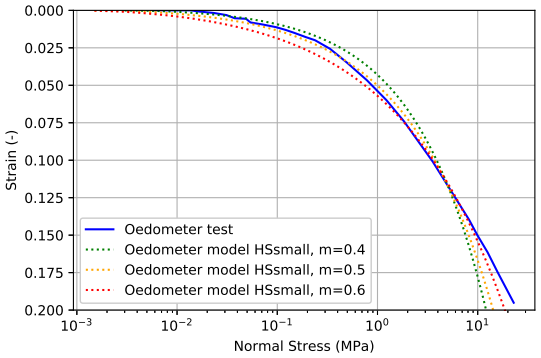

Figure 5.6: Oedometer test results compared to results of oedometer test run in the SoilTest Facility. This figure shows multiple runs done for different parameter sets, which views the process to adopt the correct parameter values.

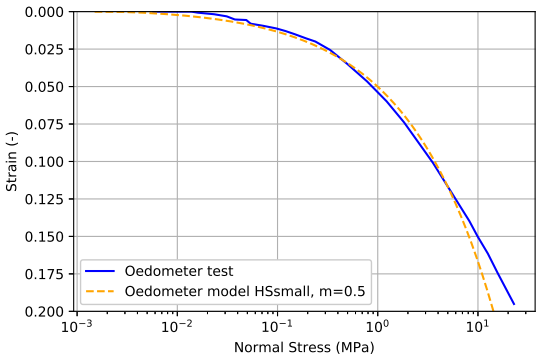

Figure 5.7: Oedometer test results compared to results of oedometer test run in the SoilTest Facility. This figure shows the adopted parameter set with m=0.5 .

For the crushed rock, the values by Lovera are taken to create the Mohr-Coulomb parameter set. These values include a Young's Modulus (E) of 60 MPa, poisson's ratio (ν) of 0.3, friction angle (ϕ') of 32° and cohesion of 0, like shown in Table 5.3. The values show that Lovera retrieved a stiffness for the crushed material of approximately a hundred times smaller than that of the intact rock. For the HSsmall material sets more parameters should be adopted. In the SoilTest Facility the stiffnesses (E_{50}^{ref}, E_{oed}^{ref}, E_{ur}^{ref}), power function (m) and Small-strain stiffness (G_0^{ref}) are varied to match the test data. The reference stress for the power function, p_{ref} was kept constant at 100 kN/m^2. For a detailed formulation of the constitutive models and parameter description please refer to manual of PLAXIS, (BENTLEY, 2022) . As can be seen in Figure 5.7 a value of 0.5 was adopted for m. The line matches the oedometer test best if you take into account that the zone of lower stress levels is of most interest. Also, this value was taken as it is a typical value for m for cohesion-less soils. The lower stress levels are important to match because this influences the initial response of the pile. The cohesion and friction angle values for the crushed rock in Table 5.3 were taken from the dissertation of Lovera (2019). The material set that resulted from the calibration is material set C1, see Appendix A.

5.3. 2D horizontal model

This model is created in order to check the typical strains that happen around a monopile when it is deflecting in lateral direction. The model is not used to calculate a soil-pile response but is meant as an aid for the constitutive model selection. If the model shows most strains occur within close vicinity to the pile for example that can lead to the choice of a simpler model further away from the pile. Since the area further away consists of intact rock that would be convenient. In that way it is not needed to calibrate the HSsmall model for the intact rock, furthermore it is questionable of the HSsmall model is

applicable for rock at all. Also in terms of computing time a simpler model could save time. Further on in this research a full 3D FEM model will be executed for the full soil-pile response.

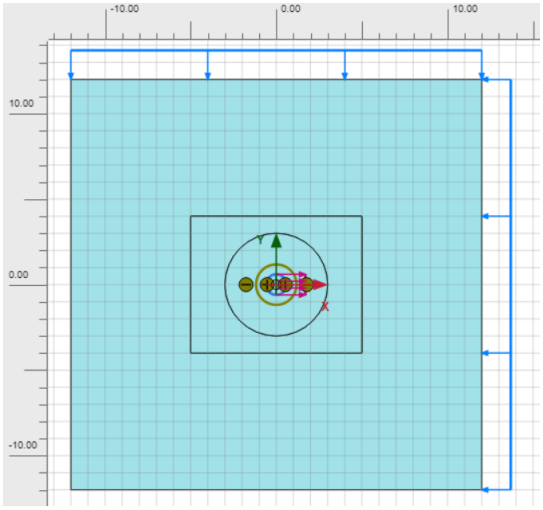

Figure 5.8: Horizontal FEM model setup in 2D. The line loads that create the correct stresses can be seen in blue.

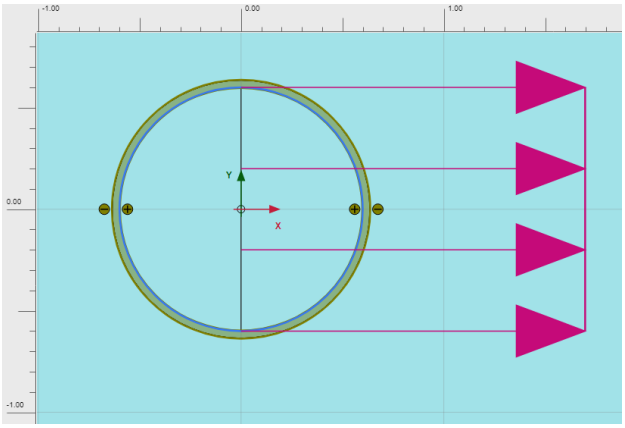

Figure 5.9: Zoomed in cross-section of the tunnel element that is set up as a plate to act as the monopile wall.

5.3.1. Setup

The model is set up as a horizontal slice through the monopile and soil at a depth of 0.5m below the surface. Since PLAXIS 2D is essentially made for vertical cross sections a work around was needed to get to the right stress conditions for the problem. The approach that was taken was creating a model with calculation type: Gravity Loading. Then the materials were assigned a unit weight of zero and line loads were added to the model in the way that is depicted in Figure 5.8. Using a material with Poisson's ratio = 0.499 and line loads in x- and y- direction of 10 kN/m^2 the effective stress in z- direction σ'_{zz} = 10 kN/m^2 was created in the initial phase. Secondly a material with Poisson's ratio = 0 was chosen to make sure the stress in z- direction was not affected, in this step the x- and y line loads then were reduced to 5 kN/m^2. This finally led to a model with $\sigma'_{xx}, \sigma'_{yy}$ = 5 kN/m^2 and σ'_{zz} = 10 kN/m^2 which are the correct stresses for a depth of 0.5 m in $z-direction$ for ground material with a unit weight of 20 kN/m^3. The water level was put under the lower boundary of the model. Adding a water table would create a differential water stress increasing from the top downwards in y-direction as PLAXIS would treat this as a vertical water table. Since this is not wanted in this model the water table is under the model, making all total stress also effective stresses.
In the model a tunnel element with the diameter of the monopile (D = 1.2 m) was added to create the circle geometry of the pile wall, see Figure 5.9. A plate was then created on this circle and a material set for steel assigned to this plate, parameter presented in Table 5.4. The pile is then pushed to the side by a prescribed displacement of 0.012m, that acts on the centre line of the tunnel element. Since the tunnel element is much stiffer than the ground and shows minimal deformation this prescribed displacement functions the way it is intended to.

Table 5.4: Steel plate parameters for the 2D horizontal model.

Parameter	Value
EA (kN/m)	60 *10^6
EI (kN m^2/m)	60 *10^3
ν	0.28

5.3.2. Geometry

The square geometry for the model can be seen in Figure 5.8. The dimension go from -12 m to 12 m in $x-direction$ as well as -12 m to 12 m in $y-direction$, making it $10 * diameter$ in all directions, which should be big enough to minimize boundary effects (Gelagoti et al., 2019). This was also verified

by checking the stresses at the boundaries in the results. The σ'_{xx} stress was checked on x-max side, the side where it is pushed towards, and increased by 30% to 6.5 kN/m^2 which is an acceptable increase to conclude the boundary effect is minimal. In the centre of the model, as mentioned above, a tunnel element is added to act as the monopile wall. Around this plate a circle with a width of 0.035m $(= 1 * wallthickness)$ is added. This volume surface area operates as the crushed zone and is assigned different strength parameters. Two different constitutive models were made use of in this model. The crushed zone can be treated as a cohesion-less material (Stevens et al., 1982), (Irvine et al., 2015), (Lovera, 2019) and the movement around the pile is influenced by small-strain stiffness and stress-dependant stiffness also is important to be captured. Therefore this part was assigned the HSsmall model. Outside of this area the weak rock is present. Because the main strains are foreseen to be inside the crushed rock, no post peak behaviour is expected in the weak rock outside. For that reason, in combination with the sake of simplicity, the Mohr-Coulomb model is used. The squares and circles in the geometry in Figure 5.8 are made for mesh refinement. In Figure 5.9 the interfaces added at the boundaries of the crushed rock can be seen. Both at the pile wall and the weak rock - crushed zone boundary an interface is added. The interfaces at the pile wall has decreased parameters by a factor of 0.67, while the crushed rock - intact rock boundary has an interface with no reduced parameters.

5.3.3. Overview

- The model is setup in Gravity Loading conditions and effective stress conditions of 0.5m depth are created.
- A steel tunnel element of diameter 1.2m is inserted and used as pile wall.
- A crushed zone 0.035m is created, around it intact rock material is added. For information on the material set, see Appendix A.
- Interfaces are added on both sides of the crushed zone, the interfaces at the pile wall includes decreased strength parameters, the interface at rock-rock interface does not.
- The pile is pulled to the side by 0.012m, being 1% of the diameter of the pile.

5.4. 2D vertical model

The goal of the 2D vertical model is to see whether crushing or softening of material under and around the pile wall tip can be captured in a FEM model. Since the movement in the model is vertically it is possible to create it as a 2D asymmetric model, which saves computing time compared to a 3D analysis. Modelling of the full driving process of a pile is difficult in a FEM model as the dynamic nature of the process is hard to capture and a FEM is not able to handle the big displacements that will take place. The mesh of the model will get too distorted to finish in an equilibrium state and so the model will collapse. What is possible though is to create a wished-in-place (WIP) monopile and push down the structure for a bit. This vertical push will create a plastic zone under the pile. By assessing the plastic zone, combined with available information found in literature, possibly conclusions on the size of the remoulded zone can be drawn. This model therefore represent static vertical loading and not a pile driving process.

5.4.1. Setup

An axisymmetric model is created in PLAXIS 2D. In the model a soil polygon is added, to which properties of the pile wall are assigned. In this way the soil polygon can act as the pile wall and be pushed down. A material set for steel is created for this. Unlike the model described in section 5.3 this model uses K0 procedure as a calculation type as the model slice is vertical and so the issues to flip stress directions is not a problem here. The water level is set at the top of the model to make the influence of water is captured in the model. Since the soil polygon is inserted into the model the pile wall is WIP, it is then pushed down by a prescribed LineDisplacement of 3.5mm (10% of the wall thickness) down from the top of the polygon. This displacement was used as too big displacements caused distortion and failure of the model. 10% of the wall thickness was deemed a reasonable displacement for the vertical push. The soil polygon that represent the pile wall is made up of a very stiff ($E_{ref} = 30 * 10^{12} kN/m^2$ and $\nu = 0.49$) Linear Elastic material model. Interfaces are added to the sides of the pile wall and extend into the rock. This adopted setup of the model is based on a method suggested by Van Langen and Vermeer (1991). The interfaces extend into the rock to allow for movement of the nodes. In this way it reduces the extreme pressure that will otherwise stack on the singular plasticity points at the pile

tip edges. The interfaces adjacent to the pile wall have a reduced interface strength of $2/3$ times the strength of the rock. The parts extending into the rock do not have reduced properties to make sure no preferential failure plane is created.

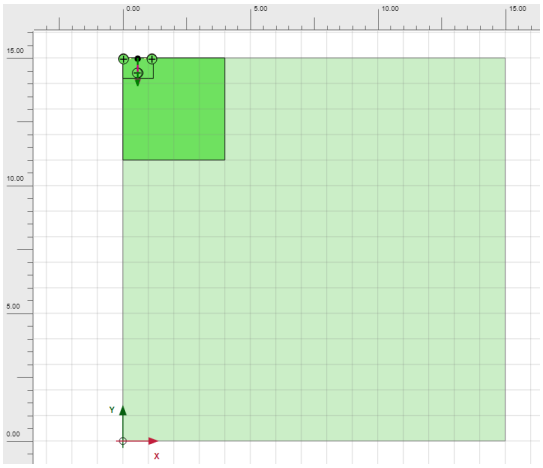

Figure 5.10: Vertical FEM model setup in 2D. On the top left the pile wall that is pushed down is shown.

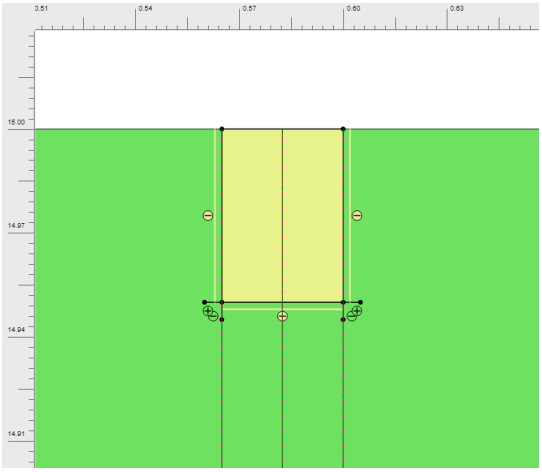

Figure 5.11: Zoomed in cross-section of the pile wall.

5.4.2. Geometry

The geometry of the model can be seen in Figure 5.10. The model extends from 0 m to 15 m in both $x-$ and $y-direction$. On the top left you can see the soil polygon that acts as a pile, with a wall thickness of 35 mm. In Figure 5.11 the configuration of the interfaces can be seen. It can be seen that the pile in Figure 5.11 does extend only 50 mm into the ground. Multiple starting depths and pile lengths were tried, but the pile walls that were WIP deeper showed a bigger plugging effect when pushing down. In the results in Figure 6.3 this effect can also be seen. Since the goal of the model is to check the local behaviour under the pile, a global response like plugging of the inside of the pile is not of interest. The model is therefore created with a starting depth for the pile wall of 50 mm for most cases. Also see Appendix B for the different model variations that were set up. The constitutive model that is used in this model is the HBS model for the intact rock. It has already been discussed that the HBS model is the most suitable for modelling the rock, and that it is of interest to have softening behaviour incorporated in the model. In the development process of the model, also runs were done using MC and HB. These models showed plastic zone going very far into the model. Expected is that the softening in the HBS model reduces the propagation of the strains and creates a more fitting plastic zone. Also the HBS model regularizes strain localizations through visco-plastic behaviour during the softening, if correctly calibrated. By this a mesh independent model can be created. The fluidity parameter γ plays a key role in the regularization of the strains and so mesh independence of the problem. To regularize the strain localization correctly γ has to be calibrated, which is done using a sensitivity analysis. The different material sets that were set up to check the influence of the fluidity can be found in Appendix A.

5.4.3. Overview

- An axisymmetric model is created in which a stiff soil polygon with a width of 0.035m is added to act as the pile wall.
- A material set for rock is inserted in the model, see Appendix B for an overview of all used material set variations.
- Interfaces are added on both sides and under the pile. The interfaces are also extended into the rock mass in horizontal and vertical direction at both sides of the pile tip. The interfaces are extended 0.005m into the rock. The interfaces extending into the rock do not include reduces strength parameters while the interfaces on the steel-rock interface do.
- A vertical prescribed displacement is applied on top of the pile, pushing the pile down 0.0035m, which is 10% of the pile wall thickness.

5.5. 3D model

To assess the lateral pile response of the monopile in weak rock a 3D FEM model is created. In this model a pile is pulled to the side to see the force that is needed to displace the pile. Goal of the model is to see the lateral pile capacity difference due to a crushed zone around the pile. By comparing the results of a model containing only intact rock, a model with a crushed and intact zone and a model containing only crushed material the effect of the weak zone can be seen. Since the exercise executed at the 2D vertical model was not able to come to a definite answer on the crushing that happens around the pile, a sensitivity analysis will be done with different crushed zone thicknesses. Also the stiffness of the crushed rock is altered, in different models, to see the effect. To compare the model to data by Lovera also a model is run with similar properties to the model in her dissertation. All results are also compared to the OnPT's in the dissertation (Lovera, 2019).

5.5.1. Setup

Also this model is set up in PLAXIS. A 3D model is created in which half a pile is added at the center of the model. Since the model is mirrored in the y = 0 plane, only half the model is needed, which saves computing time. The pile is modelled as a weightless plate, in Table 5.5 the stiffness parameters are presented. The pile is modelled weightless to make sure the small zone around the pile is not affected when loading in the plate and interfaces. Also, a model that was run which had a pile with a unit weight of 78.5 kN/m^2 showed the influence of the self weight of the pile is negligible. The dimensions of the pile are set up the same as pile P5 in Lovera (2019), for comparison. As mentioned in section 5.5 multiple models will be set up. An overview of the models that are run can be found in Appendix B. The table shows the model variations with different crushed zone thicknesses and stiffnesses. All models that include a crushed zone around the pile, also include crushed material inside the pile. All the rock that moves inside the pile during installation is expected to be crushed, this is based on the findings by Jafari et al. (2019) that are discussed in chapter 4. For a more detailed description of the materials sets of the different stiffnesses, inspect Appendix A. Figure 5.12 shows the structural elements that are set up in the model. The interfaces are added in the model because of the reduction in strength at the steel-rock interface of course, but also to allow for gapping behind the pile, which is an important factor influencing the lateral pile response according to Lovera (2019). The loading procedure is simple. After loading in the interfaces and plate elements in the first phase, a prescribed surface displacement is induced at the top of the pile as is visible in the figure. The prescribed displacement is 0.4m, which is big enough to create enough displacement of the pile at the mudline level to asses the lateral response of the pile.

Table 5.5: Steel plate parameters for the 3D model.

Parameter	Value
E (kN/m^2)	210 *10^6
G (kN m^2/)	105 *10^6
d (m)	0.035

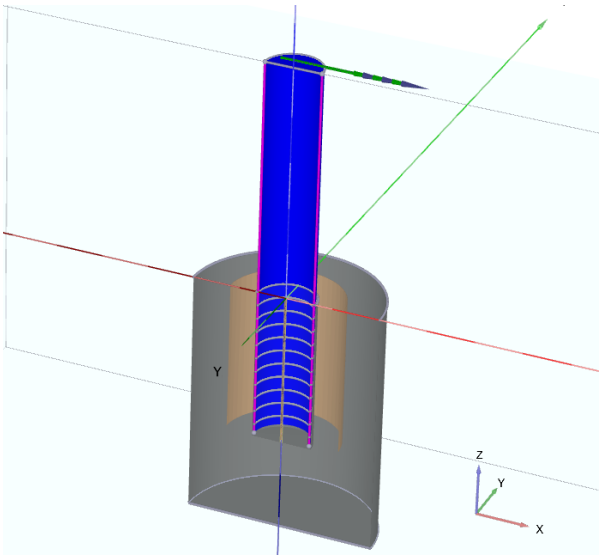

Figure 5.12: The structural parts that are included in the 3D model

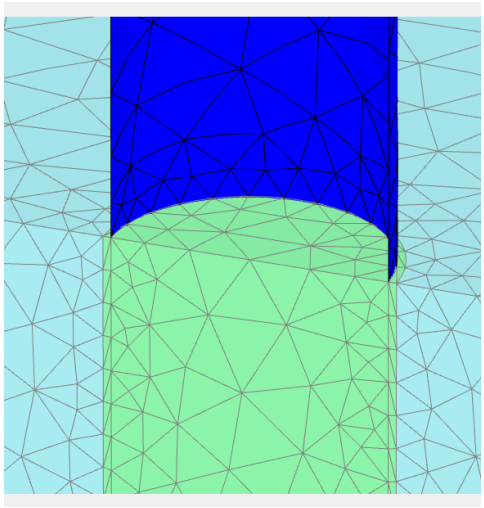

Figure 5.13: Zoomed in cross-section of the 3D model mesh, the crushed zone is shown in green and extends one wall thickness outside the monopile volume.

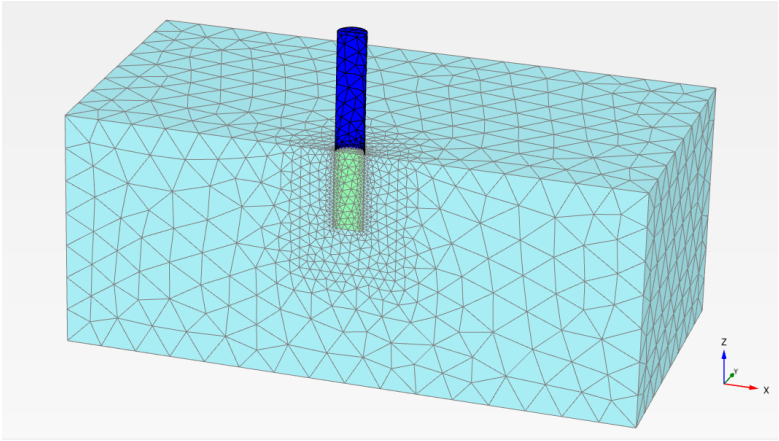

Figure 5.14: Graphic of the 3D model geometry and mesh, including a pile in the center and crushed zone in green.

5.5.2. Geometry

Figure 5.12 shows the created geometry for the model with the pile centered around x, y, z = 0. The model extends from -12 m to 12 m in $x - direction$, 0 m to 12 m in $y - direction$ and 0 m to -10 m in $z - direction$. This means $10 * Diameter$ in all lateral directions, to make sure the boundary effect is minimized. The pile dimension is a diameter of 1.2m, 3.2m embedment level and a height above ground level or pile eccentricity of of 5m. The load is applied at 5m above ground level just as in the OnPTs of Lovera (2019). An overview of the dimension is shown in Table 5.6. The crushed zone is created around and inside the pile, and is extended twice its size outside the pile under the pile. So that means for a model with a crushed zone of one times the wall thickness, it extends two wall thicknesses under the pile. This configuration was chosen as the literature suggests that crushing happens under the pile and so the crushed zone will also extend under the pile. The interfaces have a reduced strength for the inside and outside of the pile, at the interface between crushed and intact rock, no strength reduction is applied in the interface. This interface was added to allow the crushed material to move down the gap that the pile leaves behind during lateral loading. When the interface is removed the model fails after minimal movement of the pile because the annulus of crushed rock is so small and elements get distorted. Considering the downward movement of the cohesion-less crushed material is expected and

the fact that no strength reduction was applied justifies the presence of the interface. As described in the setup section above, the geometry of the crushed zone is varied over the different model variations as described in Appendix B.

Table 5.6: Overview of the pile dimensions in the 3D model.

	Dimension (m)
Pile Diameter (D)	1.2
Pile Embedment Depth	3.2
Height of applied displacement above mudline (Pile Eccentricity)	5
Wall Thickness (t)	0.035

5.5.3. Overview

- A 3D model is created in which half a pile is inserted. The pile has a diameter of 1.2m, embedment depth of 3.2m and extends 5m above mudline. On top of the pile also a surface of half a circle is created.
- A crushed zone is created in and around the pile by creating a volume around the pile. For the different geometrical variations, see Appendix B.
- A material model is assigned for the crushed and intact rock, see Appendix A for the different variations that were used.
- Interfaces are added on both the in and outside of the pile wall and on the interface between the crushed and intact rock. The pile wall interfaces include reduced strength values but the rock-rock interface does not.
- A prescribed surface displacement is applied on top of the pile, pushing the pile 0.4m to the side at a height of 5m. This displacement creates enough displacements at mudline level to assess the lateral pile response. The loading therefore is monotonic in this model.

6 Results

6.1. 2D horizontal model

For this model only one case was run, as described in section 5.3. The 2D horizontal results are depicted in two screenshots of the FEM mesh. Figure 6.1 shows the total deviatoric strains that were induced by the push in x-direction (from left to right in the picture). The prescribed displacement of the tunnel element that was activated was 0.012m, which is 1% of the pile diameter. It can be seen that the strains are localized in the crushed zone annulus close to the pile.

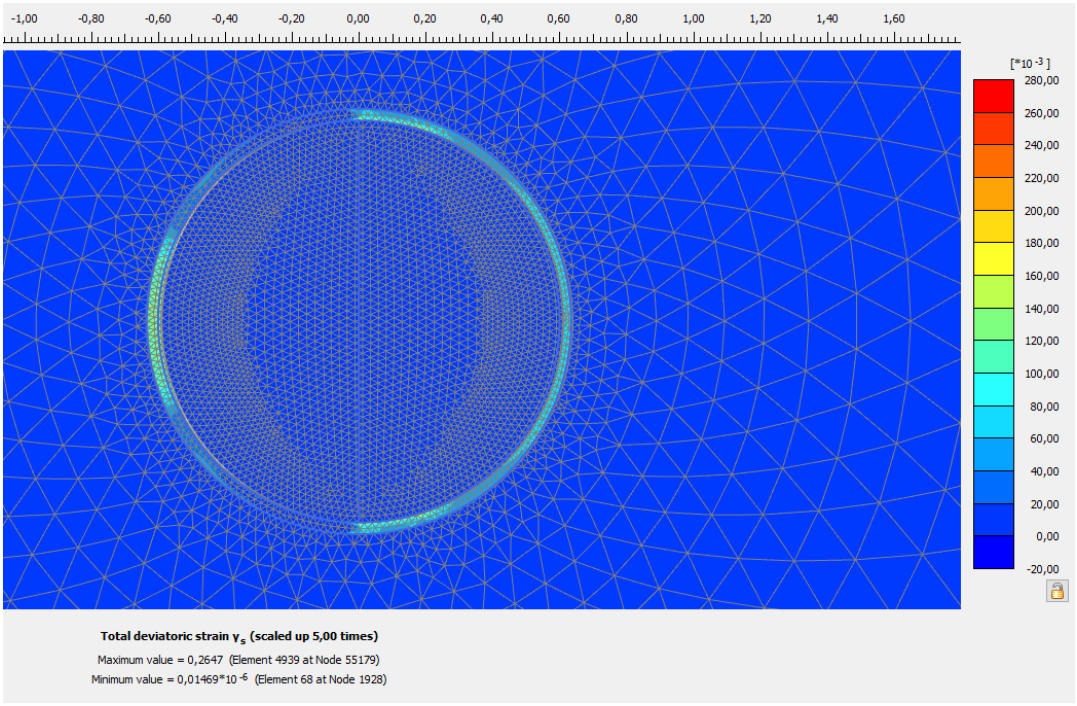

Figure 6.1: Graphic of the 2D model geometry and mesh, including a pile in the center and crushed zone in green. The tunnel element was pushed to the side for 0.012m.

Figure 6.2 shows the total displacements happening after the prescribed displacement of the tunnel element to the right. Just like with the deviatoric strains in Figure 6.1 the displacements are concentrated in the crushed zone just outside the pile.

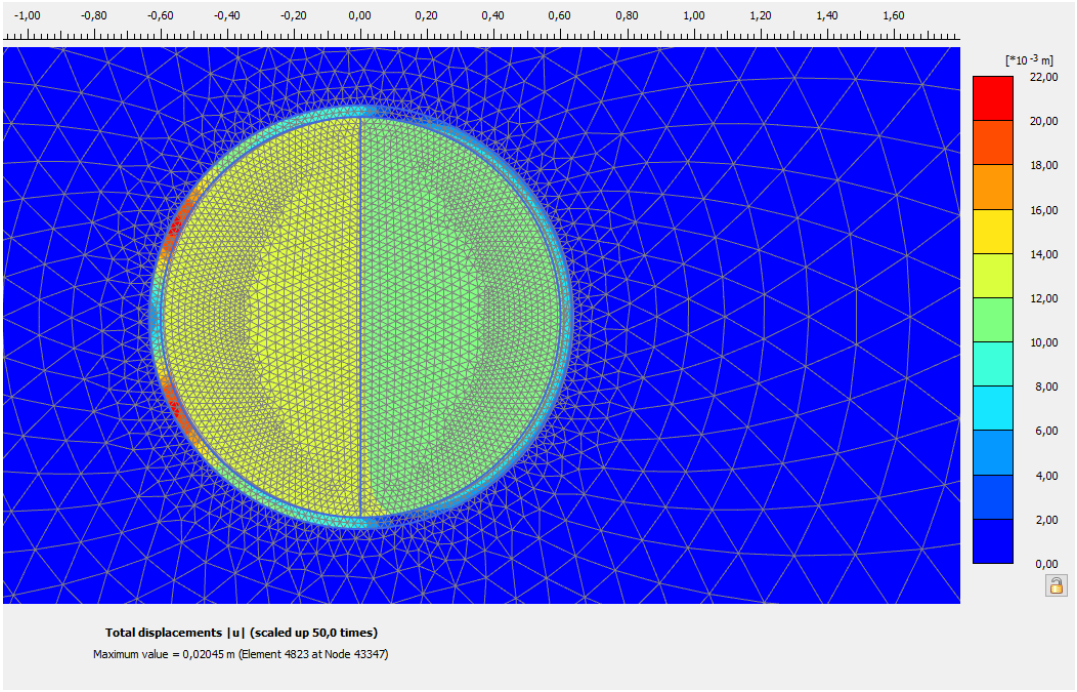

Figure 6.2: Graphic of the 2D model geometry and mesh, including a pile in the center and crushed zone in green. The tunnel element was pushed to the side for 0.012m.

6.2. 2D vertical model

For the 2D vertical model, multiple model variations were run. See Appendix B to see which variations. The detailed setup of the model is discussed in chapter 5. The models include a vertical push of a rigid pile wall volume. This is a simplified way of describing the problem and does not cover a dynamic pile driving response. The geometry was changed to see the effect the initial embedment depth (see Appendix B) of the pile wall has. Secondly the gamma parameter was varied to check if a mesh independent result could be generated. Lastly also the residual strength values were varied. This was done to see which effect this has on the crushed zone size. Allowing the rock to get weaker might mean the crushed zone last less wide for example.

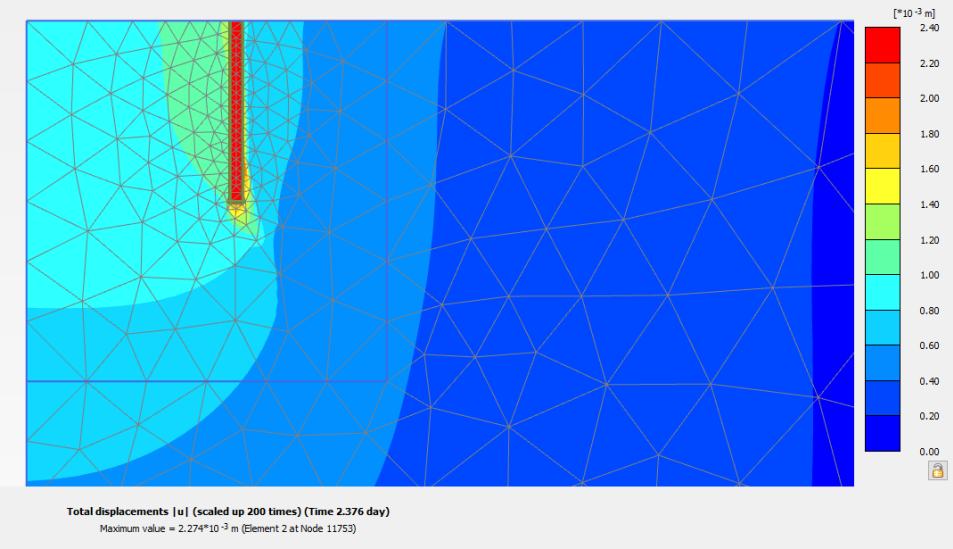

Figure 6.3: Total displacement around the pile tip after the vertical push for the model with a deeper starting embedment depth (model 4).

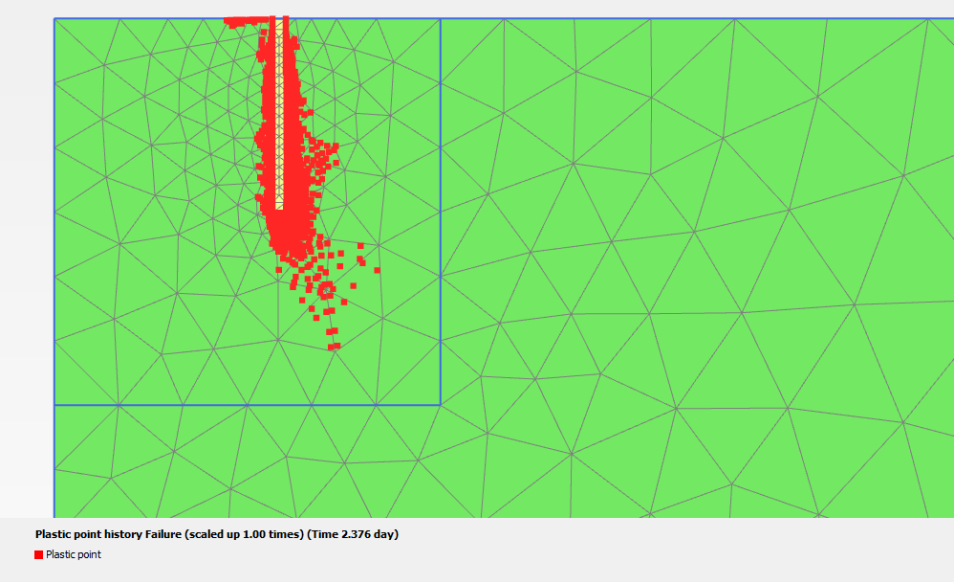

Figure 6.4: Plastic points around the pile tip after the vertical push for the model with a deeper starting embedment depth (model 4).

Comparing Figure 6.3 and Figure 6.5 it can be seen that the movement inside the pile is much bigger for the model where the initial embedment depth is bigger. This plugging effect is caused by the friction of the inner pile wall that is longer. The piles in these models are wished in place to this starting depth and therefore are surrounded by undisturbed ground. In real life however, the rock at the sides of the pile wall will be crushed already by the driving that happened before. The strength of the interface between the rock and the pile at the pile wall sides and the associated plugging therefore is unwanted to happen in this model. The response including the plugging is more of a global pile response while we are interested in the local behaviour under the pile, where the crushing is happening. Figure 6.4 shows a big part of the plastic points are also occurring adjacent to the pile. It is therefore decided that the shallower geometry in Figure 6.5 is better suited for the analysis in this section.

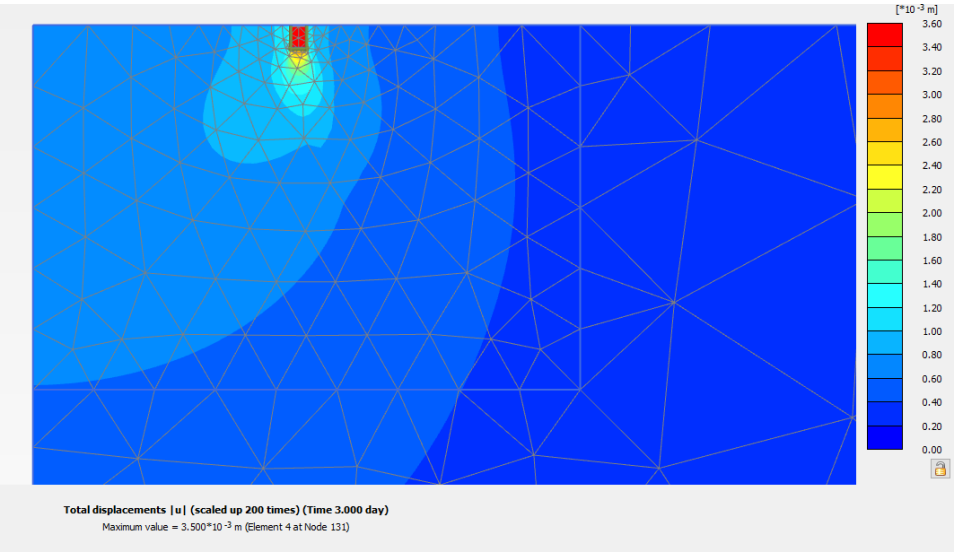

Figure 6.5: Total displacement around the pile tip after the vertical push for the model with a shallower starting embedment depth (model 3).

The Hoek&Brown Softening model was employed for this model because of the capacity to regularize strain localization, or in other words create a mesh independent model in terms of plastic zone. For different models the fluidity factor γ has a different optimal value to get to this mesh independence. That is why a check was done by running multiple models. The plastic zones for the different fluidity's and mesh coarseness are shown in Figure 6.6 to Figure 6.17.

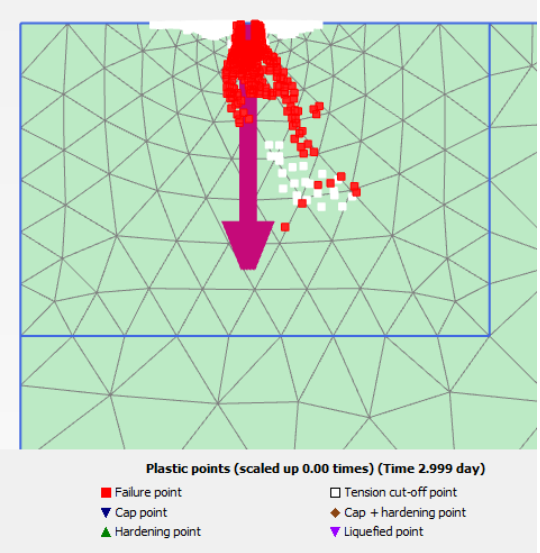

Figure 6.6: Plastic point under the pile tip for the gamma = 5 case (model 7), fine mesh.

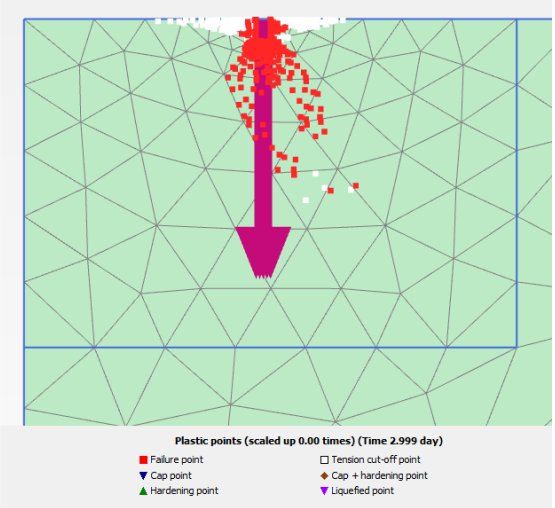

Figure 6.7: Plastic point under the pile tip for the gamma = 5 case (model 7), coarse mesh.

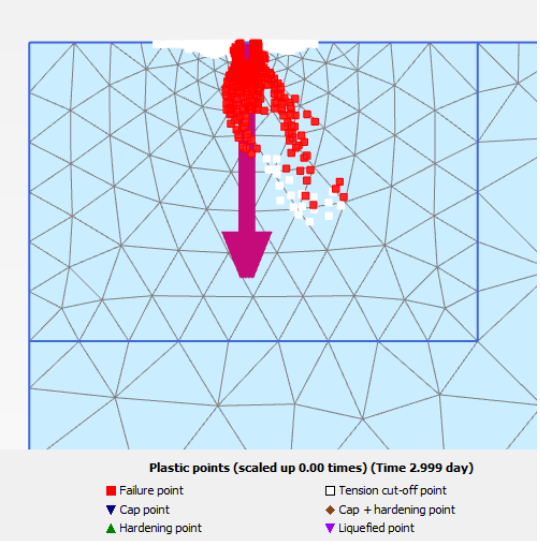

Figure 6.8: Plastic point under the pile tip for the gamma = 3 case (model 6), fine mesh.

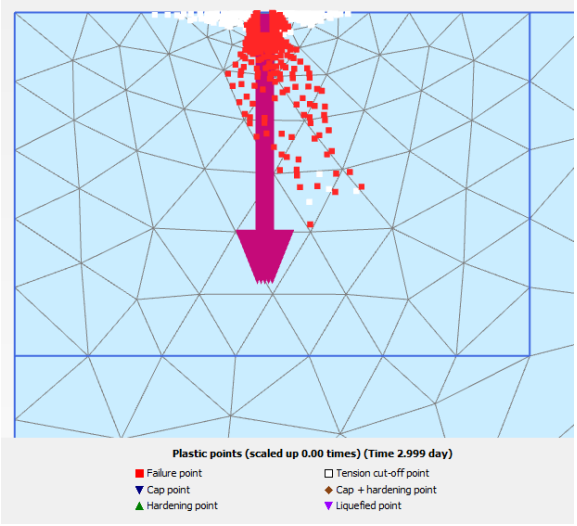

Figure 6.9: Plastic point under the pile tip for the gamma = 3 case (model 6), coarse mesh.

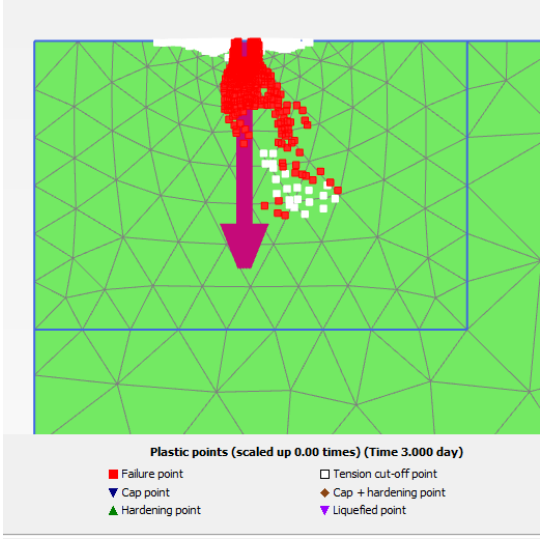

Figure 6.10: Plastic point under the pile tip for the gamma = 1 case (model 3), fine mesh.

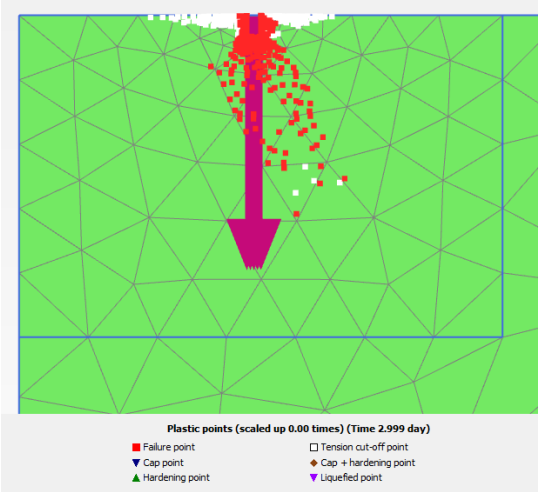

Figure 6.11: Plastic point under the pile tip for the gamma = 1 case (model 3), coarse mesh.

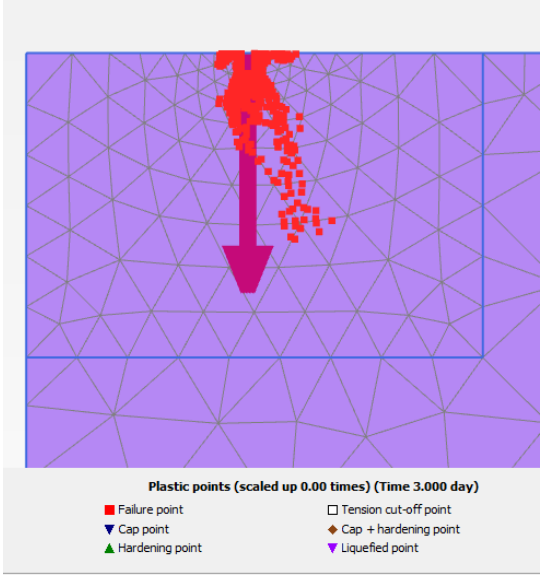

Figure 6.12: Plastic point under the pile tip for the gamma = -1 case (model 2), fine mesh.

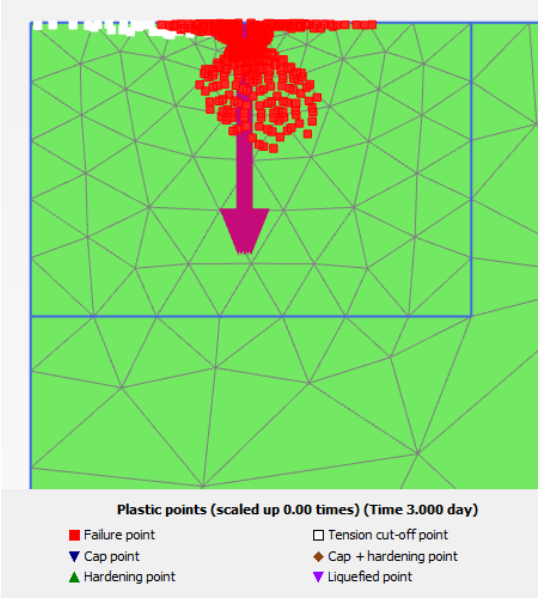

Figure 6.13: Plastic point under the pile tip for the gamma = -1 case (model 2), coarse mesh.

Model 2 is shown in Figure 6.16 and has a negative γ value which means it models an elasto-plastic material and shows the rate-independent response. When comparing the response for different mesh coarseness the difference in response and so mesh dependency is most visible at the elasto-plastic cases, indicating the strain regularization does its work in the visco-plastic models. When looking at the results, the shape for the different γ values is coherent for the different meshes, although slight mesh dependency is still visible. Ideally the difference in coarseness would be bigger, to better view this. Based on the results it was decided to take the value of γ = 3 for the following analysis as this result was most mesh independent.

The comparison in Figure 6.14 to Figure 6.17 is done to check if the value of the residual strength is of influence of the size of the crushed zone. Since the reduction in strength of the rock due to the crushing is not well defined this is interesting to see. Also, the Hoek&Brown Softening model works better for residual strengths of 75% or higher of the original strengths. On the other hand the reduction is expected to be higher than that, so by decreasing the value in steps it can be checked up to how far the model works. Ribacchi (2000) suggested the residual conditions of a rock mass are relatively independent of initial conditions of the rock and can be described as in terms of Hoek&Brown parameters as:

$$\frac{s^{res}}{s} = 0.04, \frac{m_b^{res}}{m_b} = 0.65. \tag{6.1}$$

Therefore a model using these values was also used.

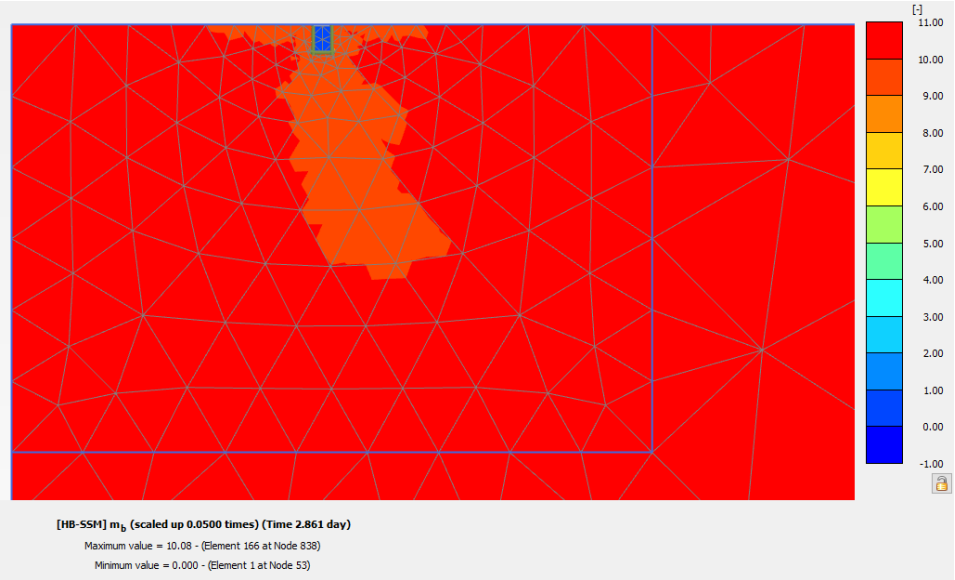

Figure 6.14: Strength reduction around the pile tip after the vertical push for a residual strength value m_b allowed to reduced to 0.9 of the original strength (model 8).

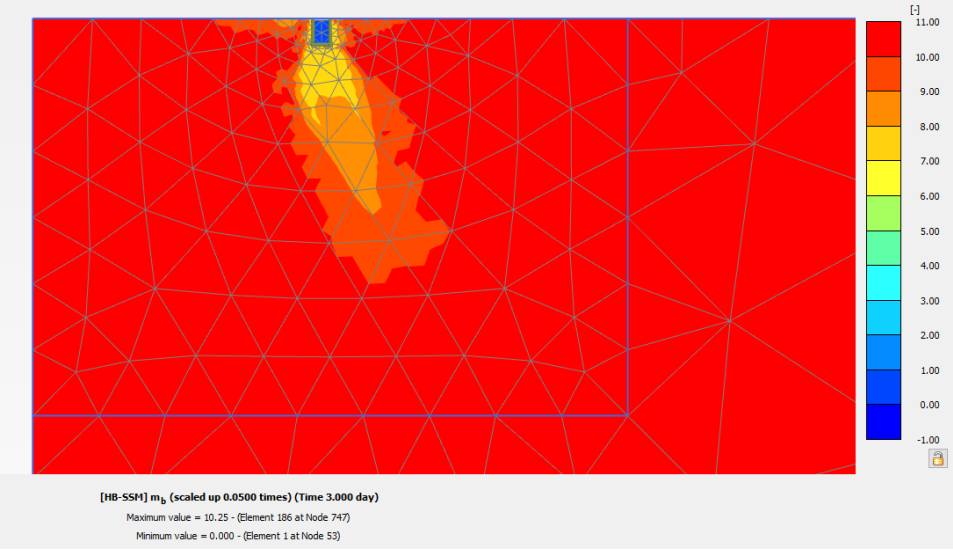

Figure 6.15: Strength reduction around the pile tip after the vertical push for a residual strength value m_b allowed to reduced to 0.75 of the original strength (model 9).

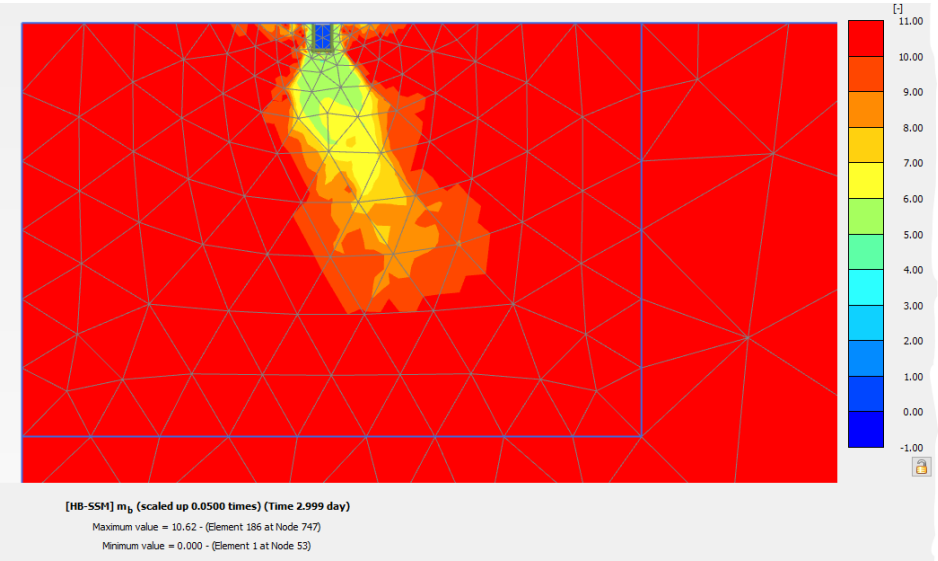

Figure 6.16: Strength reduction around the pile tip after the vertical push for a residual strength value m_b allowed to reduced to 0.5 of the original strength (model 10).

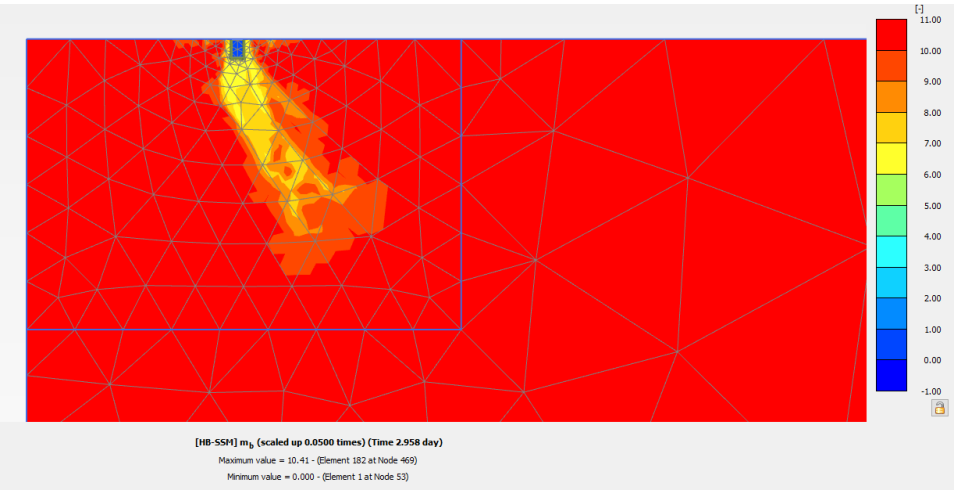

Figure 6.17: Strength reduction around the pile tip after the vertical push for a residual strength value mb and s as adviced by Ribacchi (2000).

It can be seen that the residual strength parameters do have an effect on the size of the crushed zone. A lower residual strength leads to a bigger crushed zone, however this effect is small. Especially when comparing to the total size of the softening area the difference is minimal. The model using the values as adviced by Ribacchi (2000) also shows a weakened area of similar size.

6.3. 3D model

An example of the model in which the pile is loaded in lateral direction can be seen in Figure 6.18. The figure shows a side view of the pile. The loading direction can be seen on top of the pile and the deformation it creates is also visible at and around the pile. The model shown in this figure includes a crushed zone that extends 1 wall thickness outside of the pile.

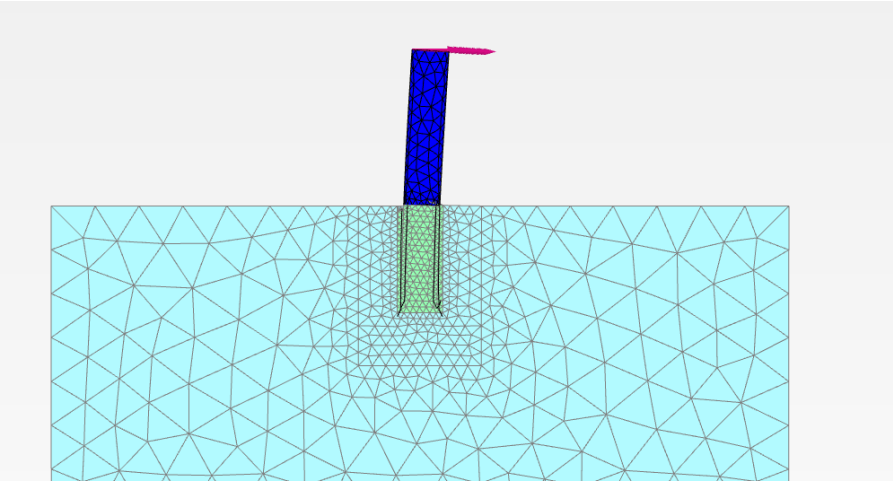

Figure 6.18: Side view of the deformed mesh, showing the lateral deflection on the pile

In order to compare and benchmark the results of the investigation done for this thesis to the results of the OnPT's by Lovera (2019), the force-displacement curves of the piles are compared. The OnPT and FEM results of Lovera are shown in Figure 6.19. For detailed explanation on the derivation of this curve please refer to the dissertation of Lovera (2019). It can be seen that the OnPT and FEM results do not align perfectly, this is due to the fact that the measurements taken at the test, were taken 10cm above mudline and the FEM results show a global stiffness of the pile deduced at ground level as stated in het dissertation. The load-displacement curves in this thesis will also be the curves at mudline level as the displacement at mudline is of interest.

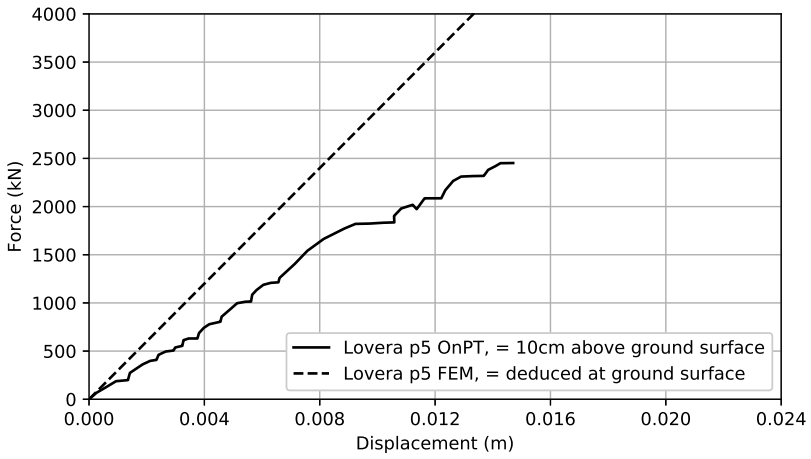

Figure 6.19: Graph of the OnPT response of pile 5 and the calculated FEM response of pile 5, presented in Lovera (2019).

As described in Table B.3, multiple configurations in terms of geometry and material models were run. All the models yield force-displacement curves of the pile, which can be compared to see the difference in lateral stiffness of the ground around the pile. Figure 6.21 shows the first comparison, where the full intact (Model 12), partly crushed (Model 17) and fully crushed (Model 15) responses are compared.

For all configurations of the models please refer to Appendix B.

The force-displacement curves are taken from the PLAXIS software in the following way. The two nodes at mudline on both sides of the monopile are selected (see Figure 6.20). For each node, using the curves manager in the PLAXIS Output interface, the total displacement (u_x) is extracted. The u_x values are divided by two to get the average displacement of the two nodes. The equivalent force (F_x) in the direction of the prescribed displacement (x axis in this case) is also extracted. Since the model includes only half a pile, the equivalent force F_x also only accounts for half a pile and is multiplied by two to get the correct value for the whole pile. Then, the force-displacement curve is calculated as follows:

$$u_x = \frac{u_x^{node1} + u_x^{node2}}{2} \tag{6.2}$$

$$F_x(Wholemodel) = 2 * F_x(PLAXISoutput) \tag{6.3}$$

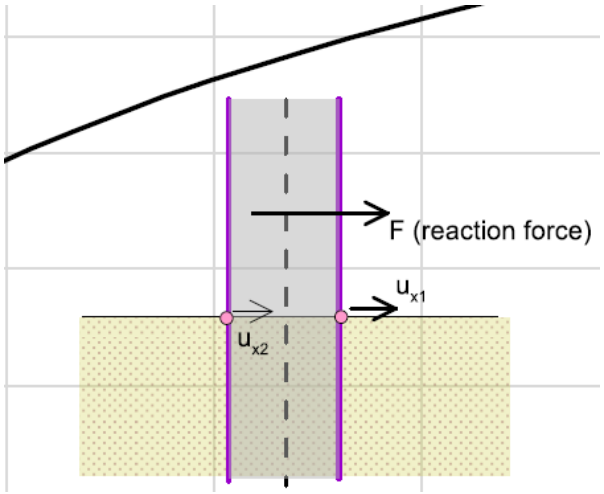

Figure 6.20: Overview of calculated pile response in the 3D model.

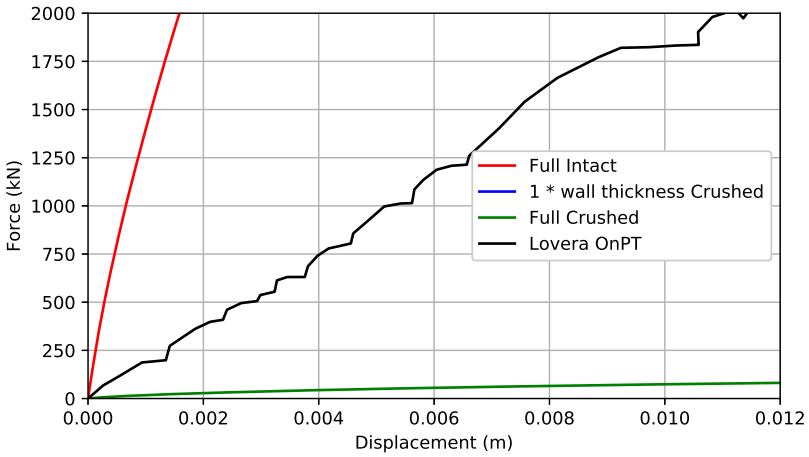

Figure 6.21: Overview of calculated pile response in the 3D model.

It can be seen in the figure that the full intact model response is very stiff and the full crushed response is very soft compared to the OnPT results. The model that includes a crushed zone coincidences best with the response of the OnPT, but in terms of initial stiffness differs significantly as well.

For the design of a monopile foundation the initial stiffness response is of interest (Seong et al., 2022) as ideally of course, no permanent displacement or rotation of the structure would occur. When looking at the tangent lines that were drawn for the global initial stiffnesses in Figure 6.22 toFigure 6.25 it can be seen that the influence of a crushed part in the model is big. The crushed zone in Model 17 results in a tangent global initial stiffness being 28 times lower than for the intact rock Model 12. The results portrayed do give an insight in the effect of introducing a crushed rock zone into a model.

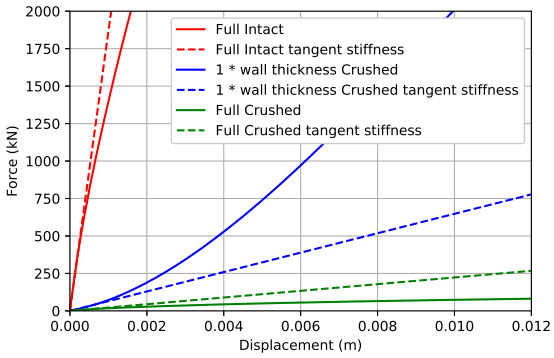

Figure 6.22: Lateral response of full intact(12), crushed zone(17) and full crushed(15) models.

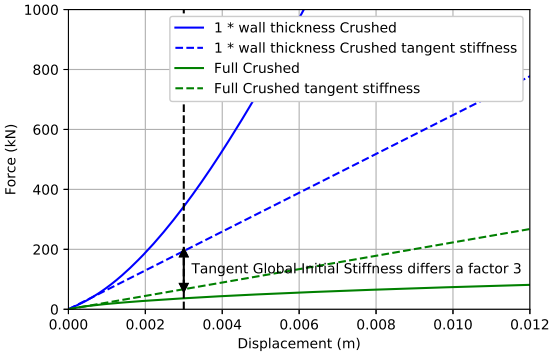

Figure 6.23: Comparison of the lateral response of the crushed zone(17) and full crushed(15) models and their tangent initial global stiffness.

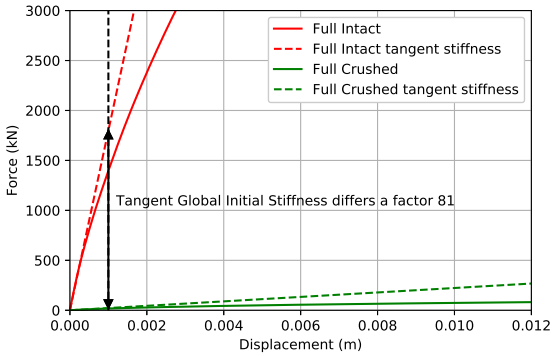

Figure 6.24: Comparison of the lateral response of the full intact(12) and crushed zone(17) models and their tangent initial global stiffness.

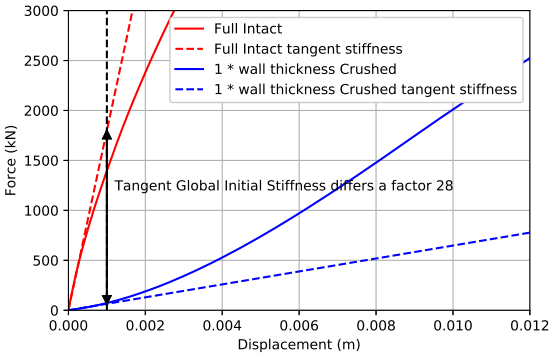

Figure 6.25: Comparison of the lateral response of the full intact(12) and full crushed(15) models and their tangent initial global stiffness.

Figure 6.26 shows the responses discussed above plotted in a logarithmic scale. This scale allows to visualise that the final lateral stiffness of the piles in the full intact rock model (12) and the full crushed rock model (15) differ approximately two orders of magnitude. Since their Young's Moduli are a factor 83 different, which is in the range of a hundred, this appears to be a reasonable result. Also the tangent global initial stiffnesses are a factor 81 apart, which is in the same range as well. The figure also shows the response of a model including a crushed zone with the blue line. It can be seen that the blue line increases in stiffness more over the displacement and for a higher displacement move closer to the intact rock response. This is caused by the increasing stress-dependant stiffness of the crushed rock modelled in HSsmall.

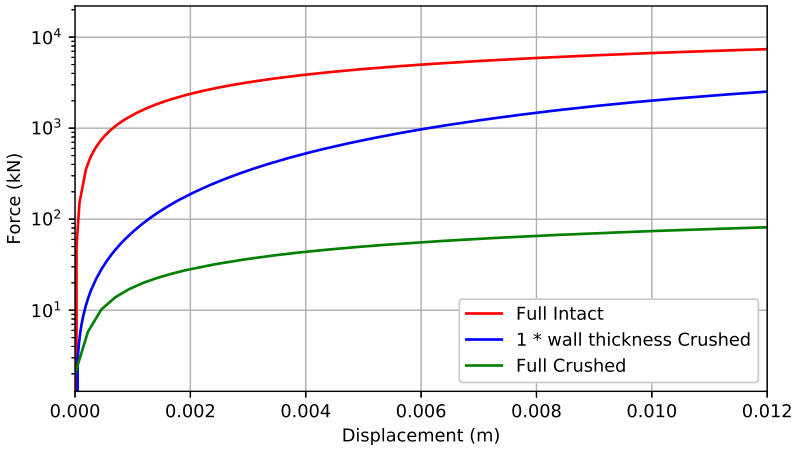

Figure 6.26: Lateral response of full intact(12), crushed zone(17) and full crushed(15) models plotted in logarithmic scale.

Since the results of the 2D vertical FEM model were not totally satisfactory it was decided to check the influence of the crushed zone for different thicknesses and stiffnesses of this crushed part. The results of the different thicknesses can be seen in Figure 6.27, where model 17,18,19 and 20 as described in Appendix B are compared. A zoomed in picture is shown in Figure 6.28. The same thing is done for the different stiffnesses in Figure 6.29, where model 20,17,21 and 22 are compared. The stiffness was increased in two models compared to the material model for a typical frictional material (C2). The stiffest material model variation was created very stiff to see the effect of the crushed zone if it's stiffness is in the same order as the intact rock. A zoomed in picture of the responses for the different stiffnesses is shown in Figure 6.30. Table 6.1 and Table 6.2 show results of the Tangent Initial Global Stiffness and the Secant Global Stiffness for 0.1% of Pile Diameter of the different model variations, since the stiffness response up untill 0.1% of pile diameter is of interest (Seong et al., 2022). The results are discussed in chapter 7.

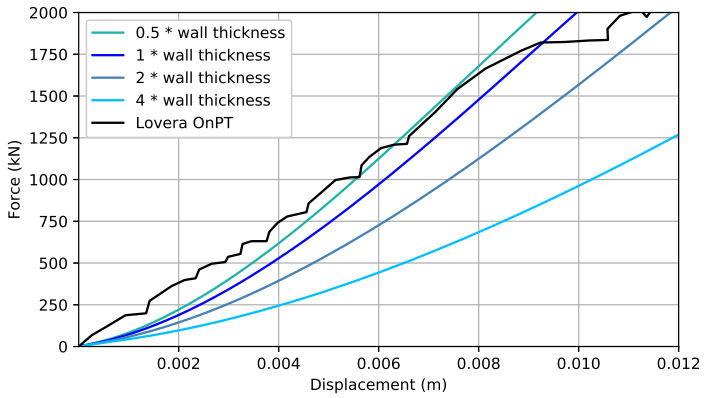

Figure 6.27: Comparison of lateral stiffness for the different crushed zone thicknesses (model 17,18,19 and 20).

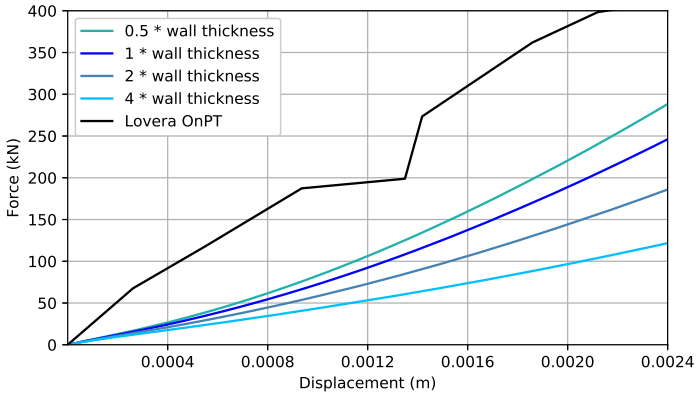

Figure 6.28: Zoomed in comparison of lateral stiffness for the different crushed zone thicknesses (model 17,18,19 and 20) to show the response are very close in the beginning of pile lateral pile movement.

Table 6.1: Overview of the different stiffness response for models with different crushed zone thickness

Model Variation	Tangent Initial Global Stiffness (kN/mm)	Secant Global Stiffness for 0.1% of Pile Diameter (kN/mm)
13 (intact)	1864	1355
16 (0.5t)	69	88
17 (1t)	65	76
18 (2t)	54	63
19 (4t)	43	46
15 (crushed)	22	16
LOVERA FEM	300	300
LOVERA OnPT	200	147

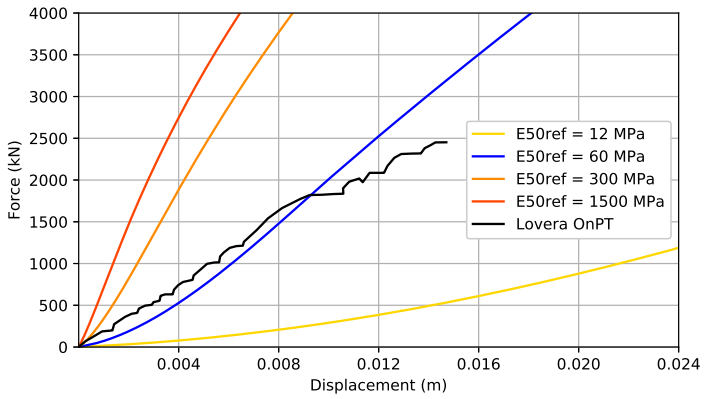

Figure 6.29: Comparison of lateral stiffness for the different crushed zone stiffness parameters (model 20,17,21 and 22).

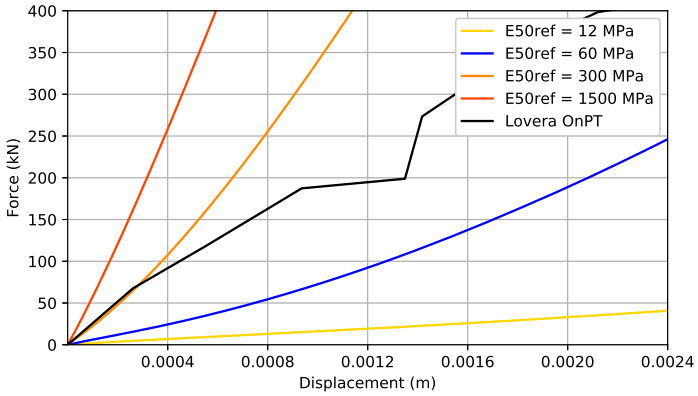

Figure 6.30: Zoomed in comparison of lateral stiffness for the different crushed zone stiffness parameters (model 20,17,21 and 22) to show the difference in response in the initial phase of lateral movement.

Table 6.2: Overview of the different stiffness response for models with different crushed zone stiffness

Model Variation	Tangent Initial Global Stiffness (KN/mm)	Secant Global Stiffness for 0.1% of Pile Diameter (KN/mm)
12 (intact)	1864	1355
20 (12Mpa)	17	16
17 (60MPa)	65	76
21 (300MPa)	221	358
22 (1500MPa)	579	714
15 (crushed)	22	16
LOVERA FEM	300	300
LOVERA OnPT	200	147

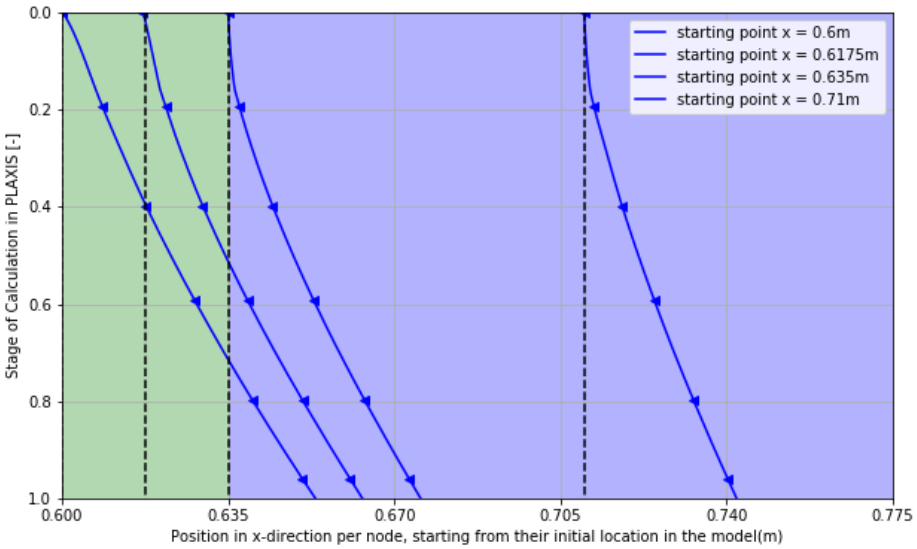

Figure 6.31: Moving path of nodes in the ground during the lateral loading in model 17. The green area represent crushed rock, the blue intact rock.

Next to the force-displacement curves, also the movement of nodes in the ground in the model were checked. Figure 6.31 shows 4 nodes that are located at ground level and on the x-axes, so x = 0 and y = 0. The y axis is labelled stage from 0 to 1, meaning 0 is the initial position and 1 the position at the end of the PLAXIS calculation. One node is located on the pile surface, one node halfway the crushed zone, one node on the border of the crushed and intact rock and one node in the intact rock. By comparing the movement during the lateral loading process, insight on what causes the increase in stiffness during lateral movement, that is seen in most models with a crushed zone, can be gained. In Figure 6.32 it can be seen that for the first part of loading movement inside the crushed zone is much higher, more than four times as much as in the intact rock. When looking at the final stages, from 0.8 to 1, it is visible that the intact rock starts to be pushed away by the pile as well. This causes that the relative extra movement in the crushed zone there is less than two times that of the intact rock.

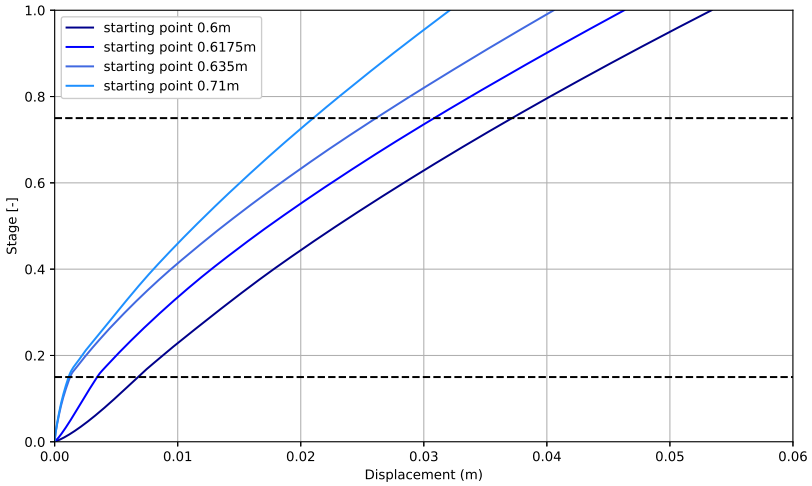

Figure 6.32: Displacement of the nodes that start at difference locations in the model.

Figure 6.33 and Figure 6.34 show screenshots of the mean effective stress and plastic point history in model 17. The graphic shows the zones of high pressure in the ground at ground level and at the pile tip due to the lateral loading. Also it can be seen that the plastic zone reaches far from the pile. It must be noted that this represents the final stage of the model, where the pile is pulled over to failure in the x-direction.

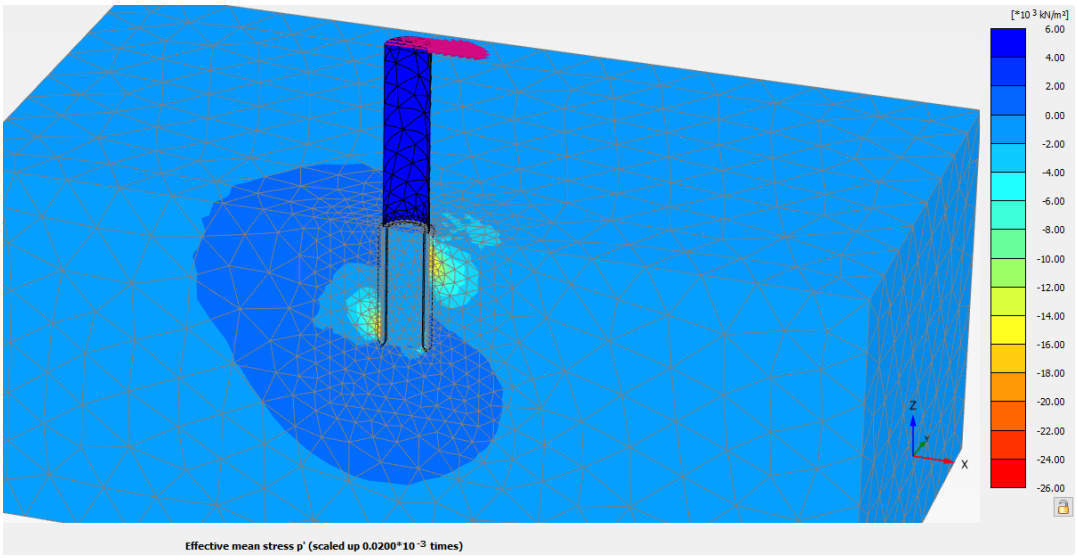

Figure 6.33: The Mean Effective Stress around the pile during the lateral loading of the pile for model 17.

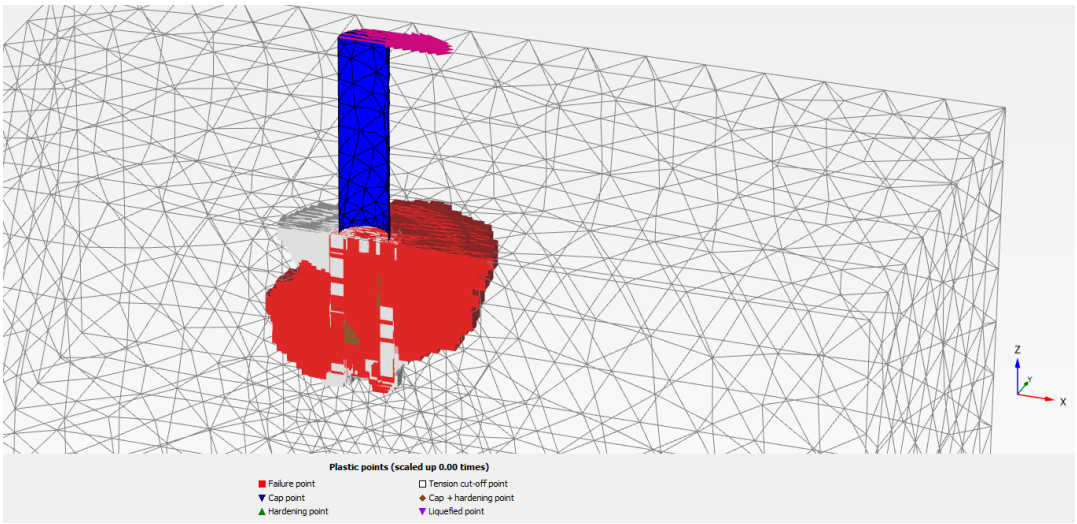

Figure 6.34: Plastic point history of the later loading of the pile, showing the failure points around the pile for model 17.

7

Discussion

7.1. 2D horizontal model

This model was created to check the typical strains around the pile. Looking at both figures presented in section 6.1, it can be seen that the movement and the strains are mostly located and concentrated in the crushed rock annulus. The thickness of the crushed zone was based on the the assumption of Lovera of the 1 wall thickness crushed zone and the stiffness of the crushed zone was based on the calibration of the oedometer test result. Considering the difference in stiffness between the materials, which are two orders of magnitude apart, the results that are seen look sensible.

When extending the prescribed displacement over 1% of the pile diameter, the zone of plastic points will start to increase into the intact rock as well. Considering that the wall thickness is 35mm and the pile diameter is 1.2m, the D/t ratio is approximately 34. That means that pushing the pile to the side for 3% of the pile diameter would make the pile reach the initial position of the intact rock, and consequently inducing plastic points in the intact rock. For ULS conditions, pushing over more than 3% of the pile diameter at mudline is common. This would however only increase the stiffness of the pile response and so be a positive support. Due to limitations of the model in 2D, the model failed with too big displacements, the push was not extended. The limitations entailed that due to the 2D nature of the model, displacement only is possible in the 2D plane. Displacing the pile to the side causes the crushed zone to move away from the area of compression and move 'around the pile'. This movement however is limited by the distortion of the elements, which becomes too big at some point. Concluded was however that the post peak behaviour of the intact material was not necessary to be included for the lateral loading in the 3D model as the influence will be small. Using a Mohr-Coulomb model for the intact material simplifies the model and makes it more quick to run, while still preserve the quality of the results of the model. Important to note that for the crushed rock an HSsmall material model is used to capture the stress-dependant behaviour.

7.2. 2D vertical model

The vertical model has as goal to see if pushing down a WIP pile can give information on a plastic zone that is created at the pile tip due to this static loading. It has to be noted this is a highly simplified, static way of describing the actual process of pile penetration and does not cover the dynamics of pile driving. However, displacing the pile wall a small length can show a zone of deformation under the pile under static loading. The material models created with Hoek&Brown Softening were used because the post peak softening property of the model is very relevant in this investigation.

Firstly however, the effect of the geometry was checked. In this comparison it could be seen in the two axisymmetric models (shown in Figure 6.3 and Figure 6.5) that for the deeper starting embedment depth, plugging inside the pile happens. The plugging of the pile is mostly caused by the inside interface of the pile wall. The strength of the intact rock along the wall of the WIP pile in this way interferes with the goal of the investigation, being to see what happens under the pile tip because of the static

loading. The shallower initial embedment depth therefore is more beneficial.

The model was run for multiple values of fluidity parameter γ to check when the failure patterns became less mesh dependent. Looking at the results for the plastic points in Figure 6.6 to Figure 6.17 however, it can be seen that for the visco-plastic cases the plastic zone is more constant for different meshes than for the elasto-plastic case. The failure patterns of plastic points for all models propagate far into the ground. They reach deep, more than ten times the displacement that is induced on the pile, and wide, more than two wall thicknesses outside the pile. When comparing to literature it is hard to correlate the results to the models or tests that were found. When looking at the graphic in Figure 4.2, where the effect of impact loading is depicted, it can be argued that the strain bands reach further into the ground represents cracks and the crushed zone is in closer vicinity to the pile tip.

Sequentially also the mb_{res} values were altered to check the effect on the size of the crushed zone. It was advised that the Hoek&Brown Softening model performs best with residual strengths of 75% of the initial strength. But for crushed rock it is not uncommon that this stiffness and strength drop way more than that, it could be in the range of two orders like Lovera (2019) presented. It was therefore checked what the effect was of decreasing the residual strength. The results showed a similar shape and size of weakened rock, for the 90%, 75%, and 50% strength reductions. Also the values proposed in literature, being 65% for mb_{res} and 4% s_{res} were used in the investigation and showed a similar size. It can be seen the size of the zone the part showing weakening is similar to the plastic zones discussed above, reach way deeper than the displacement of the pile and double the pile wall in width.

Before reaching the final models that are presented in this report, numerous configurations were tried. A model property that was altered and checked was the length of the interfaces that reach out into the ground outside the pile tip. The interfaces are assigned the same stiffness and strength properties as the rock and not the reduced values that are present on the rock-steel interface. The influence of the interfaces on the results however still could be seen. Adding longer interfaces made the model run easier and allowed for bigger displacements. Also big strains were visible around the interface, which is sensible since the nodes are more free to move. It gives the impression however preferential strain paths are created by the interface, which will not be present in a real pile penetration process. In the end the interfaces extending for 15% of the wall thickness was decided to be a reasonable length. The influence of the interfaces should be taken into account when considering the reliability of the model.

In the end the size of the crushed zone that is found in this analysis, about twice the size of the wall thickness, makes sense and looks to be reasonable when comparing to literature. The FEM software however does not allow for the modelling of a complete driving process but shows just one static push. On top of that the influence of properties like the extending interfaces on the results has a negative effect influence on the trustworthiness of the models. Also, different literature sources presented multiple different ways to define the rock crushing and thickness of the crushed zone. These facts combined lead to the decision to not make fixed conclusions on the size of the crushed zone, but to compare multiple thicknesses in the 3D analysis.

7.3. 3D model

The final goal of the investigation is to examine the lateral response of the monopile with the presence of a crushed zone. This was done in the 3D model. The 3D model was run for multiple configurations, just like the 2D vertical model. See Appendix B for an overview of the model variations. Since OnPT test results and sub-sequential FEM results were available, this model could be tested against those results.

First of all the response of a full intact rock, partly crushed and full crushed model were compared. As expected the response of the intact rock was the stiffest and the full crushed the softest. Comparing to the results of the Lovera OnPT and FEM, the model with a crushed zone suited the best, but it was not a perfect match. What also stands out is the shape of the force-displacement curve of the model with a crushed zone. The shape is bending up for increasing displacement, which means the response is getting more stiff for increasing displacement. This shape is not common for force-displacement curves of monopiles when only soil material is present. They are usually the other way around, showing soften-

ing with increasing displacement. The cause for the shape is the stress dependency of stiffness of the HSsmall model. With increasing confining stress this material model gets stiffer. Because the crushed zone annulus is confined closely around the monopile the stress will increase quickly as the pile is pushed in lateral direction. The rapid increase in stress then explains the increase in stiffness of the lateral pile response. Assessing the tangent global initial stiffness showed that introducing a crushed part in the model drastically decreases the lateral stiffness response of the ground. For a crushed zone part, it dropped by a factor 27.8 and for a full crushed model even 80.6. Considering the difference in stiffness between the two material sets (A and C2) this drop is reasonable. In Figure 6.26 the response were plot in logarithmic scale to visualise clearly that their response differ in two order of magnitude.

Next the effect of the size of the crushed zone is discussed. Four different model variations (16,17,18,19) are made up of the same material models but differ in the size of the crushed zone. It can be seen that the influence of the thickness of the crushed zone is much less than the effect of a crushed zone being present. So in other words, the presence of a crushed zone makes the response way softer, but the size does not have a major impact. To illustrate this see Table 6.1, the tangent initial global stiffness drops from 1864 kN/mm to 69 kN/mm for a $\frac{1}{2}*$ t crushed zone and 43 KN/mm for a $4*$ t crushed zone. That means the presence of a small crushed zone makes the lateral pile stiffness drop by a factor 20, while making this crushed zone eight times wider only decreases the global pile stiffness by a factor less than two compared to the small crushed zone.

Then the same investigation is presented for crushed zone material sets with different stiffness properties. The material set variation C1 that was based on the oedometer test data presented in section 5.2 was found to give a very soft response. Judging the parameters in this material set it is pictured that the material set is unrealistically soft. As the crushed rock can be treated as a frictional material a paper by Brinkgreve et al. (2010) was consulted to create a more sensible material set (material set C2). Sub-sequentially also two more stiffer material models were made to check the effect they have on the lateral response. The steps taken in increasing stiffness are times five. This was done to create a crushed zone material model that was in the same order as the intact rock. Looking at the results in Figure 6.29 and Table 6.2 it can be said that the influence of the stiffness of the crushed zone is bigger than the influence of the size of the crushed zone. On the other hand it has to be noted that the steps in increasing stiffness are bigger than extending the thickness. The force displacement curves of all model variations with an HSsmall material set for the crushed zone show a curve that is stiffening with the first displacement and then after bigger displacements starts softening again. It can be seen that the deflection point of going from stiffening to softening occurs for smaller displacements as the stiffness ratio between the intact and crushed rock decreases.

Finally the movement of four nodes in model 17 was looked at. Figure 6.31 and Figure 6.32 show the movement of these four nodes that start on the line x = 0 and y = 0. As discussed in the explanation of these figures, the nodes at the pile wall shows four times as much movement as the nodes in the intact rock for the first stage of the push over. However, after some displacement the intact rock nodes also start to be pushed to the side. The moment the intact nodes start to move along with the nodes in the crushed rock, above the dotted line in Figure 6.32, is probably correlated to the movement plastic points start to occur in the intact rock. As can be seen in Figure 6.34 the plastic points are present far into the intact rock at the end of the push-over. The movement of the intact rock also is correlated to the increase in stiffness that was seen for the HSsmall crushed zone models as discussed above. The fact that the strains start mainly in the crushed zone and get bigger in the intact rock for bigger displacement also means the lateral response is more and more 'leaning' on the intact rock for the bigger displacements, explaining the increase in global stiffness.

Last things to note on the 3D model results are the fact that it is evident the presence, stiffness and thickness of the crushed zone have a major influence on the lateral pile response, combined with the stiffness of the intact rock. The post-peak behaviour of the intact rock will not have an effect on the initial lateral pile response. When the pile is pushed over to failure, it will have a minor impact. It can therefore be said that the material set for intact rock in Mohr-Coulomb was acceptable. Although the results gave some nice insights on the effect of adding a weak zone in a model, the results do not match the test results very well.

8

Conclusion & Recommendations

By comparing the outcomes of the literature study, results and by addressing the points made at the discussion, a conclusion can be drawn on the effect of a crushed rock zone on lateral pile response in weak rock. Also the research question and sub-questions can be answered. From the literature review it could be concluded that multiple sources discussed the crushing happening around a pile, as the rock has to break to accommodate for the space that is filled with the pile wall. The extent of the crushed zone was not specified. Many different sources suggested different thicknesses for the crushed zone. About the strength reduction of a crushed rock compared to the intact rock also still unclarity exists. Field test results of Lovera (2019), combined with the residual strength values for the Hoek&Brown failure criterion coined by Ribacchi (2000) of 0.04 for s and 0.65 for mb however agreed that a drop in strength of 40% and drop in stiffness in the range of 80-90% can be realistic for crushed rock.

To investigate the size of the crushed zone a model was run in this thesis. In the 2D vertical analysis, a vertical push of a pile wall was performed. This was a static loading model, and so a simplified version of reality where impact pile driving is a dynamic process. Still, the simplified model could possibly give an insight as a plastic zone is created under the pile due to the displacement. The HBS constitutive model was used because the softening behaviour was interesting to capture. The effect of the residual strength parameters in the model were tested. The results of the vertical push showed a zone of plastic points propagating deep into the model, when compared to the small prescribed displacement. Noting the fact that the model is not representing a complete driving process, but just static push, combined with the findings in the literature review led to the decision to not make a fixed conclusion of the thickness of the crushed zone. It was therefore decided to consider multiple crushed zone thicknesses in the 3D model. The 3D model was run for multiple crushed zone thicknesses and material sets, as described in Appendix B. The 3D models all entailed monotonic lateral loading conditions and so the cyclic behaviour is not looked into. The FEM models in this thesis can be compared to the OnPT results, which were also monotonic. The results showed that the effect of the weaker crushed zone around the monopile is significant, especially when comparing to the response of the intact rock. The tangent global initial stiffness of the monopile dropped by 28 times when introducing a crushed zone into the model. The model that included a crushed zone (17) also matched the OnPT results best.

The comparisons of the different crushed zone thicknesses showed that the effect of the thickness is much less than the actual presence of the crushed zone, at least for the used stiffness parameters. Multiplying the thickness of the crushed zone by eight in the numerical models resulted only in a response that was half as stiff, compared to the 27 by introducing the crushed zone. It can therefore be concluded that the presence of the crushed zone is more relevant than the thickness, when comparing to a full intact rock model. For the different stiffnesses of the crushed zone it showed that the component had more influence, specifically when looking at the secant global stiffness for 0.1% of the pile diameter. This makes sense as the loading that has happened by this 0.1% movement will induce the stress dependent stiffness of the HSsmall model. Looking at the values, multiplication of the material stiffness at reference stress level by five times also led to the secant global stiffness at 0.1% of the pile diameter to increase five times. Conclusions on the sensitivity of the model therefore is that the

stiffness of the crushed zone has more influence than the crushed zone thickness. The influence is caused by the fact that the stiffness of the material adjacent to the pile is defining for the response in the small displacement regime.

What stands out is the shape of the curves for the models that included a crushed zone of a HSsmall material model, with an m value of 0.5 that was chosen for these frictional materials. The load-displacement curve is convex up instead of convex down, which is more common for load-displacement curves without a weaker annulus around a pile. The shape of the curves can be explained numerically. High stress areas are formed in the crushed zone due to the big difference in stiffness between the crushed and intact rock, the increase in stress then causes the stiffness of the HSsmall material to increase. This can be described as a confining effect of the stiffer intact rock, causing the stresses in the crushed zone to increase fast with pile displacement. In this way the curve shows a shape where it moves from the full crushed rock model global stiffness to the full intact rock global stiffness as the displacement increases. It can therefore be concluded that the model makes sense numerically. However, for the model to be of value, matching it with rock behaviour or pile tests is necessary. Looking at the OnPT test results of Lovera for the primary loading the shape is convex down or linear, for the cyclic loading however the curve shows a similar shape, convex up. Although cyclic loading was outside the scope of this thesis and not performed in the tests, this is interesting to note. Also normal compressive loading or triaxial loading of rock shows a convex up shape for the first part of loading, due to soft response of cracks that close upon the first loading and the subsequent stiffening. See literature review and section 7.3 for an elaborate discussion on this. Based on this conclusions can be drawn that the convex up shape, and so a stiffening response of a monopile in weak rock can be correct.

The research objective of this thesis was to investigate the monotonic lateral monopile response in weak rock and the effect of a zone of crushed rock on this response. Summing up the conclusions above it can be said that the effect of a crushed zone is big. Introducing a crushed zone in the 3D numerical models highly influenced the tangent initial global stiffness response, decreasing it at least an order of magnitude compared to an intact rock model. Considering that it is evident crushing of rock happens during impact driven installation of a monopile this is something to account for when designing a monopile foundation in weak rock using this method, and include a crushed zone in the ground model. The stiffness parameters of the crushed rock are essential when modelling the lateral response and so testing of the crushed material is important. For future cases, testing of the weak rock material found in individual situations is required to consider the amount of influence for that specific case.

8.1. Future Work

For future research on the effect of crushed rock on the lateral monopile response the following investigations are suggested :

- Performing testing and modelling in the same investigation would help out to make sure all parameters needed for the modelling are well defined by the testing,
- Investigate preloading the crushed zone by jacking the pile or stressing the rock. The HSsmall material model for the crushed rock gives a too weak response in the beginning in this thesis, due to the virgin loading of the material. Examining the influence of preloading the crushed zone is worth having a look,
- Scaled down centrifuge testing is a good option to investigate the problem of a crushed zone around a driven monopile.
- With higher D/t ratios, it is expected that not the complete pile is filled with crushed material. Investigation of the effect of an intact rock column inside the monopile therefore is of interest.
- For design of monopiles also the cyclic loading of the foundation is of importance, this was not covered in this investigation and should be looked into in future research.

A recommendation for the design of a monopile in weak rock is that including a crushed zone in your ground model is essential, because of its impact on the lateral response compared to only modelling intact material. A crushed zone with a thickness in the range of a wall thickness would be recommended. The stiffness parameters of the crushed zone are essential for the stiffness response of the pile. Therefore it would be recommended to do testing on crushed rock material, for example lab testing, that is

found at a target location for an OWT. The driving process is not described and investigated in this thesis and so also problems like driveability issues that could pop up are not discussed. However, considering that dr iving monopiles in a specific weak rock material is possible for a certain pile dimension and a driving hammer, it shows potential. Seeing that the full crushed model (16) in this thesis was based on a material model for dense sand, Figure 6.21 shows that the lateral stiffness of a monopile is bigger in a weak rock and so pile dimensions could possibly be designed smaller.

References

Achmus, M., Thieken, K., Saathoff, J.-E., Terceros, M., & Albiker, J. (2019). Un- and reloading stiffness of monopile foundations in sand. *Applied Ocean Research*, *84*, 62–73. https://doi.org/https://doi.org/10.1016/j.apor.2019.01.001

Alejano, L., Alonso, E., & Varas, F. A model to estimate the dilatancy angle of rock masses. In: In *2005*. ISRM International Symposium - EUROCK. Brno, Czech Republic, 15–21.

Alvarez-Borges, F., Ahmed, S., Bn, M., & Richards, D. (2020). Investigation of pile penetration in calcareous soft rock using x-ray computed tomography. *International Journal of Physical Modelling in Geotechnics*, *22*, 1–40. https://doi.org/10.1680/jphmg.20.00031

Arany, L., Bhattacharya, S., Macdonald, J., & Hogan, S. (2017). Design of monopiles for offshore wind turbines in 10 steps. *Soil Dynamics and Earthquake Engineering*, *92*, 126–152. https://doi.org/https://doi.org/10.1016/j.soildyn.2016.09.024

BENTLEY. (2019). *Plaxis udsm hoek & brown with softening material model manual*. https://communities.bentley.com/cfs-file/__key/communityserver-wikis-components-files/00-00-00-05-58/PLAXIS_2D00_UDSM_2D00_Hoek_5F00_Brown_5F00_with_5F00_Softenig_5F002800_V20Update1_2900_.pdf

BENTLEY. (2022). *Plaxis material models manual connection edition v22.01*. https://communities.bentley.com/products/geotech-analysis/w/wiki/46137/manuals---plaxis

Beuckelaers, W. (2017). *Numerical modelling of laterally loaded piles for offshore wind turbines* (Doctoral dissertation). University of Oxford.

Boussinesq, J. (1885). Application des potentiels: À l'étude de l'équilibre et du mouvement des solides élastiques. *(Book)*.

Brinkgreve, R., Engin, E., & Engin, H. K. (2010). Validation of empirical formulas to derive model parameters for sands. *7th Numerical Methods in Geotechnical Engineering Conference, Trondheim, Norway*, 137–142. https://doi.org/10.1201/b10551-25

Broos, E. J., Sibbes, R., & de Gijt, J. (2017). Widening a harbor basin, demolition of a deep see quay wall in rotterdam. *Conference On Maritime Energy, Hamburg*.

Cao, G., Ding, X., Liu, M., Liu, H., & Long, Q. (2023). Study on failure mechanism and soil resistance for laterally-loaded large-diameter monopiles. *Geotechnical and Geological Engineering*, *41*. https://doi.org/10.1007/s10706-023-02424-6

Charlton, T., & Rouainia, M. (2022). Geotechnical fragility analysis of monopile foundations for offshore wind turbines in extreme storms. *Renewable Energy*, *182*, 1126–1140. https://doi.org/https://doi.org/10.1016/j.renene.2021.10.092

Dai, J. (2002). Dynamic behaviors and blasting theory of rock. *Metallurgical Industry Press, Beijing*, *485*, 60.

Fan, S., Bienen, B., & Randolph, M. F. (2021). Effects of monopile installation on subsequent lateral response in sand. i: Pile installation. *Journal of Geotechnical and Geoenvironmental Engineering*, *147*(5), 04021021. https://doi.org/10.1061/(ASCE)GT.1943-5606.0002467

Gavin, K., & Doherty, P. (2012). Laterally loaded monopile design for offshore wind farms. *Proceedings of the ICE - Energy*, *165*, 7–17. https://doi.org/10.1680/ener.11.00003

Gelagoti, G., Kourkoulis, R., Georgiou, I., & Karamanos, S. (2019). Soil-structure interaction effects in offshore wind support structures under seismic loading 1. *Journal of Offshore Mechanics and Arctic Engineering*, *141*, 1. https://doi.org/10.1115/1.4043505

Gharsallaoui, H., Jafari, M., & Holeyman, A. (2020). Pile end bearing capacity in rock mass using cavity expansion theory. *Journal of Rock Mechanics and Geotechnical Engineering*, *12*(5), 1103–1111. https://doi.org/https://doi.org/10.1016/j.jrmge.2020.03.004

Hamdi, S. (2016). *Pipe pile driving into rock* (Doctoral dissertation). Université catholique de Louvain.

Hobbs, D. (1966). A study of the behaviour of a broken rock under triaxial compression, and its application to mine roadways. *International Journal of Rock Mechanics and Mining Sciences Geomechanics Abstracts*, *3*(1), 11–43. https://doi.org/https://doi.org/10.1016/0148-9062(66)90030-1

Hoek, E., & Brown, E. (1997). Practical estimates of rock mass strength. *International Journal of Rock Mechanics and Mining Sciences*, *34*(8), 1165–1186. https://doi.org/https://doi.org/10.1016/S1365-1609(97)80069-X

Hoek, E, Carranza-Torres, C., Corkum, B., Hoek, E., & Carranza-Torres, C. (2002). Hoek-brown failure criterion - 2002 edition. *Proc. NARMS-TAC Conference, Toronto*, 267–273.

Huang, S. (2016). *Mechanism of crushing of rocks under dynamic loading* (Doctoral dissertation). University of Toronto.

IRENA. (2023). *Offshore wind energy capacity worldwide from 2009 to 2022 (in megawatts)*. https://www-statista-com.tudelft.idm.oclc.org/statistics/476327/global-capacity-of-offshore-wind-energy

Irvine, J., Terente, V., Lee, L, & Comrie, R. (2015). Driven pile design in weak rock. *Proceedings of the International Symposium on Frontiers in Offshore Geotechnics, Oslo*, 569–574. https://doi.org/10.1201/b18442-73

Jafari, M., Gharsallaoui, H., Victor, K. H., & Holeyman, A. (2019). End bearing response of open-ended pipe piles embedded in rock. *International Journal of Rock Mechanics and Mining Sciences*, *119*, 46–57. https://doi.org/https://doi.org/10.1016/j.ijrmms.2019.04.008

Jorna, M. (2018). *Pile tip deformation caused by obstacles* (Master's thesis). Delft University of Technology.

Jose, N. M., & Mathai, A. (2016). A study on lateral deformation of monopile of offshore wind turbine due to environmental loads [International Conference on Emerging Trends in Engineering, Science and Technology (ICETEST - 2015)]. *Procedia Technology*, *24*, 287–294. https://doi.org/https://doi.org/10.1016/j.protcy.2016.05.038

Kaltekis, K., Panagoulias, S., Dijk, B., Brinkgreve, R., & Ramos Silva, M. (2019). Comparative concept design study of laterally loaded monopiles. *Journal of Physics: Conference Series*, *1222*, 012027. https://doi.org/10.1088/1742-6596/1222/1/012027

Kementzetzidis, E., Pisanò, F., Elkadi, A. S., Tsouvalas, A., & Metrikine, A. V. (2023). Gentle driving of piles (gdp) at a sandy site combining axial and torsional vibrations: Part ii - cyclic/dynamic lateral loading tests. *Ocean Engineering*, *270*, 113452. https://doi.org/https://doi.org/10.1016/j.oceaneng.2022.113452

Kulatilake, P., Shreedharan, S., Sherizadeh, T., Shu, B., Xing, Y., & He, P. (2016). Laboratory estimation of rock joint stiffness and frictional parameters. *Geotechnical and Geological Engineering*, *34*. https://doi.org/10.1007/s10706-016-9984-y

Lassen, S. (2022). *Sea change: Navigating the trillion-dollar offshore wind opportunity*. https://www.woodmac.com/horizons/sea-change-navigating-the-trillion-dollar-offshore-wind-opportunity/

Lehane, B. M., & Gavin, K. G. (1997). The behaviour of open and closed ended piles jacked into loose sand. *14th International Conference on Soil Mechanics and Foundation Engineering (Hamburg)*. https://www.issmge.org/uploads/publications/1/31/1997_02_0093.pdf

Lehane, B. M., & Gavin, K. G. (2001). Base resistance of jacked pipe piles in sand. *Journal of Geotechnical and Geoenvironmental Engineering*, *127*(6), 473–480. https://doi.org/10.1061/(ASCE)1090-0241(2001)127:6(473)

Lindqvist, P., Suarez, L., Montoto, M, Tan, X., & Kou, S. (1994). Rock indentation database-testing procedures, results and main conclusions. *report: Pr 44-94-023, Sweden*.

Lovera, A. (2019). *Cyclic lateral design of offshore wind turbines monopiles in weak rock* (Doctoral dissertation). Université Paris-Est.

Memija, A. (2023). *Construction of chinese xxxl monopile facility reaches next phase*. https://www.offshorewind.biz/2023/05/08/construction-of-chinese-xxxl-monopile-facility-reaches-next-phase/

Nariseti, C. (2013). *Quantification of damage in selected rocks due to impact with tungsten carbide bits* (Master's thesis). University of Toronto.

Pedone, G., Kontoe, S., Zdravkovic, L., Jardine, R., Vinck, K., & Liu, T. (2023). Numerical modelling of laterally loaded piles driven in low-to-medium density fractured chalk. *Computers and Geotechnics*, *156*. https://doi.org/10.1016/j.compgeo.2023.105252

Pisanò, F. (2019). Input of advanced geotechnical modelling to the design of offshore wind turbine foundations. *Conference: European Conference on Soil Mechanics and Geotechnical Engineering, Reykjavik, Iceland*. https://doi.org/10.32075/17ECSMGE-2019-1109

Pisanò, F. (2021). *Oe44030 offshore geotechical engineering: Piled foundations - axial loading*. https://brightspace.tudelft.nl/d2l/le/content/401351/viewContent/2373601/View

Randolph, M. Design considerations for piles jacked or driven into strong soil or weak rock. In: In *Proceedings of the second international conference on press-in engineering 2021, kochi, japan*. CRC Press. 2021, 3.

Ribacchi, R. (2000). Mechanical tests on pervasively jointed rock material: Insight into rock mass behaviour. *Rock Mechanics and Rock Engineering*, *33*, 243–266. https://doi.org/10.1007/s006030070002

Seong, J., Abadie, C., Madabhushi, G., & Haigh, S. (2022). Dynamic and monotonic response of monopile foundations for offshore wind turbines using centrifuge testing. *Bulletin of Earthquake Engineering*, *21*, 1–21. https://doi.org/10.1007/s10518-022-01524-7

Sørensen, S. P. H., Brødbæk, K. T., Møller, M., & Augustesen, A. H. (2012). Review of laterally loaded monopiles employed as the foundation for offshore wind turbines. *DCE Technical Reports, Department of Civil Engineering, Aalborg University, Aalborg, Denmark, No.137.*

Stevens, R., Willtsie, E., & Turton, T. (1982). Evaluating pile drivability for hard clay,very dense sand and rock. *Offshore Technology Conference, Houston, Texas*.

Sun, B., Zhang, Q., Zhu, W., Leng, J., & Ye, G. (2023). Borehole instability in decomposed granite seabed for rock-socketed monopiles during "drive-drill-drive" construction process: A case study. *Journal of Marine Science and Engineering*, *11*, 990. https://doi.org/10.3390/jmse11050990

Terente, V., Irvine, J., Comrie, R., & Crowley, J. (2015, June). Pile driving and pile installation risk in weak rock. In *Geotechnical engineering for infrastructure and development* (pp. 1187–1192). https://doi.org/10.1680/ecsmge.60678.vol3.168

Terente, V., Irvine, J., Torres, I., & Jaeck, C. (2017). Driven pile design methods in weak rock. *OSIG Conference*.

Tomlinson, M., & Woodward, J. (2014). *Pile design and construction practice*. CRC Press. https://doi.org/10.1201/b17526

Tsetas, A., Tsouvalas, A., & Metrikine, A. V. (2021). Installation of large-diameter monopiles: Introducing wave dispersion and non-local soil reaction. *Journal of Marine Science and Engineering*, *9*(3). https://doi.org/10.3390/jmse9030313

van Wijk, J. (2022). Friction fatigue in weak rock and non-cohesive soils with soft grains: A physical model for the role of abrasive wear in skin friction reduction. *11th International Conference*

on Stress Wave Theory and Design and Testing Methods for Deep Foundations, Rotterdam. https://doi.org/10.5281/zenodo.7148299

Van Langen, H., & Vermeer, P. A. (1991). Interface elements for singular plasticity points. *International Journal for Numerical and Analytical Methods in Geomechanics*, *15*(5), 301–315. https://doi.org/https://doi.org/10.1002/nag.1610150502

Vesić, A. S. (1972). Expansion of cavities in infinite soil mass. *Journal of the Soil Mechanics and Foundations Division*, *98*, 265–290.

Wang, L., Lai, Y., Hong, Y., & Mašín, D. (2020a). A unified lateral soil reaction model for monopiles in soft clay considering various length-to-diameter (l/d) ratios. *Ocean Engineering*, *212*, 107492. https://doi.org/10.1016/j.oceaneng.2020.107492

Wang, T., Zhang, Y., Bao, X., & Wu, X. (2020b). Mechanisms of soil plug formation of open-ended jacked pipe pile in clay. *Computers and Geotechnics*, *118*, 103334. https://doi.org/https://doi.org/10.1016/j.compgeo.2019.103334

Xu, J., Haque, A., Gong, W., Gamage, R., Dai, G., Zhang, Q., & Xu, F. (2020). Experimental study on the bearing mechanisms of rock-socketed piles in soft rock based on micro x-ray ct analysis. *Rock Mechanics and Rock Engineering*, *53*. https://doi.org/10.1007/s00603-020-02121-3

Yang, J. (2006). Influence zone for end bearing of piles in sand. *Journal of Geotechnical and Geoenvironmental Engineering*, *132*(9), 1229–1237. https://doi.org/10.1061/(ASCE)1090-0241(2006)132:9(1229)

Zhang, Q., Feng, R., Yu, Y., Liu, S., & Qian, J. (2019). Simplified approach for prediction of nonlinear response of bored pile embedded in sand. *Soils and Foundations*, *59*. https://doi.org/10.1016/j.sandf.2019.07.011

Zhang, X., & Fatahi, B. (2021). Assessing axial load transfer mechanism of open-ended tubular piles penetrating in weak rocks using three-dimensional discrete element method. *Computers and Geotechnics*, *137*, 104267. https://doi.org/https://doi.org/10.1016/j.compgeo.2021.104267

Zhang, Y., Wang, F., Bai, X., Yan, N., Sang, S., Kong, L., Zhang, M., & Wei, Y. (2022). Numerical simulation of bearing characteristics of bored piles in mudstone based on zoning assignment of soil around piles. *Buildings*, *12*, 1877. https://doi.org/10.3390/buildings12111877

A

Material Sets

Table A.1: Overview of the different material sets that were used

Material Set	Material Variation	Crushed Rock	Intact Rock	Constitutive Model
A	-	-	x	Mohr-Coulomb (5000 MPa)
B	-	x	-	Mohr-Coulomb (60 MPa)
C	C1	x	-	HSsmall (15 MPa)
	C2	x	-	HSsmall (60 MPa)
	C3	x	-	HSsmall (300 MPa)
	C4	x	-	HSsmall (1500 MPa)
D	D1	-	x	Hoek&Brown Softening (γ = -1)
	D2	-	x	Hoek&Brown Softening (γ = 1)
	D3	-	x	Hoek&Brown Softening (γ = 3)
	D4	-	x	Hoek&Brown Softening (γ = 5)
E	E1	-	x	Hoek&Brown Softening (mb_{res} = 0.9)
	E2	-	x	Hoek&Brown Softening (mb_{res} = 0.75)
	E3	-	x	Hoek&Brown Softening (mb_{res} = 0.5)
	E4	-	x	Hoek&Brown Softening (mb_{res} = 0.65)

The overview shows values with the unit MPa behind the Constitutive Model for material set A,B and C. This is just to indicate the difference between the models and not give the actual value of the stiffness. For the HSsmall models the E50ref value is given. For the complete inputs of the material sets, see Table A.2 to Table A.7. Same holds for the Hoek&Brown Softening material variations, the γ and mb_{res} are just indication of the varying parameter. Note that Material Variation D3 and E2 are actually the same, but for the sake of clarity in the sensitivity analysis they are still presented separately. For the complete inputs of the material sets, see Table A.8 to Table A.15.

Table A.2: Mohr-Coulomb material set of intact rock (Material Variation A), parameters are based on the uniaxial and triaxial tests on the intact rock.

Property	Unit	Value
Stiffness		
E'	kN/m²	5.000E6
ν' (nu)		0.3000
Alternatives		
G	kN/m²	1.923E6
E_{oed}	kN/m²	6.731E6
Strength		
c'_{ref}	kN/m²	1660
φ' (phi)	°	32.00
ψ (psi)	°	4.000
Velocities		
V_s	m/s	971.2
V_p	m/s	1817
Advanced		
Set to default values		☐
Stiffness		
E'_{inc}	kN/m²/m	0.000
z_{ref}	m	0.000
Strength		
c'_{inc}	kN/m²/m	0.000
z_{ref}	m	0.000
Tension cut-off		☑
Tensile strength	kN/m²	1540

Table A.3: Mohr-Coulomb material set of crushed rock. (Material Variation B), the friction angle is based on typical values for dense sand or gravel material.

Property	Unit	Value
Stiffness		
E'	kN/m²	60.00E3
ν' (nu)		0.3000
Alternatives		
G	kN/m²	23.08E3
E_{oed}	kN/m²	80.77E3
Strength		
c'_{ref}	kN/m²	0.000
φ' (phi)	°	40.00
ψ (psi)	°	10.00
Velocities		
V_s	m/s	106.4
V_p	m/s	199.0
Advanced		
Set to default values		☑
Stiffness		
E'_{inc}	kN/m²/m	0.000
z_{ref}	m	0.000
Strength		
c'_{inc}	kN/m²/m	0.000
z_{ref}	m	0.000
Tension cut-off		☑
Tensile strength	kN/m²	0.000

Table A.4: HSsmall material set of crushed rock based on the calibration done on the oedometer testing in section 5.2. (Material Variation C1), the friction angle is based on findings presented in Lovera (2019).

Stiffness		
E_{50}^{ref}	kN/m²	12.00E3
E_{oed}^{ref}	kN/m²	12.00E3
E_{ur}^{ref}	kN/m²	36.00E3
power (m)		0.5000
Alternatives		
Use alternatives		☐
C_c		0.02489
C_s		7.468E-3
e_{init}		0.2987
Strength		
c'_{ref}	kN/m²	1.000
φ' (phi)	°	32.00
ψ (psi)	°	2.000
Small strain		
$\gamma_{0.7}$		0.1000E-3
G_0^{ref}	kN/m²	34.00E3
Advanced		
Set to default values		☑
Stiffness		
ν'_{ur}		0.2000
p_{ref}	kN/m²	100.0
K_0^{nc}		0.4701

Table A.5: HSsmall material set of crushed rock based on Brinkgreve et al. (2010), assigning a typical material set for cohesionless material to the crushed rock. (Material Variation C2)

Stiffness		
E_{50}^{ref}	kN/m²	60.00E3
E_{oed}^{ref}	kN/m²	60.00E3
E_{ur}^{ref}	kN/m²	180.0E3
power (m)		0.5000
Alternatives		
Use alternatives		☐
C_c		5.482E-3
C_s		1.645E-3
e_{init}		0.4300
Strength		
c'_{ref}	kN/m²	0.000
φ' (phi)	°	40.00
ψ (psi)	°	10.00
Small strain		
$\gamma_{0.7}$		0.1000E-3
G_0^{ref}	kN/m²	128.0E3
Advanced		
Set to default values		☑
Stiffness		
ν'_{ur}		0.2000
p_{ref}	kN/m²	100.0
K_0^{nc}		0.3572
Strength		

Table A.6: HSsmall material set of crushed rock having a stiffness at reference stress of five times the stiffness of C2. (Material Variation C3)

Stiffness		
E_{50}^{ref}	kN/m²	300.0E3
E_{oed}^{ref}	kN/m²	300.0E3
E_{ur}^{ref}	kN/m²	900.0E3
power (m)		0.5000
Alternatives		
Use alternatives		☐
C_c		1.096E-3
C_s		0.3289E-3
e_{init}		0.4300
Strength		
c'_{ref}	kN/m²	0.000
φ' (phi)	°	40.00
ψ (psi)	°	10.00
Small strain		
$\gamma_{0.7}$		0.1000E-3
G_0^{ref}	kN/m²	700.0E3
Advanced		
Set to default values		☑
Stiffness		
ν'_{ur}		0.2000
p_{ref}	kN/m²	100.0
K_0^{nc}		0.3572
Strength		

Table A.7: HSsmall material set of crushed rock having a stiffness at reference stress of five times the stiffness of C3. (Material Variation C4)

Stiffness		
E_{50}^{ref}	kN/m²	1.500E6
E_{oed}^{ref}	kN/m²	1.500E6
E_{ur}^{ref}	kN/m²	4.500E6
power (m)		0.5000
Alternatives		
Use alternatives		☐
C_c		0.2193E-3
C_s		0.06578E-3
e_{init}		0.4300
Strength		
c'_{ref}	kN/m²	0.000
φ' (phi)	°	40.00
ψ (psi)	°	10.00
Small strain		
$\gamma_{0.7}$		0.1000E-3
G_0^{ref}	kN/m²	3.500E6
Advanced		
Set to default values		☑
Stiffness		
ν'_{ur}		0.2000
p_{ref}	kN/m²	100.0
K_0^{nc}		0.3572
Strength		

Table A.8: Hoek&Brown Softening material set of intact rock. (Material Variation D1)

User-defined model		
DLL file		hbs1_64.dll
Model in DLL		HB-SSM
User-defined parameters		
E	kN/m²	5.000E6
ν		0.3000
D		0.000
GSI_{ini}		100.0
α		0.8700
m_i		10.00
$m_{\psi_{ini}}$		0.5000
m_{res}		7.500
s_{res}		0.7500
$m_{\psi_{res}}$		0.000
σ_{ci}	kN/m²	6000
B_{m_b}		1.000E-3
B_s		1.000E-3
B_ψ		0.01000
γ	1/day	-1.000
k		-0.9999

Table A.9: Hoek&Brown Softening material set of intact rock. (Material Variation D2)

User-defined model		
DLL file		hbs1_64.dll
Model in DLL		HB-SSM
User-defined parameters		
E	kN/m²	5.000E6
ν		0.3000
D		0.000
GSI_{ini}		100.0
α		0.8700
m_i		10.00
$m_{\psi_{ini}}$		0.5000
m_{res}		7.500
s_{res}		0.7500
$m_{\psi_{res}}$		0.000
σ_{ci}	kN/m²	6000
B_{m_b}		1.000E-3
B_s		1.000E-3
B_ψ		0.01000
γ	1/day	-1.000
k		-0.9999

Table A.10: Hoek&Brown Softening material set of intact rock. (Material Variation D3)

User-defined model		
DLL file		hbs1_64.dll
Model in DLL		HB-SSM
User-defined parameters		
E	kN/m²	5.000E6
ν		0.3000
D		0.000
GSI_{ini}		100.0
α		0.8700
m_i		10.00
$m_{\psi_{ini}}$		0.5000
m_{res}		7.500
s_{res}		0.7500
$m_{\psi_{res}}$		0.000
σ_{ci}	kN/m²	6000
B_{m_b}		1.000E-3
B_s		1.000E-3
B_ψ		0.01000
γ	1/day	-1.000
k		-0.9999

Table A.11: Hoek&Brown Softening material set of intact rock. (Material Variation D4)

User-defined model		
DLL file		hbs1_64.dll
Model in DLL		HB-SSM
User-defined parameters		
E	kN/m²	5.000E6
ν		0.3000
D		0.000
GSI_{ini}		100.0
α		0.8700
m_i		10.00
$m_{\psi_{ini}}$		0.5000
m_{res}		7.500
s_{res}		0.7500
$m_{\psi_{res}}$		0.000
σ_{ci}	kN/m²	6000
B_{m_b}		1.000E-3
B_s		1.000E-3
B_ψ		0.01000
γ	1/day	-1.000
k		-0.9999

Table A.12: Hoek&Brown Softening material set of intact rock. (Material Variation E1)

User-defined model		
DLL file		hbs1_64.dll
Model in DLL		HB-SSM
User-defined parameters		
E	kN/m²	5.000E6
ν		0.3000
D		0.000
GSI_{ini}		100.0
α		0.8700
m_i		10.00
$m_{\psi_{ini}}$		0.5000
m_{res}		6.500
s_{res}		0.04000
$m_{\psi_{res}}$		0.000
σ_{ci}	kN/m²	6000
B_{m_b}		1.000E-3
B_s		1.000E-3
B_ψ		0.01000
γ	1/day	3.000
k		-0.9999

Table A.13: Hoek&Brown Softening material set of intact rock. (Material Variation E2)

User-defined model		
DLL file		hbs1_64.dll
Model in DLL		HB-SSM
User-defined parameters		
E	kN/m²	5.000E6
ν		0.3000
D		0.000
GSI_{ini}		100.0
α		0.8700
m_i		10.00
$m_{\psi_{ini}}$		0.5000
m_{res}		7.500
s_{res}		0.7500
$m_{\psi_{res}}$		0.000
σ_{ci}	kN/m²	6000
B_{m_b}		1.000E-3
B_s		1.000E-3
B_ψ		0.01000
γ	1/day	3.000
k		-0.9999

Table A.14: Hoek&Brown Softening material set of intact rock. (Material Variation E3)

User-defined model		
DLL file		hbs1_64.dll
Model in DLL		HB-SSM
User-defined parameters		
E	kN/m²	5.000E6
ν		0.3000
D		0.000
GSI_{ini}		100.0
α		0.8700
m_i		10.00
$m_{\psi_{ini}}$		0.5000
m_{res}		5.000
s_{res}		0.5000
$m_{\psi_{res}}$		0.000
σ_{ci}	kN/m²	6000
B_{m_b}		1.000E-3
B_s		1.000E-3
B_ψ		0.01000
γ	1/day	3.000
k		-0.9999

Table A.15: Hoek&Brown Softening material set of intact rock. (Material Variation E4)

User-defined model		
DLL file		hbs1_64.dll
Model in DLL		HB-SSM
User-defined parameters		
E	kN/m²	5.000E6
ν		0.3000
D		0.000
GSI_{ini}		100.0
α		0.8700
m_i		10.00
$m_{\psi_{ini}}$		0.2500
m_{res}		2.500
s_{res}		0.9000
$m_{\psi_{res}}$		0.000
σ_{ci}	kN/m²	6000
B_{m_b}		1.000E-3
B_s		1.000E-3
B_ψ		0.01000
γ	1/day	3.000
k		-0.9999

B

Models Overview

Table B.1: Overview of the different 2D horizontal FEM model set ups

Model Variation	Crushed Rock		Intact Rock
	Thickness	Material Set	Material Set
1	$1 * t$*	HSsmall (C1)	Mohr-Coulomb (A)

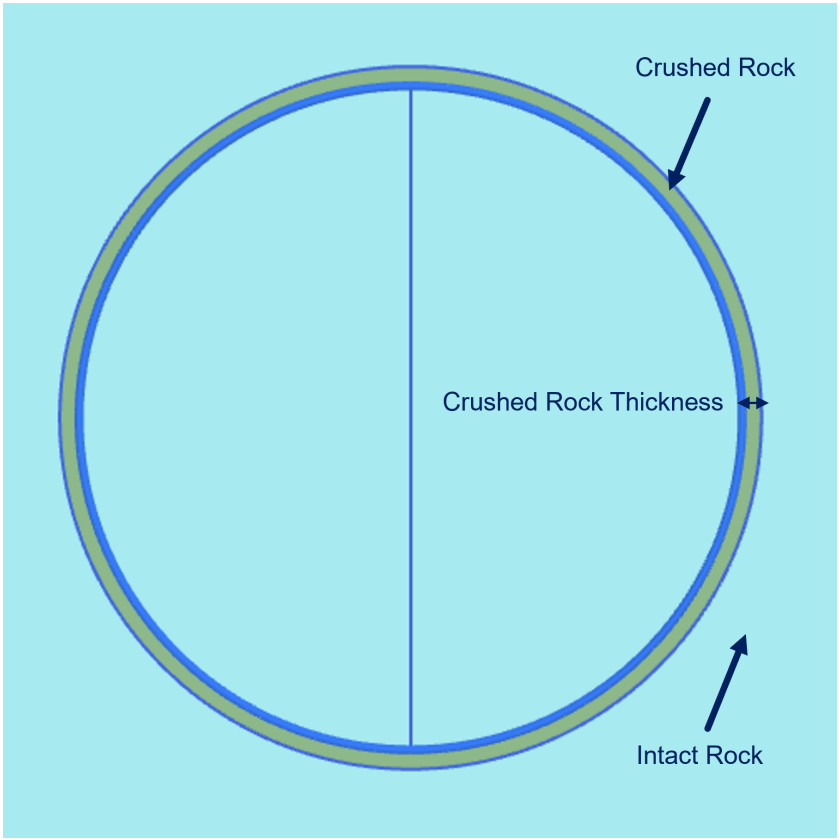

Figure B.1: Graphic of the location of the crushed and intact rock and the crushed rock thickness for the 2D horizontal model.

* t represents the wall thickness of the pile, which is 35mm.

Table B.2: Overview of the different 2D vertical FEM model set ups

Model Variation	Material Set	Embedment depth (m)	Axisymmetric/Plane-Strain
2	D1	0.1	Axisymmetric
3	D2	0.1	Axisymmetric
4	D2	0.5	Axisymmetric
6	D3	0.1	Axisymmetric
7	D4	0.1	Axisymmetric
8	E1	0.1	Axisymmetric
9	E2	0.1	Axisymmetric
10	E3	0.1	Axisymmetric
11	E4	0.1	Axisymmetric

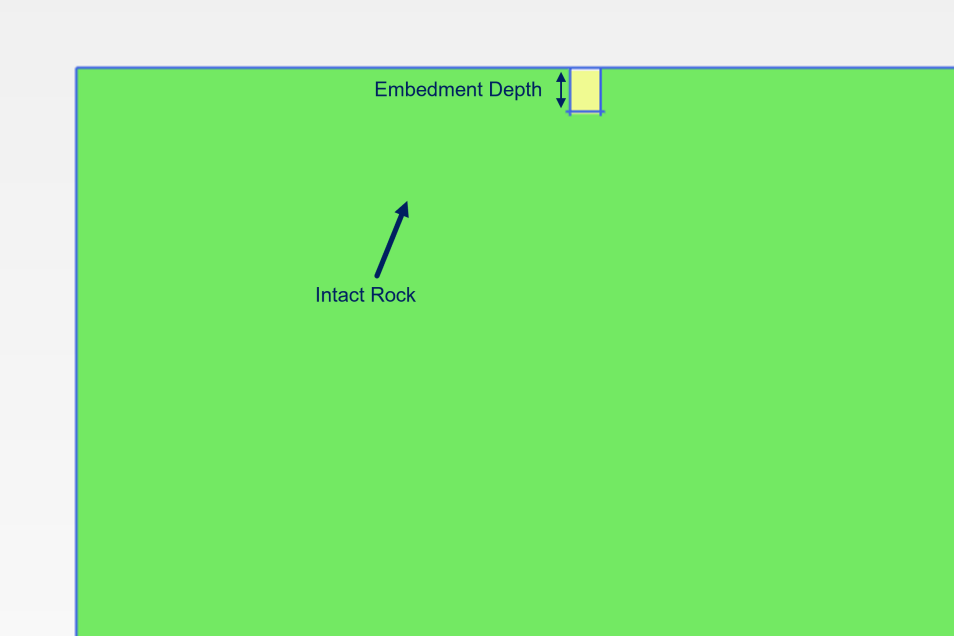

Figure B.2: Graphic showing the meaning of embedment depth in the 2D vertical model. It is the initial depth of the WIP pile before it is pushed down.

Table B.3: Overview of the different 3D FEM model set ups

Model Variation	Crushed Rock		Intact Rock
	Thickness	Material Set	Material Set
12	-	-	Mohr-Coulomb (A)
13	$1 * t$	Mohr-Coulomb (B)	Mohr-Coulomb (A)
14	Full Model	Mohr-Coulomb (B)	-
15	Full Model	HSsmall (C2)	-
16	$\frac{1}{2} * t$	HSsmall (C2)	Mohr-Coulomb (A)
17	$1 * t$	HSsmall (C2)	Mohr-Coulomb (A)
18	$2 * t$	HSsmall (C2)	Mohr-Coulomb (A)
19	$4 * t$	HSsmall (C2)	Mohr-Coulomb (A)
20	$1 * t$	HSsmall (C1)	Mohr-Coulomb (A)
21	$1 * t$	HSsmall (C3)	Mohr-Coulomb (A)
22	$1 * t$	HSsmall (C4)	Mohr-Coulomb (A)

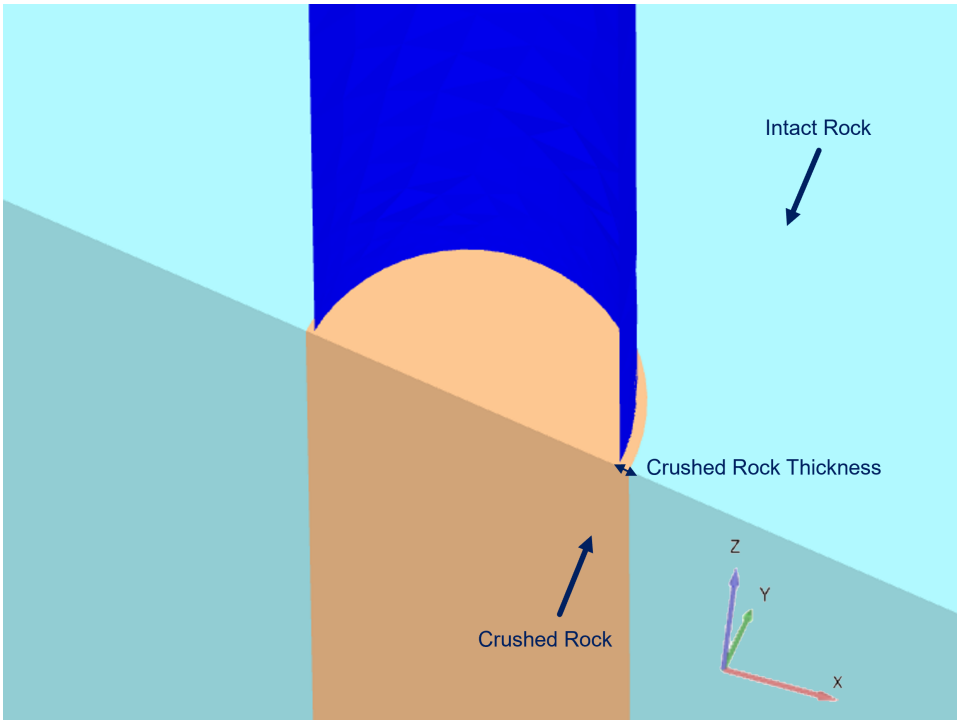

Figure B.3: Graphic of the location of the crushed and intact rock and the crushed rock thickness for the 3D model.

* t represents the wall thickness of the pile, which is 35mm.